Electronic Structures of Cluster Anions Studied by Photoelectron Spectroscopy

光電子分光法によるクラスター
負イオンの電子状態の研究

Hiroyuki Yoshida

吉田弘幸

学位論文

Electronic Structures of Cluster Anions Studied by Photoelectron Spectroscopy
(光電子分光法によるクラスター負イオンの電子状態の研究)

平成 6 年 12 月博士 (理学) 申請
東京大学大学院理学系研究科

化学専攻
吉田 弘幸

Electronic Structures of Cluster Anions Studied by Photoelectron Spectroscopy

A Thesis Presented by
Hiroyuki Yoshida

Submitted to
School of Science
The University of Tokyo
(December 1994)

Acknowledgments

I would like to express my sincere appreciation to Professor Tamotsu Kondow. His support and guidance has been a great source of encouragement.

I am sincerely grateful to Professor Takashi Nagata and Dr. Akira Terasaki for the kind advice and helpful discussion. I extend my gratitude to Drs. Shinji Nonose and Fumitaka Mafuné for the kind encouragement.

I would like to thank my experimental collaborators, Mr. Kazuhiro Okano, Ms. Naoko Takahashi, Messrs. Yuji Fukuda, Shin-ichiro Minemoto, Tetsuya Nishio, Ms. Masako Iseda, Mr. Sang Yun Han.

I also acknowledge all the members of the laboratory, Dr. Jun Hirokawa, Mr. Tsutomu Ikegami, Drs. Makoto Nagaminé, Toshiki Sugai, Tatsuya Tsukuda, Messrs. Masahiko Ichihashi, Yoshihiro Takeda, Hisato Yasumatsu, Jun-ya Kohno, Hideki Tanaka, Uwe Kalmbach, Hisashi Matsumura, Ms. Noriko Horimoto, Messrs. Tomoyuki Mizuno, Junsei Yamabe, Yuichiro Hashimoto, Shin'ichi Koizumi, Ms. Kanae Murai, Mr. Hitoshi Yamaguchi, and Ms. Maki Tsuchida.

I wish to acknowledge valuable discussions with Professors Suehiro Iwata, Masaru Tsukada, Tsuyoshi Yamaguchi, Hideo Imoto, and Dr. Katsuyoshi Kobayashi. I would like to thank Messrs. Tamotsu Inaba, Takashi Kawashima for the technical assistance.

Finally, I extend my grateful thanks to my parents, my sister and my good friends.

Contents

Chapter I

General Introduction

A cluster which is defined as an aggregate consisting of $2 \sim 10^3$ atoms or molecules is considered to be an intermediate state of matter between the gas and the condensed phases. It is expected therefore that the properties of the clusters change characteristically and drastically with the number of the constituent atoms or molecules (cluster size) and gradually approach those of the condensed matter as the cluster size increases. It is essential to examine the electronic structure as a function of a cluster size, because the electronic structure is closely related to other important properties such as the cluster bonding, reactivity, magnetism and so on.

We always encounter much difficulty in the experimental investigations of the electronic structures of the cluster, because number density of the cluster is very small. In order to overcome the difficulty, a high sensitive technique is definitely necessary at the first place, even if information derived from it is limited or indirect. This technique includes photodestruction [1] [2], photodissociation [3], and photodetachment spectroscopies [4]. Among these techniques, the photoelectron spectroscopy of cluster anions [5] is the most powerful and suitable for investigating the electronic structure of clusters with a given size.

In the photoelectron spectroscopy, the cluster anions is size-selected by mass spectroscopic technique and is subjected to intense laser light which achieves electron detachment with a sufficiently high efficiency. Information on the electronic structure of a cluster anions can be obtained as follows: spectral feature is determined from photodetachment transition between the states of the anion and the corresponding neutral with the geometry of the cluster anion. It is equally important that the electron affinity can be determined from the transition between the ground electronic and vibrational states of the anion and the neutral. In this way, the photoelectron spectroscopy provides the quantitative information which can be precisely compared with a theoretical calculation. With the aid of the theoretical calculation, the electronic structures will be examined precisely and further information such as geometrical structures will be derived from the photoelectron spectra.

From the nature of the bonding in the clusters, the studies on the electronic structures fall into molecular cluster anions and metal and semiconductor cluster anions. In a molecular cluster anion, the nature of the cluster anion bonding is closely related to the distribution of

the excess electron over the cluster anion. In the simplest case, the excess electron localizes on one of the component molecules to form the core ion, which interacts with the remaining neutral components (solvents). This case describes an ion-molecular complex which may provide a microscopic detail of solvation phenomena. In this regard, Bowen et al. have measured the photoelectron spectra of various ion-molecular complexes [6], deriving the charge distributions of the complexes and the ion-solvent dissociation energies (solvation energies). In the other case, the excess electron is delocalized among several component molecules as exemplified by water and ammonia cluster anions [7].

In the metal cluster study, on the other hand, one of the most important issue is how the electronic properties (or bulk band structures) evolve. The photoelectron spectra of cluster anions provide important information about the electronic properties of their corresponding neutral clusters. Studying an entire series of a metal cluster using photoelectron spectroscopy of the anion of clusters allows one to map out variation in the electron affinity and the valence electronic structure as a function of the cluster size. By doing this, one can trace the evolution of the electronic properties from the atom toward the bulk.

In recent years, several groups have recorded the photoelectron spectra of clusters consisting of various metals and semiconductors [6],[8]-[24]. For metal clusters consisting of Ia and Ib group metals and most of typical metal elements, the electronic structure near the highest occupied orbitals appears to be well described by a "shell model" which is successfully applied to explain the stability of nuclear [25]. In addition to cluster abundance in mass spectra and ionization potential measurements [25], the photoelectron spectroscopy of the cluster anions have provided excellent support of this simple model for small clusters of variety of metals [16]. Furthermore, in the clusters consisting of Ia and Ib group metal [6], [8], [9], [11], [12] and semiconductor elements [20]- [24], *ab initio* calculations have been performed, and their geometric and electronic structures are successfully determined [26]-[28]. On the other hand, for the clusters consisting of the transition metal atoms with open *d* shell, the studies are very limited, particularly for clusters with larger sizes; a simple picture of the electronic structures has not been proposed yet. Precise *ab initio* calculations are also inherently difficult to be performed because of many low-lying electronic states

associated with the d electrons. However, the investigation of the d electrons is of great important and interest, because the d electrons play an important role in emerging of the magnetism and the catalytic activities of transition metals and transition metal compounds [29]- [40]. The photoelectron spectroscopy will provide an avenue for solving the problems in connection with the behavior of the d electrons.

The present study is devoted to elucidation of the electronic structures and related properties of clusters consisting of molecular and transition metal atoms. The present dissertation is organized as follows:

The chapter II presents a detailed description of the experimental apparatus used in this study. Two different photoelectron spectrometers were designed and constructed together with a cluster source.Electronic circuits developed were also presented.

In chapter III, studies on the photoelectron spectroscopy of $(CO_2)_n H_2O^-$ are described. Johnson et al. [41] measured the photoelectron spectra in the size range of $2 \leq n \leq 13$ and found that the vertical detachment energy changes abruptly at the cluster size of $n = 6$. Based on the *ab initio* calculation of $(CO_2)_2^-$ [42], this result was interpreted as a size-dependent isomerization of the core ion from a dimer core ion, $C_2O_4^-$, to a monomer core ion, CO_2^-. The intent of this work is to see whether the excess electron is trapped in the binary $(CO_2)_n H_2O^-$ clusters in the same manners as in $(CO_2)_n^-$ and, if this is the case, how the introduction of H_2O into the system affects the core isomerization. It is found that two isomeric forms having the monomer core ion, CO_2^-, and the dimer core ion, $C_2O_4^-$, coexist at least in small clusters ($n = 2, 3$ and 4). This coexistence indicates that the barrier to the isomerization of the ion core increases by the introduction of a single H_2O molecule.

In chapter IV, studies on the electronic structure of Co_n^- are described. Among clusters of transition metal elements, a cobalt cluster is one of the most interesting examples to be investigated, because of significant exchange interaction and electron correlation of the $3d$ band of cobalt. In connection with the recent measurements of the magnetism of the cobalt clusters [32], their spin-polarized electronic structures are of great interest. To this end, the photoelectron spectra of Co_n^- ($3 \leq n \leq 70$) were measured, and were compared with the results of the spin-polarized DV-Xα calculation. It is found that $3d$ bands with the

majority and the minority spins are separated by $1.0 \sim 2.8$ eV with the spin differenc of about 2 electrons per cobalt atom. This result provides the evidence of ferromagnetic spin ordering in Co_n^-. In addition, a size-dependent transition was observed in the electronic structure of Co_n^- at the cluster size of about $n = 7$.

Since remarkable correlation between a reactivity and an electronic states was observed [40], the size-dependent transition in the reactivity should occur in the vicinity of $n = 7$ of Co_n^-, where the transition of the electronic structure was observed. Chapter V represents the studies on the reactivity of Co_n^- with O_2 or CO. As expected,a size-dependent transition was observed in the reactivity of Co_n^- . The reactivity of Co_n^- should be elucidated by examining the electronic structures of the reaction products, because these electronic structures are closely related to the bonding between the clusters and the adsorbate. To this end, the photoelectron spectra of $Co_nO_m^-$ $(m = 1, 2)$ and Co_nN^- were measured.

In chapter VI, studies on the electronic structure of V_n^- are described. It is interesting to see whether a similar size-dependent transition occurs as observed in the cobalt cluster anions. In addition, the magnetism of the vanadium clusters were extensively investigated theoretically, because it is predicted that both a high-spin and a low-spin states exist in these clusters [34]-[36]. The photoelectron spectra of Co_n^- will provide important information on their spin states. Another focus of this work was the experimental investigation of the properties of the s electrons in the clusters consisting of the transition metals having a partially filled d shell. Fujima and Yamaguchi calculated the electronic structure of the nickel, cobalt and iron clusters and predicted that the $4s$ electrons form the electronic shell in these transition metal clusters in the same manner as in the alkali and coinage metal clusters [43]. However, the significant influence of the s electrons was not observed by the previous studies [11], [12], probably because s bands were hidden behind the thick d bands in the photoelectron spectra of these clusters on the right-hand side of the transition metal series. The clusters of vanadium whose atomic configuration is represented as $3d^34s^2$ are an excellent candidate to examine the behavior of the $4s$ electrons, because the number of s electrons relatively to that of d electrons is larger. As a result, the same transition as in the cobalt cluster anions were observed in the vicinity of $n = 9$. In addition, the clear

distinction between $n \leq 16$ and $n \geq 17$ was observed in the spectral feature; below $n = 16$, the spectral feature varies dramatically as a function of cluster size, while above $n = 17$ the spectral feature does not vary significantly. This latter transition in the spectral feature may be understood in terms of the influence of the $4s$ and/or $4p$ electrons.

References

[1] P. C. Cosby, J. H. Ling, J. R. Peterson, and J. T. Moseley, J. Chem. Phys., **65**, 5267 (1976).

[2] R. A. Beyer, and J. A. Vanderhoff, J. Chem. Phys., **65**, 2313 (1976).

[3] A. W. Castleman, Jr., D. E. Hunton, T. G. Lindeman, and D. N. Lindsay, Intl. J. Mass Spect. and Ion Phys., **47**, 199 (1983).

[4] H. -S. Kim and M. Bowers, J. Chem. Phys., **47**, 199 (1986).

[5] D. G. Leopold, J. Ho, and W. C. Lineberger, J. Chem. Phys., **86**, 1715 (1987).

[6] S. T. Arnold, J. G. Eaton, D. Patel-Misra, H. W. Sarkas, and K. H. Bowen, in *Ion and cluster ion spectroscopy and structure*, edited by Maier (Elsevier, Amsterdam 1989).

[7] J. V. Coe, G. H. Lee, J. G. Eaton, S. T. Arnold, H. W. Sarkas, K. H. Bowen, C. Ludewigt, H. Haberland, and D. R. Worsnop, J. Chem. Phys. **92**, 3980 (1990).

[8] K. M. McHugh, J. G. Eaton, G. H. Lee, H. W. Sarkas, L. H. Kidder, J. T. Snodgrass, M. R. Manaa, and K. H. Bowen, J. Chem. Phys. **91**, 3792 (1989).

[9] J. Ho, K. M. Ervin and W. C. Lineberger, J. Chem. Phys. **93**, 6987 (1990).

[10] M. L. Polak, G. Gerber, J. Ho, and W. C. Lineberger, J. Chem. Phys. **97**, 8990 (1992)

[11] G. Ganteför, M. Gausa, K. H. Meiwes-Broer and H. O. Lutz, J. Chem. Soc. Faraday Trans. **86**, 2483 (1990).

[12] G. Ganteför, M. Gausa, K. H. Meiwes-Broer and H. O. Lutz, Faraday Discuss. Chem. Soc. **86**, 197 (1988).

[13] K. J. Taylor, C. L. Pettiette, M. J. Craycraft, O. Cheshnovsky, and R. E. Smalley, Chem. Phys. Lett. **152**, 347 (1988).

[14] C. -Y. Cha, G. Ganteför, and W. Eberhardt, J. Chem. Phys. **100**, 995 (1994).

[15] C. L. Pettiette, S. H. Yang, M. J. Craycraft, J. Conceicao, R. T. Laaksonen, O. Cheshnovsky, and R. E. Smalley, J. Chem. Phys. **88**, 5377 (1988).

[16] C.-Y. Cha, G. Ganteför, and W. Eberhardt, J. Chem. Phys. **99**, 6308 (1993).

[17] H. Handshuh, G. Ganteför, P. S. Bechthold, and W. Eberhardt, J. Chem. Phys. **100**, 7093 (1994).

[18] D. G. Leopold, and W. C. Lineberger, J. Chem. Phys. **85**, 51 (1986).

[19] K. M. Ervin, J. Ho, and W. C. Lineberger, J. Chem. Phys. **89**, 4514 (1988).

[20] O. Cheshnovsky, S. H. Yang, C. L. Pettiette, M. J. Craycraft, Y. Liu, and R. E. Smalley, Chem. Phys. Lett. **138**, 119 (1987).

[21] S. H. Yang, C. L. Pettiette, J. Conceicao, O. Cheshnovsky and R. E. Smalley, Chem. Phys. Lett. **139**, 233 (1987).

[22] S. Yang, K. J. Taylor, M. J. Craycraft, J. Conceicao, C. L. Pettiette, O. Cheshnovsky, and R. E. Smalley, Chem. Phys. Lett. **144**, 431 (1988).

[23] T. N. Kitsopoulos, C. J. Chick, A. Weaver and D. M. Neumark, J. Chem. Phys. **93** 6108 (1990).

[24] D. W. Arnold, S. E. Bradforth, T. N. Kitsopoulos, and D. M. Neumark, J. Chem. Phys. **95** 8753 (1991).

[25] W. A. de Heer, Rev. Mod. Phys. **65**, 611 (1993) and references therein.

[26] (a)V. Bonačić-Koutecký, P. Fantucci and J. Koutecký, Chem. Rev. **91**, 1035 (1991); (b)V. Bonačić-Koutecký, P. Fantucci and J. Koutecký, J. Chem. Phys. **91**, 3794 (1989); (c)V. Bonačić-Koutecký, P. Fantucci and J. Koutecký, J. Chem. Phys. **93**, 3802 (1989); (d)V. Bonačić-Koutecký, L. Češpiva, P. Fantucci, J. Pittner and J. Koutecký, J. Chem. Phys. **100**, 490 (1994).

[27] (a) K. Raghavachari and C. M. Rohlfing, J. Chem. Phys. **94**, 3670 (1991); (b) C. M. Rohlfing and K. Raghavachari, *ibid*, **96**, 2114 (1992).

[28] J. D. Watts and R. J. Bartlett, J. Chem. Phys. **97**, 3445 (1992).

[29] D. M. Cox, D. J. Trevor, R. L. Whetten, E. A. Rohlfing, and A. Kaldor, Phys. Rev. B **32**, 7290 (1985).

[30] W. A. de Heer, P. Milani, and A. Châtelain, Phys. Rev. Lett. **65**, 488 (1990).

[31] J. P. Bucher, D. C. Douglass, and L. A. Bloomfield, Phys. Rev. Lett. **66**, 3052 (1991).

[32] D. C. Douglass, A. J. Cox, J. P. Bucher, and L. A. Bloomfield, Phys. Rev. B **47**, 12874 (1993).

[33] S. N. Khanna, and S. Linderoth, Phys. Rev. Lett. **67**, 742 (1991).

[34] K. Lee and J. Callaway, Phys. Rev. B **48**, 15 358 (1993).

[35] F. Liu, S. N. Khanna, and P. Jena, Phys. Rev. B **43**, 8179 (1991)

[36] (a) J. Dorantes-Dávila and H. Dreyssé, Phys. Rev. B **47**, 3857 (1993); (b) P. Alvarado, J. Dorantes-Dávila and H. Rreyssé, *ibid.* **50**, 1039 (1994).

[37] P. Fayet, A. Kaldor, and D. M. Cox, J. Chem. Phys. **92**, 254 (1990).

[38] J. L. Elkind, F. D. Weiss, J. M. Alford, R. T. Laaksonen, and R. E. Smalley, J. Chem. Phys. **88**, 5215 (1988).

[39] R. L. Whetten, M. R. Zakin, D. M. Cox, D. J. Trevor, and A. Kaldor, J. Chem. Phys. **85**, 1697 (1986).

[40] R. L. Whetten, D. M. Cox, D. J. Trevor, and A. Kaldor, Phys. Rev. Lett. **54**, 1494 (1985).

[41] M. J. DeLuca, B. Niu and M. A. Johnson, J. Chem. Phys. **88**, 5857 (1988).

[42] S. H. Fleishman, and K. D. Jordan, J. Phys. Chem. **91**, 1300 (1987).

[43] N. Fujima, and T. Yamaguchi, J. Non-Crystal. Solid, **117/118**, 2885 (1990).

Chapter II

Detailed Description of Experiments

II.1 $(CO_2) - H_2O$ cluster anions

II.1.1 Overview

Figure II-1 shows a schematic drawing of an apparatus used for the photoelectron spectroscopy of $(CO_2)_nH_2O^-$ clusters. This apparatus is a time-of-flight (TOF) photoelectron spectrometer with a reflectron time-of-flight (TOF) mass spectrometer and a cluster anion source, and is composed of four chambers; a source chamber, first and second TOF chambers and a photoelectron spectrometer. The binary cluster anions, $(CO_2)_nH_2O^-$, were formed by injecting electrons into a supersonic expansion of CO_2 gas containing a trace amount of H_2O ($\sim$ 0.05 %) from a pulsed valve. The bare carbon dioxide cluster anions, $(CO_2)_n^-$, were merely formed from pure (CO_2) gas. The cluster anions thus produced were extracted by applying a pulsed electric field and accelerated up to 2 keV. Mass selection was achieved by using a 3-m reflectron TOF mass spectrometer prior to the PES measurement. At the spatial and temporal focus of the cluster anions, the unfocused third harmonics of a Nd YAG laser was introduced to interact the ion beam. The kinetic energy of the photoelectrons were analyzed by a TOF photoelectron spectrometer which has the flight path of 14 cm. The flight tube was set to be perpendicular to the ion beam axis, and the direction of the polarization vector of the photodetachment laser was set to be parallel to the flight tube. The pulsed valve , the acceleration voltage, and irradiation laser were operated in a pulsed mode and synchronized by a pulsed generator (SRS DG535). Detailed description will be given in the following sections.

II.1.2 Cluster Ion Source

The cluster source chamber is evacuated by a 4900 ls^{-1} oil diffusion pump (ULVAC ULK-14) and a 2400 ls^{-1} oil diffusion pump (ANELVA CDP-2400). The binary cluster anions, $(CO_2)_nH_2O^-$, were formed in a supersonic jet of CO_2 gas containing a trace amount of water ($\sim$ 0.05 %) by injecting electrons. The stagnation pressure of sample gas was 1 atm. For mixing the trace amount of water with CO_2, 1 atm of CO_2 gas was allowed to path

through the surface of water at the temperature of $\sim -20\,^{\circ}\mathrm{C}$.

The electrons were produced by two different methods which would provide the different conditions of the cluster anion formation. In one method the electrons were produced by focusing XeCl excimer laser light (Lambda Physik EMG101) onto a Mg metal surface located at distance of $\sim$ 5 mm downstream from the nozzle orifice. In the other method, the electrons were generated by an electron gun. The electron current was typically 100 μA at an impact energy of 100 $\sim$ 200 eV. In the latter case, the diameter of the electron beam was estimated to be less than 5 mm and the electron beam was interacted with the supersonic jet at distance of 3 $\sim$ 5 mm downstream from the nozzle orifice.

II.1.3 Reflectron TOF mass spectrometer

After drifting 150 mm from the nozzle orifice, the cluster anions thus produced were mass-selected by the time-of-flight mass spectrometer with a reflectron. This spectrometer was composed of an accelerating region, ion optics, a field free region and a reflectron.

The acceleration region was consist of three grids which divided the region into two parts, namely "s-region" and " d-region". The cluster ions accelerated in s-region by applying a pulsed electric field was further accelerated in d-region by a pulsed electric field which is usually different from that of s-region in strength. The ratio of these electric fields and the dimension of the acceleration grids were chosen in order to focus the ion packet spatially. On this desirable condition (a space focusing condition), the length of the field free region, D, was approximated by [1]

$$D = 2s_0 k_0^{3/2} \left(1 - \frac{d}{s_0} \frac{1}{k_0 + k_0^{1/2}} \right), \qquad \text{(II.1)}$$

where k_0 denotes the ratio of the ion kinetic energy given by the electric field of the s-region to the total kinetic energy, s_0 and d denote the flight length of the ions in the s-region and in the d-region, respectively. An acceleration voltage amounted to 2.0 keV was divided to each region by two resisters. Typically, the pulsed voltage of 400 V was applied to the 35-mm s-region, and that of 1600 V to the 20-mm d-region. In this experiment, as the space focusing condition was determined so as to achieve optimum mass-resolution together with

the reflectron, the actual space focusing condition differs from that given above equation. The pulsed acceleration voltage was generated from the power supply (Veronex 350) in which the unregulated high-voltage direct current was switched by vacuum tubes. Special care was taken to produce uniform fields in the acceleration regions. It is found that the large electrode with compared with the distance between the nascent grids is hardly disturb the electric field, and hence the higher mass-resolution is achieved. In this experiment the electrodes (about 160 mm in diameter) with the center hole (50 mm in diameter) on which a stainless steel mesh (0.05 mm in diameter wire, 50 mesh/inch^2) was fixed was used.

The accelerated cluster anions were introduced into the TOF chambers. The first and second chamber was evacuated by a 2400 ls^{-1} oil diffusion pump (ANELVA CDP-2400) and a 1500 ls^{-1} turbo molecular pump (Mitsubishi PT-1500), respectively. The ambient pressure was maintained to be 10^{-7} – 10^{-8} Torr. In the first TOF chamber, an einzel lens and two sets of vertical and horizontal deflectors served to steer and to focus the ion beams.

In these chambers, after traveling in a field free region without changing the transverse components of the velocity, the cluster anions were reflected by the reflectron. The reflectron serves to suppress the dispersion of the initial kinetic energy of the ions [2] [3]. This operation is called energy focusing. The ions having larger kinetic energies travel faster and reach at the entrance of the reflectron earlier than that having smaller kinetic energies. The ions are subjected to the retarding field in the reflectron, where ions having larger energies penetrate deeper in the reflectron and reflected, and *vice versa*. The difference of the flight length compensate for the difference of the initial kinetic energies.

The anions reflected by the reflectron further traveled in the field free region and were introduced into the photoelectron spectrometer to intersect the laser beam.

II.1.4 TOF photoelectron spectrometer

A pulsed laser photodetached the mass-selected ions at the focus of the mass spectrometer, and the resulting photoelectrons are energy-analyzed by time-of-flight technique.

Figure II-2 shows a schematic diagram of the TOF photoelectron spectrometer.

Unfocused third harmonic from a 10 Hz repetition rate the Nd YAG laser (Quanta Ray DCR-11) was introduced to intersect the ion beam with a $\sim$ 10 mm beam diameter. The ions are detected by an electron multiplier (Murata Ceratron). After amplified the ion signals were recorded and averaged over 100 events by a transient digitizer (Iwatsu DM-2350).

The cluster size was selected by setting an appropriate time delay between the pulsed ion acceleration and the laser irradiation. This time delay was optimized by deflecting the ion beam by floating the electron multiplier and selectively detecting the fast neutral fragment. Since the arrival time of the neutral peak with voltage applied to the electron multiplier is the same as that of the undeflected parent ion, the mass of the photodetached ion can be confirmed.

The photoelectron field-free flight tube, which was oriented perpendicular to the ion beam axis and laser beam propagation axis, was 140 mm long and magnetically shielded by two concentric cylinders made of 78-permalloy (1.0 mm thick). The inside of the tubes was gold-plated in order to suppress the charging effect and the background photoelectron from the wall of the tubes. Two apertures of 8 mm diameter which was quite similar to a light baffle used in a laser induced fluorescence experiment were located 2 cm and 4 cm apart from the laser/ion interaction region, respectively. They serve to reduce the photoelectron acceptance angle and improve the resolution of the spectrometer; the aperture also eliminates contributions to the signal from electrons which bounce off the walls of the flight tube before reaching the detector. The detector end of the tube was covered with two layer of non-magnetic meshes (tungsten 0.03 mm in diameter and 30 mesh inch^{-2}) which were 5 mm apart, so that the micro channel plate's electric field is kept from intruding into the field-free region.

The photoelectrons were detected by a tandem microchannel plate (HAMAMATSU F2223-21S). The electron signal was amplified by two stage of fast preamplifiers (ORTEC 9301, ORTEC 474) and discriminated by a constant fraction discriminator (ORTEC 473A) prior to the time of flight measurement. The electron signals thus amplified and

discriminated were recorded by a 1 GHz time-to-digital converter (LeCroy 4208) which was triggered by a laser light by use of a pinphoto diode and co-added by the personal computer (NEC 9801VX21).

Laser fluence was kept in the range of 25–50 $mJcm^{-2}pulse^{-1}$. In this range no multiphoton effect was observed. The direction of the polarization vector of the photodetachment laser was set to be perpendicular to the ion beam axis and parallel to the electron flight tube because preliminary measurements indicated a strong anisotropic angular distribution of the photoelectrons along the polarization vector.

II.2 Metal cluster anions

II.2.1 Overview

Figure II-3 shows a schematic diagram of the apparatus used for photoelectron spectroscopy of metal cluster anion. This apparatus is composed of four chambers; a cluster source chamber, first and second TOF chambers and a photoelectron spectrometer. The vacuum chamber and the pumping system is the same that used $(CO_2)_nH_2O^-$ experiments as described in the previous section except for the photoelectron spectrometer chamber.

Cluster anions were generated by laser vaporization from a metal disc in the presence of a helium carrier gas. The cluster anions thus produced were mass-selected by a time-of-flight technique. The temporally mass-selected anions of interest were separated by a mass-gate and were decelerated prior to intersected with a pulsed laser so as to suppress the Doppler broadening in photoelectron energy. Kinetic energies of the photodetached electrons were analyzed by a magnetic-bottle type photoelectron spectrometer. Detailed description will be given in the following subsections.

II.2.2 Metal cluster source

Introduction

In the metal cluster experiment, the first step is development of a metal cluster anion source for producing an intense and stable beam of the metal cluster anions. It must be also suitable for the photoelectron spectroscopy with a pulsed laser beam as described below. There have been developed many types of metal or semiconductor sources in the recent ten years. These can be classified into two under the character of the generated cluster beam: the continuous ion beam and the pulsed ion beam.

In the continuous ion beam, an oven source is the most commonly used metal cluster source, in which the metal vapor is coexpanded with an inert gas through a pin hole into a vacuum. The mixture is cooled in the supersonic expansion and cluster formation takes place. This technique has been successfully applied to alkali metals [9]-[14], but could not be applied to refractory metals because it requires a high vapor pressure ($\sim$ 100 Torr). Gas-aggregation sources [15]-[19] have been used to produce continuous cluster beam not only of alkali metals but also of more refractory metals. In the gas-aggregation source, metal is vaporized and introduced in a flow of cold inert gas. Due to the low temperature of the inert gas, cluster production proceeds primarily by successive single-atom addition. Although these continuous ion source have been combined with the pulsed technique [19], usually it is not effective because only small fraction of the ions can be used with pulsed technique.

For the pulsed cluster source, a laser vaporization source originally developed by Smalley [27] is widely-used and well established one. High-intensity pulsed laser light is focused onto a sample and a small amount of the material is vaporized into a flow of inert carrier gas introduced from a pulsed valve. The inert gas quenches the vapor, which condenses into clusters. The mixtures are then allowed to expand into a vacuum.

The PACIS (pulsed arc cluster ion source) is also powerful technique to generate an intense pulsed metal cluster beam [26]. In this source, the metal vapor is produced by a pulsed electric arc between an anode and a sample cathode rod in stead of the laser pulse.

It was reported to be 100 times as intense as that produced from the conventional laser vaporization source [26].

These pulsed ion sources have been applied to for all solid material, and have following two advantages; it allows small vacuum pumps to maintain a good background pressure by reducing the duty cycle of the supersonic expansion. It is particularly suited to pulsed spectroscopic techniques, notably those based on pulsed lasers.

In this study, the laser vaporization source with a cavity [22] was adopted. In this source, the processes involved in the vaporization, cluster formation and thermalization takes place in a small cavity, which would reduces the material deposition to the wall and would allow the larger cluster formation. Therefore larger clusters, higher beam intensities and better stability can be obtained than those from the conventional laser vaporization source. Moreover the internal temperature of the cluster can be controlled by adjusting the temperature of the cavity.

Source design

The cluster source chamber is evacuated by a 4900 ls^{-1} oil diffusion pump (ULVAC ULK-14) and a 2400 ls^{-1} oil diffusion pump (ANELVA CDP-2400). The ambient pressure was maintained below 1×10^{-5} Torr (Typically it was 1×10^{-5} Torr).

A schematic view of the cluster source is shown in Fig. II-4. The source body is machined from a rectangular stainless steel block. The cylindrical cavity in which the vaporization takes place before expansion is formed by a 8-mm hole drilled in this block capped with an adjustable stainless steel plug on rear and a nozzle on the front. The nozzle had a 1-mm diameter central exit hole, and a 3-mm long 90 ° cone facing the cavity and a 10-mm long 30 ° cone facing the vacuum. A Teflon block was attached on the side of the first block. A pulsed valve (General Valve series 9) is mounted on this Teflon block. Both the carrier gas of helium injected by pulsed valve and a second harmonics of Nd YAG laser beam (Quanta Ray DCR-11) focused by a 450-mm focal length lens enters the cavity via a 4-mm diameter channel of this block which is perpendicular to the axis of the cavity and the nozzle. On

the end of this channel, a plug with a 0.8 mm in diameter hole is inserted to reduce the gas losses. A sample disc was 5 mm in thickness and 10 mm or 20 mm in diameter depending on a material. This disc was mounted in a circular housing, which was pressed to the stainless steel block by a compression spring. The sample disc was separated from the cavity by a 0.7 mm thin stainless steel wall with a 1.5 mm diameter hole through which the laser beam was focused onto it. It rotated and translated to expose as much of the surface as possible to the vaporization laser. For this purpose, the sample disc was loosely attached to a shaft of a ac-synchronous motor (1 rpm) and rotational motion was transmitted with the pin which was driven perpendicularly into the shaft. The whole rotating components were translated gradually (typically with a period of 10 min) over a 1-4 mm. This translational motion was generated by rotating a screw having a 0.7-mm pitch with a stepping motor which was located outside the vacuum chamber. A thin Teflon ring (1 mm in thickness, 30 mm in outer diameter and 20 mm in inner diameter) was attached on the disc housing in order to prevent a gas leakage and to make the sample move smoothly.

The stagnation pressure of the He carrier gas was 5 atm. It was essential for the cluster formation to optimize the diameter of the exit hole of the nozzle and the time duration between the firing the laser and the actuating the pulsed valve.

In the metal cluster formation which is reactive, it is necessary to eliminate the contamination such as oxides. To this end, the helium carrier gas having 99.9999 % purity was further purified by passing through tree layers of molecular sieve (3A, activated charcoal and 13X) which were stuffed into a 1/4-inches diameter and 1-m long pipe. The whole valve component was baked out up to $\sim$ 100 °C before each experiment.

Performance

Fig. II-5 shows a mass spectrum of aluminum cation clusters generated by this source. The laser power used was 30 mJ/pulse. Duration of actuating the pulsed valve and the laser firing was 5300 μs. The clusters produced from the source was extracted perpendicularly by applying the 2-kV pulsed voltage, 480 μs after the laser firing. The mass-analysis was achieved by the reflectron time-of-flight mass spectrometer described in section II.1.3. The

mass-selected cluster ions were detected by a microchannel plate (HAMAMATSU F2221-21S). After amplified the ion signals were recorded and averaged over 500 events by the transient digitizer (IWATSU DM-2350). It is noted that in this spectrum the clusters are not further ionized.

The cluster cations containing up to 100 atoms were detected. From this source, both aluminum anion and neutral clusters were observed. The mass spectra of the cluster anions consisting of cobalt and vanadium metals are shown in chapters IV and VI, respectively.

II.2.3 TOF mass spectrometer

The outline of a TOF mass spectrometer was the same as that described previous section, except for two points; anions produced from the source was extracted colinearly and the reflectron was not used for the limitation of the space.

The cluster anions drifted $\sim$ 100 mm from the nozzle of the metal cluster source were extracted colinearly by applying a pulsed voltage with a width of up to 50 μs. The acceleration voltage was between 300 V and 1000 V depending on the mass of the cluster anions interest.

This time, the velocity of the anions at the detachment region must be low enough to suppress the Doppler broadening. Therefore the acceleration voltage was lower than that in the $(CO_2)_2H_2O^-$ experiment described previous section in order to decelerate the anions effectively. At the low acceleration voltage, the acceleration perpendicular to the primary ion beam axis might cause the reduction of an ion intensity, because the ion drifting from the source has a high transverse energy which is approximately proportional to ion mass. Assuming a cluster velocity as 1000 ms^{-1} [22], the transverse kinetic energy is 10 eV at the ion mass of 2000 u (This is on the order of cobalt clusters containing 34 atoms). The larger clusters are deflected away in the perpendicular acceleration of low voltage. For example, the ion of 500 u in mass detected in the colinear acceleration was about ten times as intense as that in the perpendicular at the acceleration voltage of 500 V.

The space focusing condition (see equation II.1) was carefully chosen by varying the di-

viding resisters as mentioned above. Typically, the ratio of the voltage of s-region to that of d-region was 1/20 so as to spatially focus the ion packet at 3 m downstream from the acceleration grids where the anions intersect with the laser beam.

II.2.4 Magnetic-bottle type photoelectron spectrometer

Introduction

To apply the photoelectron spectroscopy to cluster anions, the difficulty comes from their low signal intensity. In the apparatus described below, a typical negative cluster ion count in the roughly 1 cm^3 detachment region of the photoelectron spectrometer is only $10 \sim 10^3$. Therefore intense laser pulses must be used to achieve a high yield of photoelectrons, and these electrons must be collected with high efficiency and energy analyzed so as to accumulate the photoelectron spectrum of the entire energy range from each laser shot. On this condition, another difficulty comes out. Such a intense laser light with high photon energy easily causes background photoelectrons from a wall of the vacuum chamber and from multi-photon ionization of the background gases. It is necessary to contrive to minimize these background noise as well as to maximize the collection efficiency of the photoelectron signal.

The magnetic bottle type photoelectron spectrometer which was first developed by Kruit and Read [23] is the most suitable apparatus for the photoelectron spectroscopy of cluster anions. In principle this design provides a solid angle of 4π sr collection efficiency and sufficient energy resolution in a time-of-flight mode. It involves a use of a divergent magnetic field to parallelize the photoelectrons without changing their kinetic energy and a weak, guiding magnetic fields which is directed them down a flight tube for time-of-flight analysis.

Principle

Figure II-6 shows the principle of the magnetic bottle type photoelectron spectrometer. An electron initially emitted at an angle θ_i to the z direction, and with an energy E and

velocity v, undergoes helical motion in the magnetic field B_i. The angular momentum of the helical motion l_i is

$$l_i = \frac{m^2 v^2 sin^2\theta_i}{eB_i}. \tag{II.2}$$

Under the adiabatic approximation, which means that the magnetic field experienced by an electron changes negligibly in the course of one revolution of the helical motion, then the angular momentum is a conserved quantity [23]. This implies that the relation between the angle θ_f of the helical motion in the region of the low field B_f and θ_i of B_i is given by

$$\frac{sin\ \theta_f}{sin\ \theta_i} = \left(\frac{B_f}{Bi}\right)^{1/2}. \tag{II.3}$$

The electron trajectories are therefore parallelized in the type of magnetic field, and the electron orbit is always bounded by the same magnetic field lines. Then a collection efficiency in initial angle θ_i is obtained. An electron which initially emitted toward stronger magnetic field region in the magnetic field, B_i, at an angle, $\theta_i > 90°$, can be reflected by the stronger magnetic field. If the maximum magnetic field is B_{max}, the electrons initially emitted at an angle θ_i from 0 to θ_i are parallelized, where $\theta_i^{(max)}$ is given by

$$sin\ \theta_i^{(max)} = \left(\frac{B_i}{B_{max}}\right)^{1/2}. \tag{II.4}$$

If the maximum field, B_{max}, is sufficiently stronger than B_i, the collection efficiency will be a solid angle of $4\pi sr$.

The transverse component of the velocity is therefore reduced. Since the total velocity is unchanged the longitudinal component increases from $v\ cos\theta_i$ to

$$v_{zf} = v\left(1 - \frac{B_f}{B_i} sin^2\theta_i\right)^{1/2}. \tag{II.5}$$

The time of flight during the parallelization depends greatly on the angle, θ_i, but the time of flight in the drift tube itself is

$$T_{drift} = \frac{L_{drift}}{v_{zf}} \sim \left(1 + \frac{B_f\ sin^2\theta_i}{2B_i}\right), \tag{II.6}$$

which is almost independent of θ_i. The energy spread, ΔE, of the electron with the kinetic energy, E, is expressed as

$$\frac{\Delta E}{E} = \frac{\Delta T_{drift}}{2T_{drift}}$$

$$= \frac{B_f}{B_i} sin^2\theta_i$$
$$\leq \frac{B_f}{B_i}. \qquad \text{(II.7)}$$

Therefore the limit on the energy resolution in the drift region is approximated as B_f/B_i.

On the other hand, there is another limitation in the collection efficiency, namely the special collection efficiency. The electrons emitted in the finite volume of the high magnetic field can be detected by the detector with the finite size. Because the electron moves toward the detector along the same magnetic field line as mentioned above, the bundle of the electrons in the magnetic field of B_i are magnified in the course of the movement toward the low magnetic field region. The total magnification, M, is expressed as

$$M = \left(\frac{B_f}{B_i}\right)^{1/2}. \qquad \text{(II.8)}$$

This implies the bundle of the emitted electrons with the diameter of $1/M$ of the detector diameter can be detected. Therefore the energy resolution and the spatial collection efficiency conflict each other concerning the choice of the B_f/B_i ratio. This difficulty can be avoid in some extent by strengthen the local magnetic field around the detector region. For this purpose, a thin coil having about 150 mm in dameter was added over the long solenoid in this apparatus.

Design

The magnetic bottle photoelectron spectrometer can be classified under three types by how to generate the strong magnetic field; a cone-shaped polepieces [23], [24], a tip polepieces [25],[26], and a simple helical solenoid without any polepieces [27]. In the first two types with polepieces, the strong magnetic field and steep magnetic field gradient are easily generated, which can reduce the ratio of B_f/B_i (see equation II.7) and the length of parallelization and/or reflection in which the time of flight of electrons strongly depends on initial angle θ_i. These conditions are advantageous to achieve higher energy resolution. On the other hand, the cone-shaped polepieces and the simple solenoid have critical advantage to reduce background electrons emitted from the metal surface, because the field lines

all pass through the center of solenoid [27]. However, the cone-shaped polepieces are rather diffucult to construct and to tune up, because the magnetic field shape produced using the polepieces may be significantly sensitive to their shape and the magnetization of their material. Moreover the simple solenoid was found to have sufficient properties in the energy resolution and in the collection efficiency for the photoelectron spectroscopy of cluster anions as mentioned below. Therefore the third type was adopted in this work.

In order to achieve optimum property, including to determine lay-out and strength of the electromagnets to be used, the magnetic field and the electron trajectories in the field were calculated computationally prior to drawing the plan. The magnetic field was calculated by the finite element method program [28]. In order to calculate the electron trajectory in a non-uniform magnetic field, this computer program was modified as follows. At first, the magnetic field $\boldsymbol{B} = (B_r, B_\theta, B_z)$ in the cylindrical coordinates is obtained by differentiating the vector potential, A_θ, which is calculated by the above program,

$$\begin{aligned} B_z &= \frac{A_\theta}{r} + \frac{\partial A_\theta}{\partial r}, \\ B_r &= -\frac{\partial A_\theta}{\partial z}. \end{aligned} \tag{II.9}$$

It is noted that the radial and axial components are zero on the rotationally symmetric condition. Then the coordinates are converted from the cylindrical coordinates to the Cartesian coordinates, and the Newton's motion equation,

$$\begin{aligned} \frac{d\boldsymbol{v}}{dt} &= \frac{e}{m}\,\boldsymbol{v} \times \boldsymbol{B}, \\ \frac{d\boldsymbol{r}}{dt} &= \boldsymbol{v}, \end{aligned} \tag{II.10}$$

is integrated by the Runge-Kutta-Gill method [29]. The step length used was varied during the integration so as to be proportional to reciprocal of the local magnetic field, in order to minimize the computing time necessary for a given accuracy. The results of the calculation were checked by examining that the final kinetic energy of the electron did not change under the given accuracy when the step length varied. In the present experiments, following conditions were used: the solenoids generates a peak magnetic field at the center of the

strong solenoids $\sim$ 7000 G, a magnetic field at laser interaction region of $\sim$ 1000 G, and at the drift region of 10 G.

By use of the above information, the energy resolution of the spectrometer was estimated. The first effect which will govern the energy resolution comes from the principle of the magnetic bottle photoelectron spectrometer itself; the dependence of the flight time on the initial angle θ_i, which can be divided into two parts. One is the parallelization time, T_{para}, i.e., the reflection and/or redirection time in the inhomogenious magnetic field, and the other is the drifting time, T_{drift}, in the homogeneous field. $T_{para}/E^{1/2} \sim 80$ ns eV$^{-1/2}$ was obtained by the simulation mentioned above, and $T_{drift} \sim 1/200$ was reduced from the equation II.7. Then the energy resolution was estimated as,

$$\Delta E/E = \Delta T/T \sim 0.045. \tag{II.11}$$

The second effect which will govern the resolution is Doppler broadening due to the finite velocity of the cluster anions. Since the detached electrons are collected from nearly 4π sr solid angle, the velocity of the detached electron in the cluster center of mass, v_e, will range between $v_e + v_i$ and $v_e - v_i$ in the laboratory frame. The resultant energy spread is expressed as

$$\Delta E = 4\left(\frac{m_e}{m_i}E_e E_i\right)^{1/2}, \tag{II.12}$$

where E_e and E_i denote the kinetic energies of the electron in the center of mass and of the clusters, respectively, while m_e and m_i denote the masses. For this reason the ions must be decelerated prior to the detachment.

The duration of the laser pulse which is usually less than $\sim$ 10 ns is sufficiently smaller than the time of flight of the photoelectrons (2–10 μs).

Description of apparatus

Fig. II-7 is a schematic drawing of the magnetic-bottle type photoelectron spectrometer which was developed in this work. The magnetic field line calculated above are superimposed. The photoelectron spectrometer was evacuated by a 150 ls^{-1} turbo molecular

pump (MITSUBISHI PT-150). A background pressure was maintained less than 1×10^{-8} Torr.

The cluster anions of interest which were mass selected temporally by time-of-flight technique were chosen by the mass-gate consist of two grids. The first was always grounded and the second was usually applied the voltage enough to repel the anions. Just before the anions of interest came in front of the first grid, the voltage of the second grid dropped rapidly to ground so that the anions could pass through, and then recovered just after the anion traveled into a potential switch. The potential switch which consists of 6 cm long pipe capped with grids at the both ends. During the anions traveled in this pipe which was always kept field-free, the potential of this assembly rose rapidly to the voltage, V_{pot}, lower than the kinetic energy of the anion, U_{ion}, so that the anions were decelerated to the kinetic energy, $U_{ion} - V_{pot}$, by the electric field between the end grids of the potential switch and a grounded grid positioned 5 mm downstream. Typically the primary anions with the kinetic energy, U_{ion}, of 600 eV were decelerated to 50 eV by applying the pulsed voltage, V_{pot}, of 550 V to the potential switch. After interacting with a pulsed laser beam, the decelerated anions were detected by the microchannel plate with the diameter of 14.5 mm (HAMAMATSU F2221-21S).

The photodetached electrons were guided by the magnetic field produced by the strong magnet and the long solenoid , and detected by a microchannel plate with 27 mm in diameter(HAMAMATSU F2223-21S). The laser time delay was optimized so as to maximize the photoelectron signal intensities.

The strongest magnetic field was produced by a pulsed electromagnet located outside the vacuum chamber. This magnet was prepared from $\sim$ 500 turns of 0.4 mm in diameter wire wound on a water-cooled copper core. The maximum electric current of 30 A was sent to the electromagnet during the generation and drift of the photoelectrons. The current was provided by applying 150 V pulsed voltage with the duration of 1 ms by use of the electric circuit described in section II.5.3. Note that this magnet mount has a central hole facing the detachment region . The purpose of this hole is to ensure that in the vicinity of the detachment laser there is no metal surface for which the local magnetic field maps

onto the photoelectron detector. The uniform magnetic field was produced by the solenoid prepared from a 1 mm in diameter wire wound on a 2 m long aluminum pipe. This solenoid was also located outside the vacuum chamber.

Special care was taken to exclude the electric field from the trajectory of photoelectrons caused by the MCPs or the deceleration assembly. The long solenoid was covered by a single magnetic shielding (78-permalloy) to avoid the disturbance by the earth's magnetic field.

Performance

Figure II-8 shows the photoelectron spectrum of the copper anion measured by this apparatus with a 4.025 eV laser (XeCl excimer) at a beam energy of $\sim$ 30 eV. The three peaks centered at the electron binding energy of 1.235 eV, 2.624 eV, and 2.877 eV [30], correspond to detachment of Cu $^2S(d^{10}s^1) \leftarrow$ Cu$^-$ $^1S(d^{10}s^2)$, Cu $^2D_{5/2}(d^9s^2) \leftarrow$ Cu$^-$ $^1S(d^{10}s^2)$, and Cu $^2D_{3/2}(d^9s^2) \leftarrow$ Cu$^-$ $^1S(d^{10}s^2)$, respectively. Since the peak width is limited by an instrumental resolution for the atomic species, the resolution of this spectrometer was determined from this spectrum. The energy resolution was 150 meV fwhm and 30 meV fwhm at the kinetic energy of 2.79 eV and 1.148 eV, respectively. A detailed description of the data analysis is given in section II.4.

II.3 Reactions involving metal cluster anions

Fig. II-9 shows the schematic diagram of the apparatus used for a metal cluster reaction experiment. The metal cluster source and the reflectron TOF mass spectrometer including the vacuum chambers and the pumping system are the same that described above.

The cluster anions produced from the laser vaporization source were allowed to collide with the reactant gas (ex. CO or O_2) injected by the pulsed valve (General Valve series 9) in the reactor which is locate $\sim$ 5 cm downstream from the exit nozzle of the cluster source. The reaction product anions were analyzed by a time-of-flight mass spectrometer with a reflectron. The mass resolution was better than $\triangle m/m \sim 200$. The intensity of

reactant and product ions was determined by the area of the each peak in the spectrum. The accuracy was estimated to be $\sim$ 20%. Special care was taken that the reactant gas should not enter the cluster growth chamber and should not mix with the metal vapor which might be energetically hot and ready to react.

II.4 Data analysis of photoelectron spectra

In these studies an electron energy is analyzed by time-of-flight. Accordingly, it is necessary to convert the arrival times into electron kinetic energies. The energy scale of the photoelectron spectra is calibrated by using the reported photoelectron spectra. Usually the photoelectron spectra of O^- and O_2^- [4] [5] were used. In addition, the photoelectron spectrum of Cu^- [30] [31] was used during the metal cluster experiments . These photoelectron spectra are fit using a nonlinear squares routine [6] to the three parameter formula [7],

$$Ek = \frac{m_e L^2}{2(t - t_0)^2} + V_c, \tag{II.13}$$

where m_e is the electron mass, L is the electron flight length, t_0 is an inherent delay in the detection system, and V_c is a contact potential of the laser interaction region. Typically L and t_0 is on the order of 140 mm and 60 ns, respectively. The V_c parameter generally has values of ± 0.05 eV.

The electron kinetic energy thus obtained is a laboratory kinetic energy, E_{lab}, rather than a center-of-mass kinetic energy, $E_{c.m.}$. By use of the ion velocity E_i, the ion mass, m_i, the electron mass, m_e, and the angle between the electron-collection direction and the ion-beam direction, θ, the $E_{c.m.}$ is reduced from following formula [8],

$$E_{c.m.} = E_{lab} + \frac{m_e E_i}{m_i} - 2\left(\frac{m_e E_{lab} E_i}{m_i}\right)^{1/2} cos\ \theta. \tag{II.14}$$

In the case of the simple TOF photoelectron spectrometer, only the electrons emitted perpendicular to the ion beam axis, $\theta = \pi/2$, are detected with a small solid angle (in this case $\sim$ 0.037 sr). Omitting the third term of equation II.14,

$$E_{c.m.} = E_{lab} + \frac{m_e E_i}{m_i}, \tag{II.15}$$

is obtained. Actually the formula II.15 instead of II.14 is used for the data analysis of the simple TOF photoelectron spectrometer. In the magnetic bottle type photoelectron spectrometer by which the whole photoelectrons are collected, the transformation from E_{lab} to $E_{c.m.}$ is not necessary, because the velocity of the parent anion only gives the broadening of the spectrum peaks and the center of the distribution in E_{lab} should correspond to $E_{c.m.}$.

Since the time-of-flight is converted into the kinetic energy by the equation II.13, the intensities in the kinetic energy spectrum must be adjusted so that the integrated peak intensities are to remain the same. The energy dependent intensity, $I(E)$, is related to the experimentally determined time-of-flight intensity, $I(t)$, by the Jacobian $(\partial E/\partial t)$:

$$I(E) = -I(t)\left(\frac{\partial E}{\partial t}\right) = I(t)\left(\frac{t^3}{m_e L^2}\right). \qquad \text{(II.16)}$$

II.5 Electronic circuits

Several electric circuits used in these experiment have been developed and constructed by the author. This section presents overviews and diagrams of these circuits.

II.5.1 Nozzle driver

In the pulsed cluster source, it is essential that a pulsed valve opens rapidly (within few hundred micro seconds) to form clusters. For rapidly actuating an electromagnet of the pulsed valve, it is necessary to send a current enough to overcome the high inductance of the electromagnet. Usually it is achieved by applying a pulsed high voltage ($\sim$ 300 V) with short duration ($10 \sim 50\mu$s) prior to applying a long-pulse voltage just enough to opening the valve ($10 \sim 20$ V).

In the circuit shown in Fig. II-10, field effect transistors (FET) serve as switches. At first, when the FETs of 2SK787 turn on, the high voltage (V3) stored in capacitors is applied to pulsed valve which is connected to between out and com terminals. After few ten micro seconds, another FET (2SK785) turns on and it removes the high voltage from

the capacitor through a resistor. Then a low voltage (V4) whose value is now higher than that stored in the capacitor is allowed to be applied to the pulsed valve through a diode. Until either of the FETs turns off, the pulsed valve continues to open. The timing and duration of these pulses for driving the FETs is generated by a TTL-monostable IC (74LS221) followed by transistors.

II.5.2 High voltage power supply

For accelerating, decelerating or rejecting the ions by pulsed high voltage, it was necessary to develop a high-speed high voltage ($\sim$ 1kV) power supply. A single semiconductor element such as a transistor or a FET can not switch such a high voltage. This problem was solved by a cascade of several FETs. Figure II-11 shows the circuit diagram of the high voltage power supply. A pulsed transformer drives the gates of the FETs in spite of the voltage of the drain. The pulsed transformer was made by wounding the wire around a troidal ferrite core (#43, 850 in permeability). The number of the turns (typically from 15 to 30) were adjusted so as to optimize two contradictory properties, sufficient rise-time and enough pulse duration. By this circuit, both positive and negative pulsed voltage of up to 1.5 kV having a rise time of less than 200 ns was obtained. The pulse width was maintained up to $\sim$ 50 μs without reducing the voltage. This rise time limitation is caused by the response of the pulsed transformer.

II.5.3 Solenoid driver

Figure II-12 shows a diagram of a pulsed solenoid driver. By this circuit, a electron current of up to 30 A is send to the pulsed solenoid having $\sim 5\Omega$ in resistance. The circuit is consist of five parallelized FETs (2SK785) on a large heat sink so as to treat large currents.

References

[1] W. C. Wiley and I. H. McLaren, Rev. Sci. Instrum. **26**, 1150 (1955).

[2] V. I. Karataev, B. A. Mamyrin, and D. V. Shmikk, Sov. Phys.-Tech. Phys. **16**, 1177 (1972).

[3] B. A. Mamyrin, V. I. Karataev, D. V. Shmikk, and V. A. Zagulin, Sov. Phys. JETP **37**, 45 (1973).

[4] L. M. Brancoumb, D. S. Burch, S. J. Smith, and S. Geltman, Phys. Rev. **111**, 504 (1958).

[5] R. J. Cellota, R. A. Bennett, J. L. Hall, M. W. Siegel, and J. Levin, Phys. Rev. A **6**, 631 (1972).

[6] F. James, Function Minimization in Proc. of the 1972 CERN Computing and Data Processing school, CERN 72-21 (1972).

[7] L. A. Posey, and M. A. Johnson, J. Chem. Phys. **88**, 5383 (1988).

[8] M. W. Siegel, R. J. Cellota, J. L. Hall, J. Levin, and R. A. Bennett, Phys. Rev. A **6**, 631 (1972).

[9] E. J. Robbins, R. E. Leckenby, and P. Willis, Adv. Phys. **16**, 739 (1967).

[10] A. Herrmann, E. Schumacher, and L. Wöste, J. Chem. Phys. **68**, 2327 (1987).

[11] M. M. Kappes, R. W. Kunz, and E. Schumacher, Chem. Phys. Lett. **91**, 413 (1982).

[12] K. I. Peterson, P. D. Dao, and A. W. Castleman, Jr., J. Chem. Phys. **79**, 777 (1983).

[13] W. D. Knight, K. Clemenger, W. A. de Heer, W. A. Saunders, M. Y. Chou, and M. L. Cohen, Phys. Rev. Lett. **52**, 2141 (1984).

[14] C. Bréchignac, and Ph. Cahuzac, Chem. Phys. Lett. **117**, 365 (1985).

[15] K. Sattler, J. Mühlbach, and E. Recknagel, Phys. Rev. Lett. **45**, 821 (1980).

[16] D. Rayane, P. Melinon, B. Tribollet, B. Chabaud, A. Hoareau, and M. Broyer, J. Chem. Phys. **91**, 3100 (1989).

[17] K. E. Schulze, B. Winter, and I. Goldenfeld, Phys. Rev. B **38**, 2937 (1988).

[18] K. M. McHugh, H. W. Sarkas, J. G. Eaton, C. R. Westgate, and K. H. Bowen, Z. Phys. D **12** 3 (1989).

[19] T. P. Martin, U. Nahen, T. Bergmann, H. Göhlich and T. Lange, Chem. Phys. Lett. **183**, 119 (1991).

[20] R. E. Smalley, Laser Chem. **2**, 167(1983), and references therein.

[21] G. Ganteför, H. R. Siekmann, H. O. Lutz, and K. H. Meiwes-Broer, Chem. Phys. Lett. **165**, 293 (1990); H. R. Siekmann, Ch. Lüder, J. Faehrmann, H. O. Lutz, and K. H. Meiwes-Broer, Z. Phys. D **20**, 417 (1991).

[22] P. Milani, and W. A. de Heer, Rev. Sci. Instrum., **61**, 1835 (1990).

[23] P. Kruit and F. H. Read,
J. Phys. E: Sci. Instrum.,**16**, 313, (1983).

[24] T. Tsuboi, E. Y. Xu, Y. K. Bae, and K. T. Gillen, Rev. Sci. Instrum. **59**, 1357, (1988).

[25] G. Ganteför, M. Gausa, K. H. Meiwes-Broer and H O. Lutz,
Z. Phys. D, **9**, 253, (1988).

[26] C.- Y. Cha, G. Ganteför, and W. Eberhardt, Rev. Sci. Instrum., **63**, 5661, (1992).

[27] O. Cheshnovsky, S. H. Yang, C. L. Pettiette, M. J. Craycraft, and R. E. Smalley, Rev. Sci. Instrum., **58**, 2130, (1987).

[28] E. Munro,
in *A set of computer programs for calculating the properties of electron lenses*, Cambridge University Engineering Department Report CUED/B-ELECT/TR 45 (1975).

[29] Ayao Amemiya and Takeo Taguchi,
in *Suuchi kaiseki to FORTRAN* Maruzen, (1969),p. 358.

[30] Joe Ho, Kent. M. Ervin, and W. C. Lineberger, J. Chem. Phys., **93**, 6987, (1990).

[31] C. F. Moore, Natl. Bur. Stand. (U. S.) Circ. No.467 (U.S. GPO, Washington, D. C., 1952).

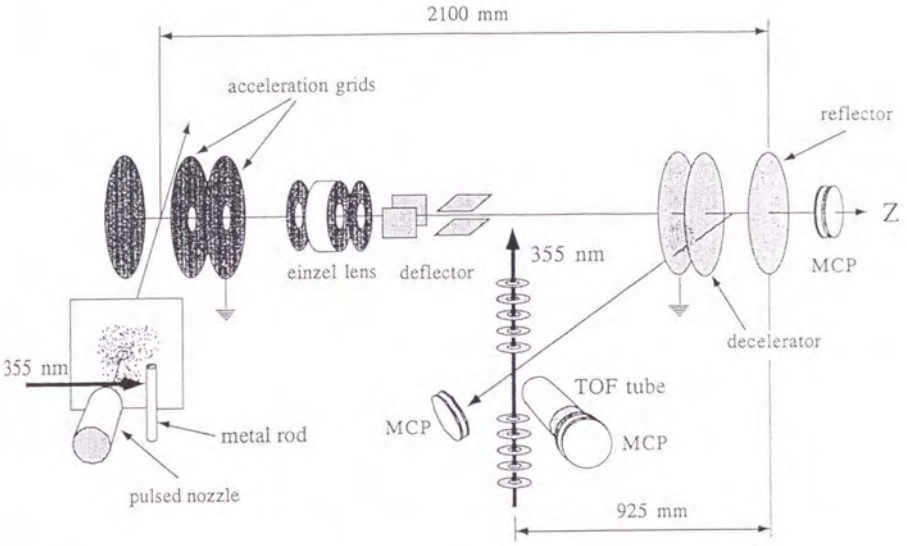

Fig. II-1 Schematic drawing of the experimental apparatus used in the photoelectron spectroscopy of $(CO_2)_nH_2O^-$.

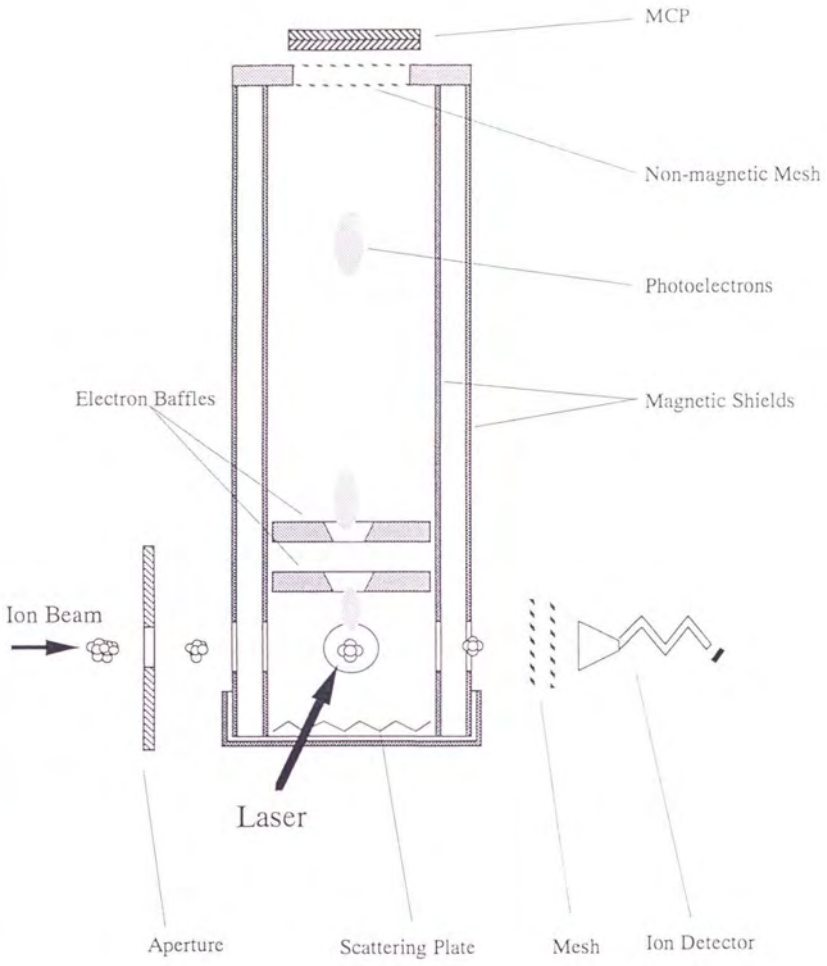

Fig. II-2 Schematic drawing of the TOF photoelectron spectrometer.

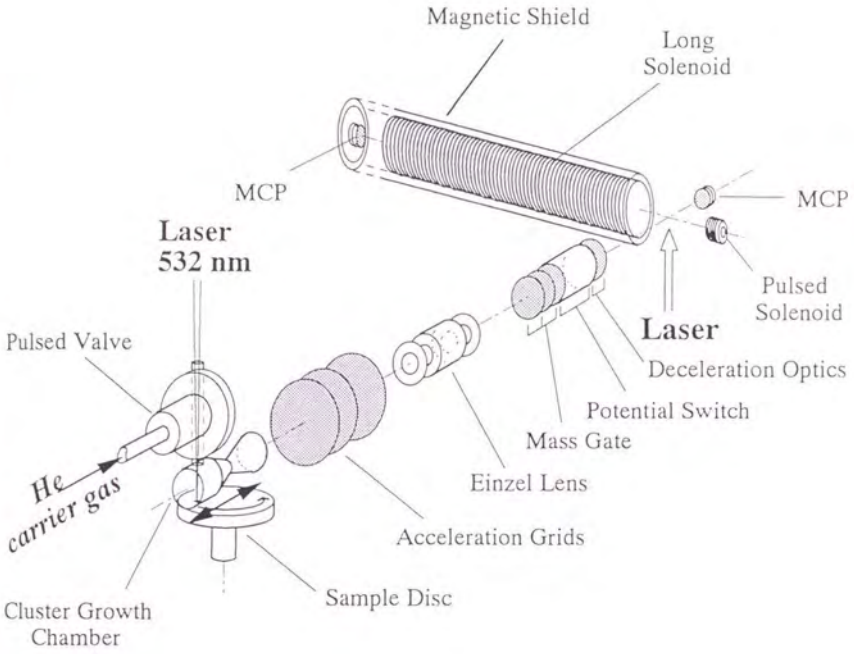

Fig. II-3 Schematic drawing of the experimental apparatus used in the photoelectron spectroscopy of metal clusters.

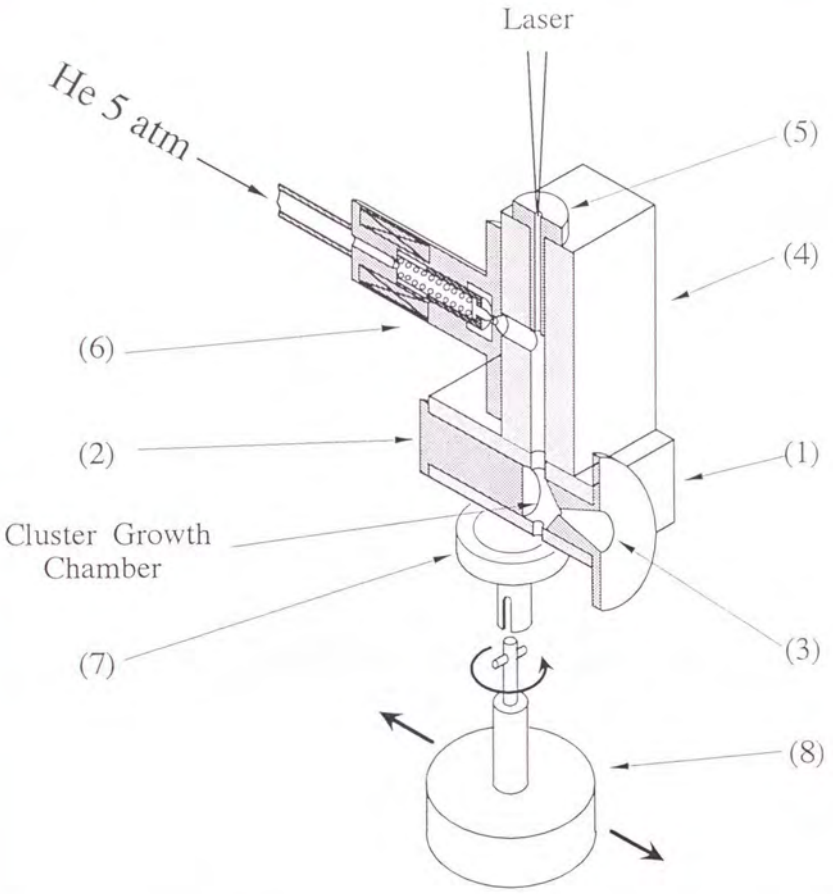

Fig. II-4 Schematic drawing of the metal cluster source: (1) Stainless steel block. (2) Adjustable plug. (3) Nozzle. (4) Teflon block. (5) Plug. (6) Pulsed valve. (7) Sample disc and housing. (8) Ac synchronous motor.

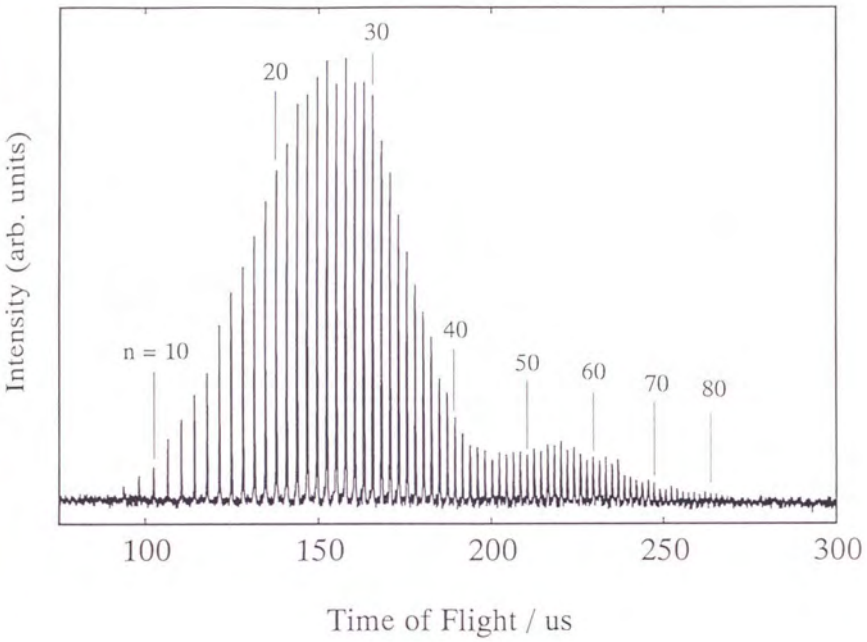

Fig. II-5 Time of flight mass spectrum of aluminum cluster cations produced from the metal cluster source.

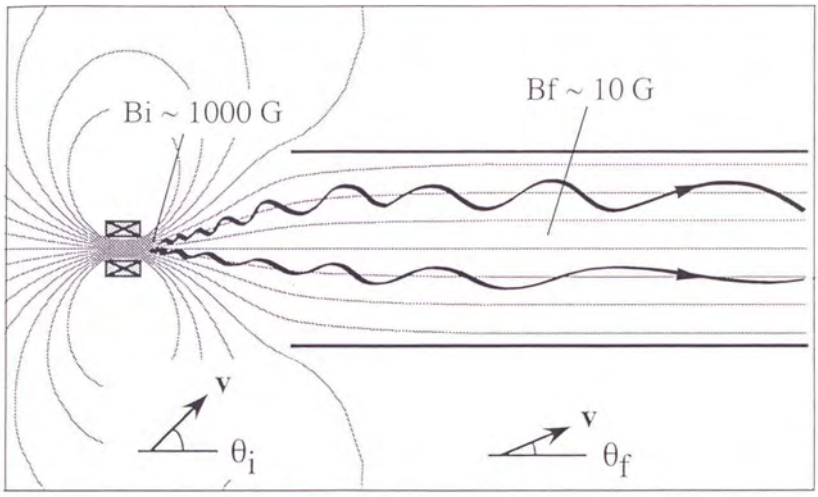

Fig. II-6 Schematic diagram showing the helical motion of an electron moving in a magnetic field generated by a strong magnet (left) and a long solenoid (right).

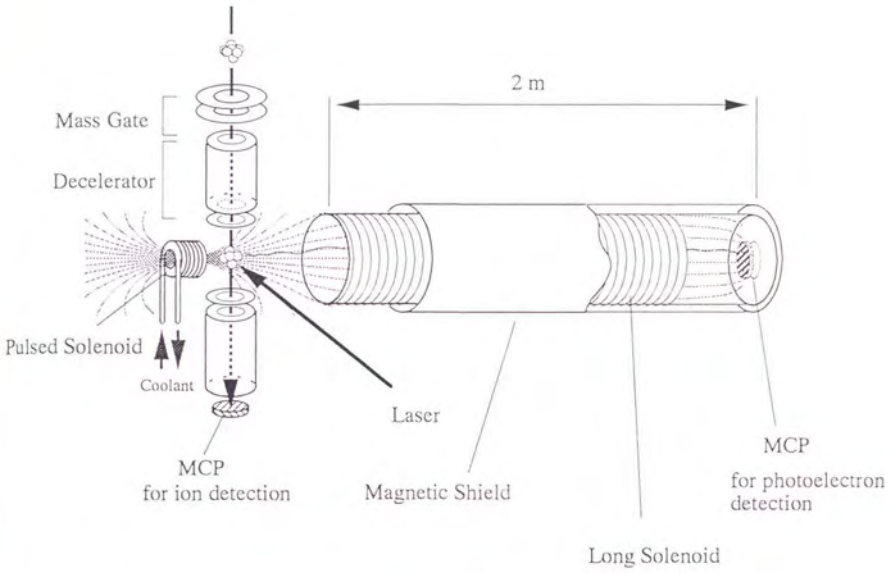

Fig. II-7 Schematic drawing of the magnetic bottle type photoelectron spectrometer.

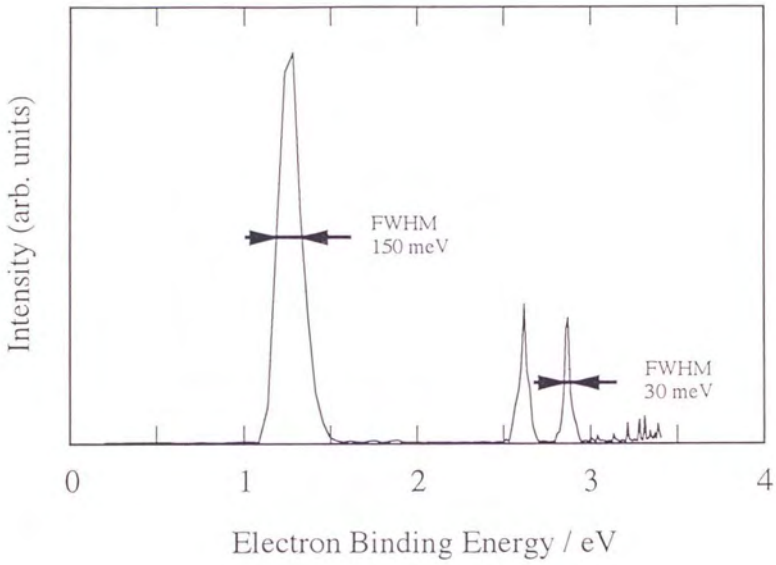

Fig. II-8 Photoelectron spectrum of Cu^- measured by the magnetic bottle type photoelectron spectrometer at the photon energy of 4.025 eV.

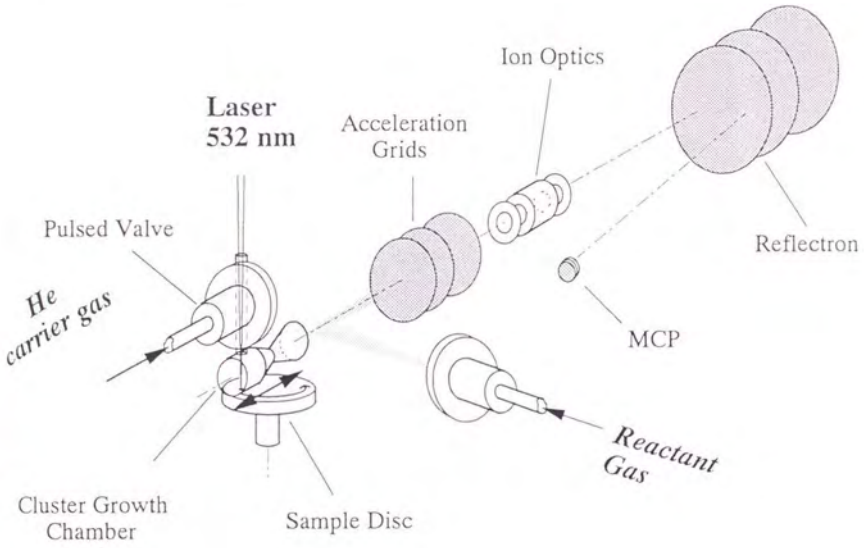

Fig. II-9 Schematic drawing of the experimental apparatus used for examining the reactivity of metal cluster anions.

VARIABLE WIDTH GENERATOR

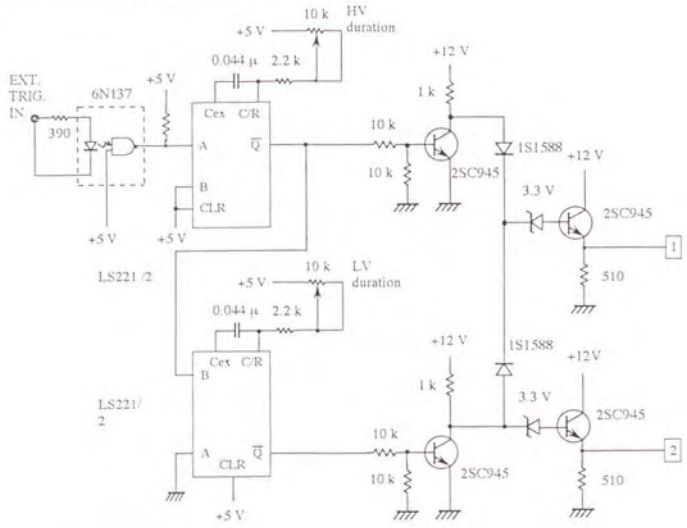

PULSE AMPLIFIER

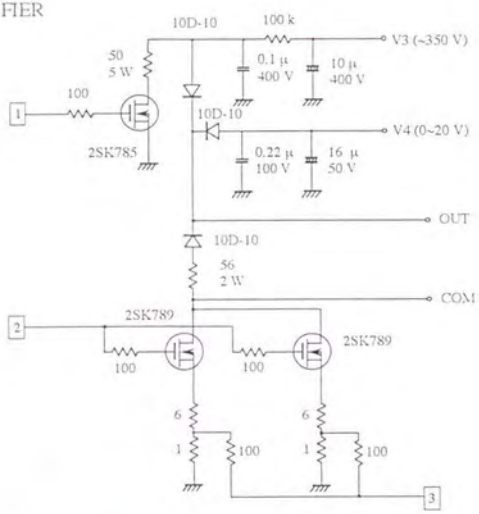

Fig. II-10 Circuit diagram of the pulsed nozzle driver (continued on the next page).

CURRENT MONITOR AND INDICATOR

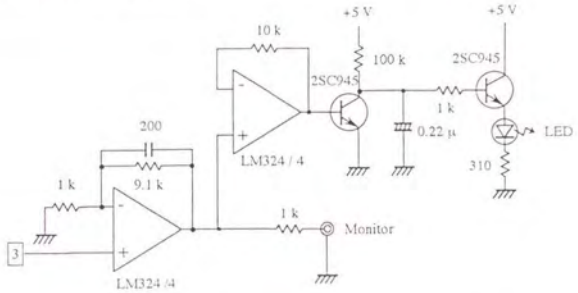

POWER SUPPLIES

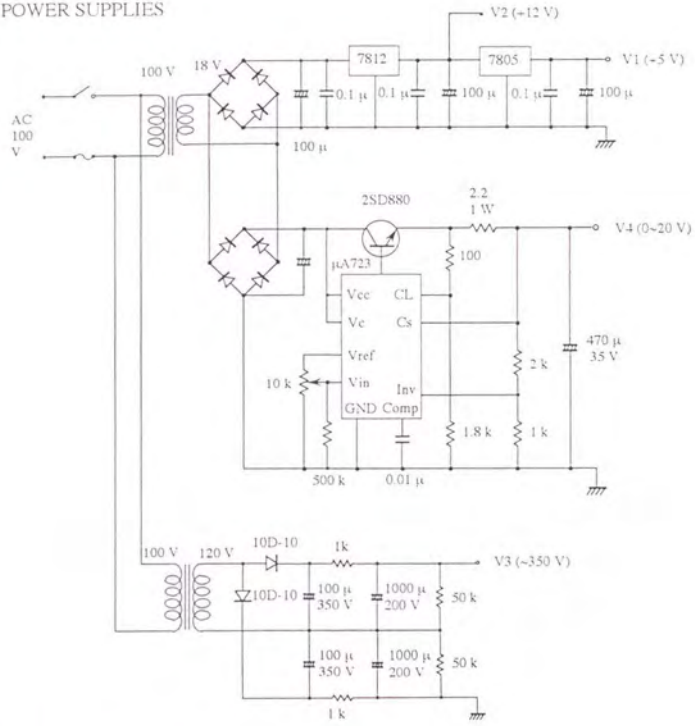

(continued from the previous page)

VARIABLE WIDTH GENERATOR

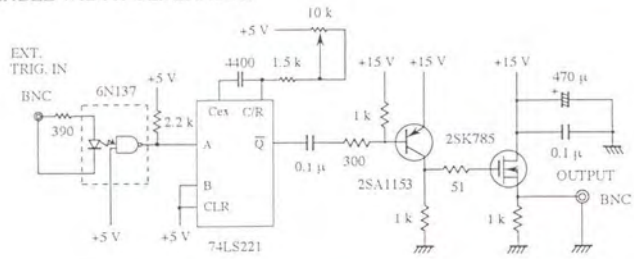

PULSE AMPLIFIER FOR NEGATIVE PULSE

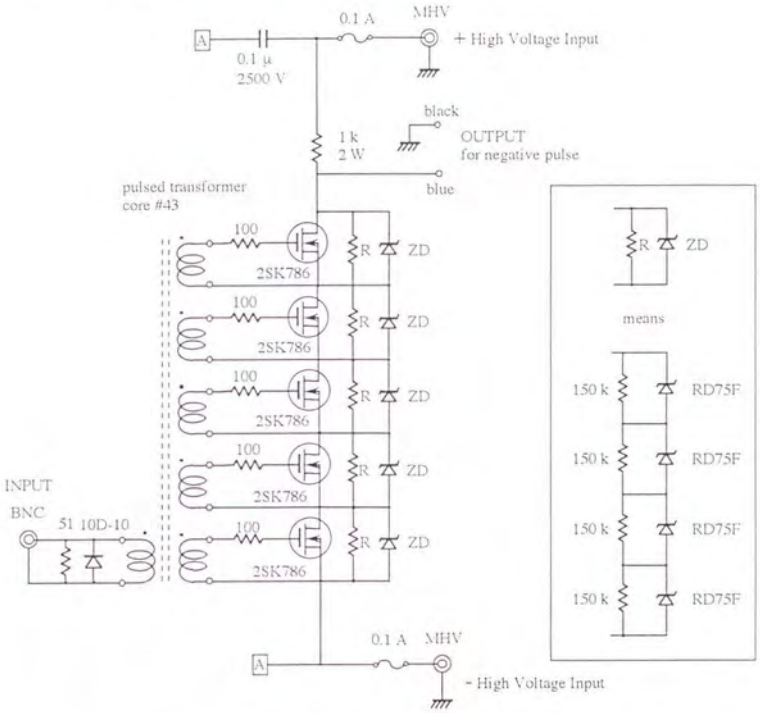

Fig. II-11 Circuit diagram of the pulsed high voltage power supply (continued on the next page).

POWER SUPPLY

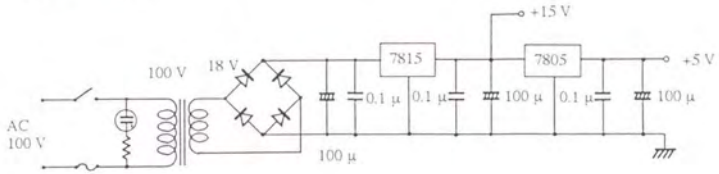

PULSE AMPLIFIER FOR POSITIVE PULSE

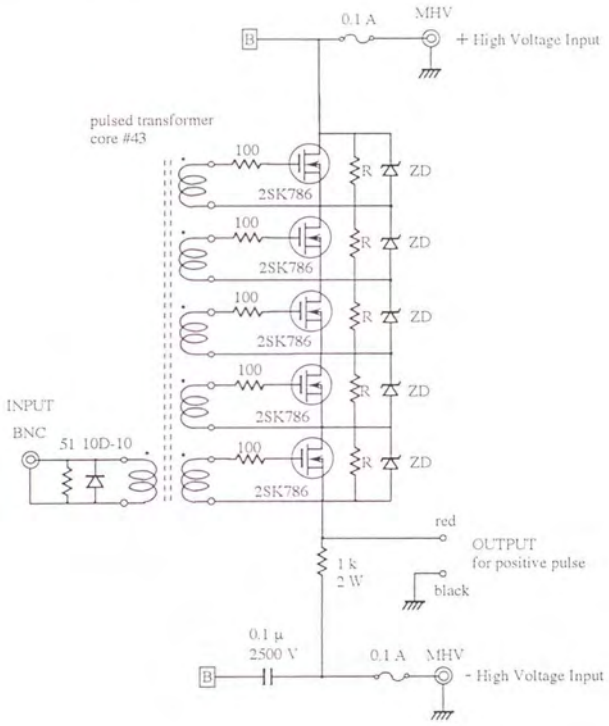

(continued from the previous page.)

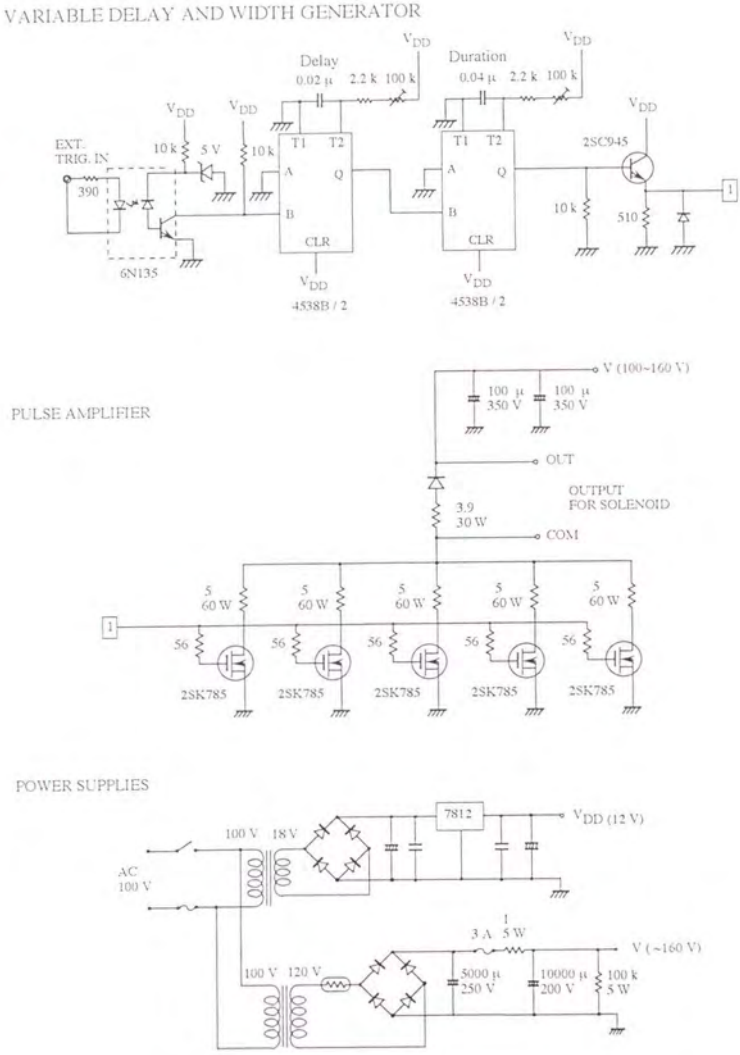

Fig. II-12 Circuit diagram of the pulsed solenoid driver.

Chapter III

Photoelectron spectroscopy of $(CO_2)_nH_2O^-$

abstract

Photoelectron spectra of $(CO_2)_nH_2O^-$ $(2 \leq n \leq 8)$ were measured at the photon energy of 3.49 eV. The spectra shows unresolved broad features, which are approximated by Gaussians. Comparing with the recent *ab initio* calculations and the photoelectron spectra of $(CO_2)_n^-$, it is concluded that a core ion of $(CO_2)_nH_2O^-$ are either CO_2^- or $C_2O_4^-$. In particular, for $n = 2, 3$ and 4, the spectra are approximated by sums of two Gaussians. These findings are interpreted as the coexistence of the two isomeric forms of the different core ions.

III.1 Introduction

Since the pioneering work of Klots and Compton [1],there have been a number of reports on the formation, stability and structure of negatively charged clusters of carbon dioxide, $(CO_2)_n^-$ [2]-[15]. The experiments in which neutral CO_2 clusters are collided with slow electrons [2]-[6] or high-Rydberg atoms [7]-[10] have revealed that $(CO_2)_n^-$ $(n > 3)$ clusters are readily formed through electron attachment to neutral clusters, whereas a bare CO_2 molecule does not capture an excess electron [16]. The size distribution of $(CO_2)_n^-$ shows distinct intensity anomalies at $n = 10, 14$ and 16 [2], [5], [6], [8]-[10]. Those experimental results indicate the presence of energetically favorable structures for $(CO_2)_n^-$ of particular sizes. Accordingly, much attention continues to be focused on the electronic properties of these $(CO_2)_n^-$ ions; whether the excess electron is localized over a larger moiety of the cluster.

Fleishman and Jordan have predicted two possible isomers for the structures of $(CO_2)_2^-$ [14]. One has a symmetrical D_{2d} form where the excess electron is delocalized over the two equivalent CO_2 molecules as represented by a $C_2O_4^-$ molecular ion. The other has an asymmetrical C_s form having a $CO_2 \cdot CO_2^-$ ion-solvent structure. These two isomers are close in energy; the D_{2d} form is only ~ 0.2 eV more stable than C_s. The *ab initio* calculations also predict a large difference in the vertical detachment energy (VDE) between these two isomers. The VDE values are calculated to be 2.8 eV and 1.7 eV for the D_{2d} and C_s forms, respectively. This difference in VDE arises from the fact that the molecular structure of CO_2 is distorted from the neutral equilibrium geometry more strongly in the D_{2d} form than in the C_s form. They further anticipate that the $CO_2 \cdot CO_2^-$ complex is stabilized more efficiently than the $C_2O_4^-$ ion by attaching one additional CO_2 "solvent" molecule. This implies that two isomers, $C_2O_4^-(CO_2)_n$ and $CO_2^-(CO_2)_n$ could be nearly isoenergetic at a certain size n.

Recently, Johnson and co-workers have measured photoelectron spectra of $(CO_2)_n^-$ and determined VDE as a function of the cluster size in the range of $n = 2 - 13$ [11]. The n dependence of VDE shows a sharp discontinuity at $n = 6$. The VDE decreases suddenly

by ~ 1 eV as the cluster size increase from $n = 5$ to 6. The magnitude of this decrease in VDE is nearly equal to the calculated difference in VDE between $C_2O_4^-$ and $CO_2 \cdot CO_2^-$ [14]. They have concluded from these findings that the $C_2O_4^-$ dimer ion is the core of $(CO_2)_n^-$ for $2 \leq n \leq 5$, while a CO_2^- monomer ion behaves as the core in larger clusters with $n \geq 6$.

In this work the photoelectron spectra of $(CO_2)_n H_2O^-$ $(2 \leq n \leq 8)$ was measured at 355 nm. The particular stability of ionic species with the formula $(CO_2)_x(H_2O)_y^-$ $(x, y \geq 1)$ has been reported by Klots [17]. The intent in this study is to see whether the excess electron is trapped within these binary clusters in the same manner as in $(CO_2)_n^-$.

III.2 Experimental

Experiments were performed in the apparatus which is described in detail in Chapter II. The binary cluster anions, $(CO_2)_n H_2O^-$, were formed by injecting electrons into a supersonic expansion of CO_2 gas containing a trace amount of H_2O ($\sim$ 0.05 %). The electrons were produced by two methods. In one method, the electrons were produced by focusing XeCl excimer laser light (Lambda Physik EMG101) onto a Mg metal surface located at a distance of $\sim$ 5 mm downstream from the nozzle orifice. In the other, an electron gun was used; the electron current was typically 100 μA at an impact energy of 100 $\sim$ 200 eV. These two methods were expected to provide different source condition. However, no essential difference in the photoelectron spectra between the two methods. Further analysis described below also reveal no difference within experimental error.

The cluster anions thus produced were extracted by applying a pulsed electric field and accelerated up to 2 keV. Mass selection was achieved by using a 3-m reflectron TOF mass spectrometer prior to the PES measurement. At the spatial and temporal focus of the cluster anions, the unfocused third harmonics of a Nd YAG laser (Quanta-Ray DCR-11) was interacted with the ion beam. The kinetic energy of the photoelectrons were analyzed by a TOF photoelectron spectrometer which has the flight path of 14 cm. The flight tube was set to be perpendicular to the ion beam axis.

Laser fluence was kept in the range of 25–50 mJ $cm^{-2}pulse^{-1}$. In this range no multiphoton effect was observed. The direction of the polarization vector of the photodetachment laser was set to be perpendicular to the ion beam axis and parallel to the electron flight tube because preliminary measurements indicated a strong anisotropic angular distribution of the photoelectrons along the polarization vector.

Under the present experimental conditions, photoelectron having a center-of-mass kinetic energy smaller than 0.3 eV could not be detected with sufficient reproducibility. This low-energy cut-off corresponds to the electron binding energy of ~ 3.2 eV.

III.3 Results

III.3.1 Mass spectra

Figure III-1 shows a typical time-of-flight spectrum of anions produced by the cluster sources where electron beams were injected into the supersonic expansion of CO_2 and H_2O mixtures; the electrons were generated by the laser sputtering. A series of intense peaks are assigned to $(CO_2)_n^-$ starting from $n = 3$; the size distribution peaks around $n = 7$. The anomalies in the intensity of $(CO_2)_n^-$ at $n = 7, 14$ and 16 are observed. Almost all the other peaks arise from the binary cluster ions of $(CO_2)_n(H_2O)_m^-$ $(n + m \geq 3, 1 \leq m \leq 4)$. Although there seems to be anomalies in the size distribution of $(CO_2)_nH_2O^-$, the spectral feature is rather sensitive to the source condition, especially to the concentration of the water in the CO_2 gas. In contrast to the $(CO_2)_n^-$ case, no distinct " magic number" was observed around $n \sim 14$. In addition, CO_3^- molecular ion is observed which is known to have a formation threshold of about 3 eV [1]. Because of the presence of both the CO_3^- and the larger clusters $(n > 4)$ which are efficiently formed with near zero energy electrons [3],[4],[16],[19], the kinetic energy of the electrons were likely ranging from near zero to more than 3 eV.

III.3.2 Photoelectron spectra

The photoelectron spectra of $(CO_2)_nH_2O^-$ $(2 \leq n \leq 8)$ are shown in Fig. III-2. The dots represent the experimental data. All spectra consist of bell-shaped envelopes containing no reproducible fine structures. For $n = 2$ and 4, each spectrum seems to be comprised of two broad peaks. In the other clusters, the spectrum consist of a single broad peak which is quite similar to that of $(CO_2)_n^-$ obtained by DeLuca et al. [11] except for the position of the maximum.

III.3.3 Analysis

As shown above, the photoelectron spectra of $(CO_2)_nH_2O^-$ are similar to that of $(CO_2)_n^-$ except for the shoulders appeared in the $n = 2, 4$. In the photoelectron spectra of other water-containing clusters, such as NO $(H_2O)_n^-$, X $(H_2O)_n^-$ (X = I, Br, Cl) [20] [21], overall feature of the photoelectron spectra does not change significantly by addition of a H_2O molecule, except that the fine structures are broadened and the envelopes of the spectra shifts by 0.1–0.5 eV higher in electron binding energy. These changes caused by adding a H_2O are interpreted as follows: the electron localizing on a constituent of the cluster is stabilized by H_2O through charge-dipole interaction, while the charge distribution essentially remains unchanged. Therefore if the excess electron is trapped in the $(CO_2)_nH_2O^-$ in the same manner as in $(CO_2)_n^-$, the overall feature of the photoelectron spectra of $(CO_2)_nH_2O^-$ should be similar to that of $(CO_2)_n^-$ except that the envelopes shift by 0.1-0.5 eV.

In the $(CO_2)_n^-$ $(1 \leq n \leq 13)$, DeLuca et al. proposed that there are two isomeric core ions [11]. They further proposed that the contours of the photoelectron spectra regarding of both core ions are well represented by a Gaussian having the FWHM of ~ 1 eV; $(CO_2)_6^-$ is an only exception where the contour is represented by a sum of two Gaussians which is interpreted as coexistence of two isomeric forms. The Gaussian shape of the spectral feature results from the large geometry change from the bent form of the anion core to bound neutral surface in a strong repulsive region of the bending mode.

In order to examine the core ion in $(CO_2)_nH_2O^-$, the Gaussian model was tested. The contour of the photoelectron spectra were fitted to a Gaussian profile of the form,

$$g(E) = Nexp\left[-\left(\frac{E-\varepsilon}{\delta}\right)^2\right] + C, \qquad \text{(III.1)}$$

using a non-linear squares procedure. If the contour could not be reasonably fitted to a single Gaussian III.1, it was fitted to a sum of two Gaussians,

$$g(E) = \sum_{i=1}^{2} N_i exp\left[-\left(\frac{E-\varepsilon_i}{\delta_i}\right)^2\right] + C. \qquad \text{(III.2)}$$

Here the ε_i parameter defining the maximum was associated with the vertical electron detachment energy (VDE). The parameter δ_i is related to the width of the envelope by FWHM $= 2(\ln 2)^{1/2}\delta_i$. The best-fit profiles are displayed in Fig. III-2 with solid lines. For $n = 2$–4, the contour of the photoelectron spectra is not characterized as a single Gaussian (III.1) but a sum of two Gaussians (III.2). For $n = 5 - 8$, the contours were well fitted to single Gaussians (III.1); although these contours were also tried to be fitted to sums of two Gaussians (III.2), none of them were reasonably represented. The VDE values determined by the maxima, ε_i, of the Gaussians are collected in Table III-1 along with each FWHM. The FWHMs of $(CO_2)_nH_2O^-$ were around 1 eV, which is similar to that of $(CO_2)_n^-$. In addition, the photoelectron spectra are well characterized as Gaussian profiles. These facts strongly indicates that $(CO_2)_nH_2O^-$ have the same core ions as that in $(CO_2)_n^-$ as discussed following section.

III.4 Discussion

The VDE values determined in the previous section are plotted against the cluster size, n, in Fig. III-3. The $(CO_2)_n^-$ values determined by DeLuca et al. [11] are also shown for comparison. These VDE values of $(CO_2)_nH_2O^-$ fall into two progressions; one is continuation of the trend from 2.06 eV of $n = 2$ to 3.12 eV of $n = 8$, and the other is that from 3.08 eV of $n = 2$ to 3.27 eV of $n = 4$. The VDE of the former progression is about 1 eV lower than that of latter in each cluster size where two components are observed

at the same time. Within each progression, the VDE increase by 0.1-0.4 eV with each additional CO_2 molecule. Since these energy shifts are on the order of magnitude expected for solvation of an ionic core, it is expected that each progression corresponds to the same ion core.

To examine the core ion in $(CO_2)_nH_2O^-$ in another aspect, the VDE of $(CO_2)_nH_2O^-$ is to be compared for each cluster size with that of $(CO_2)_{n+1}^-$ consisting of the same number of molecules. For each cluster size of n = 2, 3 and 4, the value of the higher VDE for $(CO_2)_nH_2O^-$ is about 0.1 eV larger than that for corresponding $(CO_2)_n^-$, while the value of the lower VDE for $(CO_2)_nH_2O^-$ is about 0.7 eV less than that for corresponding $(CO_2)_n^-$. On the other hand, the VDE of $(CO_2)_nH_2O^-$ for $n = 6, 7$ and 8 is systematically about 0.3 eV larger than that of corresponding $(CO_2)_n^-$ ($n = 6, 7$ and 8); in the $(CO_2)_6^-$, the lower VDE of the two is comparable to the VDE of $(CO_2)_5H_2O^-$. These energy shifts are on the order of the magnitude expected for solvation of an core ion by single H_2O. Therefore, the $(CO_2)_nH_2O^-$ belonging to the progression of the higher VDEs should have the same core ion, $C_2O_4^-$, as that of $(CO_2)_n^-$ for $n = 2, 3, 4$ and 5, while the $(CO_2)_nH_2O^-$ belonging to the progression of the lower VDEs should have the same core ion, CO_2^-, as that of the $(CO_2)_n^-$ for $n = 6, 7, 8$ and 9. Moreover, the lower VDE of 2.19 eV for $(CO_2)_2H_2O^-$ is larger than the VDE of 1.4 eV for CO_2^- [22] by 0.8 eV, which is reasonable value for the solvation of CO_2^- with one CO_2 and one H_2O molecules.

These discussions will be further supported by the recent *ab initio* calculation by Iwata et al [23]. They calculated the equilibrium geometric structures of different conformers of $(CO_2)_2H_2O^-$ and found two stable forms, shown in Fig. III-4. These forms correspond to an essentially $(CO_2)^-$ ion solvated by a CO_2 and a H_2O molecules and a $C_2O_4^-$ ion having slightly distorted D_{2d} symmetry solvated by a H_2O molecule; these geometrical structures of core ions are quite similar to that of $(CO_2)_2^-$, namely the monomer core ion and the dimer core ion, respectively. Although they have not calculated the energy levels including the VDEs which is to be compared with the experimental results, the VDEs can be estimated from the calculated VDEs for $(CO_2)_2^-$ by Fleishman and Jordan; the VDEs of $(CO_2)_2H_2O^-$ should be higher than that of corresponding $(CO_2)_2^-$ by 0.1–0.5 eV which is

expected for the energy change caused by adding a H_2O. Since the calculated values were 1.2 eV and 2.8 eV for $(CO_2)_2^-$ having the monomer core ion and that having the dimer core ion, respectively [14], the measured VDEs of 2.06 eV and 3.08 eV for $(CO_2)_2H_2O^-$ having the monomer core ion and that having the dimer core ion, respectively, is fairly good agreement with above estimation.

For larger clusters, the cluster size dependence of the VDE shown in Fig. 3 reveals that in the progression which start from the VDE of 2.06 eV for $n = 2$ to that of 3.12 eV for $n = 8$, the VDE increases by 0.1 eV with each additional CO_2 molecule, except for a small deviation at $n = 6$; these components maintain a monomer core ion which is weakly solvated with H_2O and CO_2 molecules. On the other hand, in the other progression which starts from the VDE of 3.08 eV for $n = 2$ to that of 3.27 eV for $n = 4$, the VDE also increases by 0.1 eV with each additional CO_2 molecules; these components maintain the dimer core ion. Summarizing, CO_2^- and/or $C_2O_4^-$ forms the core of $(CO_2)_nH_2O^-$, and at least in $n = 2, 3$ and 4 the two isomeric forms exist simultaneously.

Comparing $(CO_2)_nH_2O^-$ with $(CO_2)_n^-$, the striking difference is the cluster size where two isomeric forms were observed at the same time. In the $(CO_2)_n^-$, two isomers were observed simultaneously only at $n = 6$, and possibly in $n \geq 6$; even if two isomers coexist for $n > 6$ of $(CO_2)_n^-$ or for $n > 6$ of $(CO_2)_nH_2O^-$, one of them cannot be observed with 355-nm light, because the electron binding energy of this component would exceeds the experimental cut-off of 3.2 eV. Anyway, the two isomers coexist at least for $n = 2, 3$ and 4 of $(CO_2)_nH_2O^-$, while no evidence of the coexistence of the two isomers was observed in the same cluster size of $n \leq 5$ for $(CO_2)_n^-$. In these small clusters, the total energy of the clusters are expected vary dramatically as a function of the cluster size because the one constituent molecule will strongly influence the electric structure of the cluster consisting of few molecules. This result obviously indicates that H_2O molecule hydrate incipiently the core of the $(CO_2)_2^-$ clusters and causes the coexistence of the two isomeric forms through the strong charge-dipole interaction. This prediction about the role of the dipole moment of H_2O would be supported by the geometrical structures shown in Figs. III-4 (a) and (b). In Fig. III-4 (a), the H_2O directs its dipole toward the center of the excess charge

possessed by one CO_2 molecule, while in Fig. III-4 (b), the excess charge is spread over two CO_2 molecules and each H atom of H_2O direct the oxygen atom of the CO_2 molecule.

These geometrical structures further indicate that the H_2O molecule stabilize the core ion of each form in its stable structure; consequently, the two isomeric forms were observed in $n = 2, 3$ and 4 for $(CO_2)_nH_2O^-$, because the isomerization is suppressed by the H_2O molecule.. In other word, the introduction of the H_2O makes the barrier to the isomerization between the two isomeric forms high. On the other hand, in the $(CO_2)_n^-$ of $n = 2 - 5$, the barrier of the isomerization is not high enough to isolated the each isomeric form, therefore only more stable form was observed. At $n = 6$ of $(CO_2)_n^-$, as the energy of the two isomeric forms are *accidentally* the same, the two isomers exists at the same time. It is unlikely that the energy levels of two isomeric forms are accidentally the same ranging from $n = 2$ to $n = 4$ for $(CO_2)_nH_2O^-$.

If the isomerization of the core ion is really 'locked' by the introduction of H_2O, the intensity ratio of the two isomers should depend on the detailed source conditions. However, the experiment revealed no essential difference in the photoelectron spectra depending on the source condition as mentioned in section III-2. This experimental result seems to conflict with the above discussion. It is probably due to the process of the cluster formation in this experiment. Since CO_2^- monomer anion or even $CO_2H_2O^-$ was never observed, the cluster anions are formed by dissociative electron attachment onto larger neutral clusters. After the attachment of the electron, the clusters stabilize quickly; the excess energy is released by evaporation of monomers which ultimately leads to anomalies in ion intensities depending on the subsequent unimolecular decomposition kinetics [24] [25]. Accordingly, the ratio of the two isomeric conformers of the core ions are probably controlled by the kinetics of the latter stabilization process. This prediction is supported by the similarity of mass-spectral pattern under the different source conditions.

In order to further understand the mechanism of the isomerization, it is necessary that the photoelectron spectra measured in the present work are compared with that of anions generated by a utterly different process. For example, if the cluster anions are formed by adding solvent molecules of H_2O and CO_2 to CO_2^- core, it is expected that the anions having

the monomer core ions are preferentially generated. In addition, the internal temperature of the cluster anions have to be controlled, or at least have to be measured to discuss the possibility of the isomerization caused by thermal agitation.

References

[1] C. E. Klots, and R. N. Compton, J. Chem. Phys. **67**, 1770 (1978); **69** 1636 (1977).

[2] M. Knapp, D. Kresle, O. Echt, K. Sattler and E. Recknagel, Surface Sci. **156**, 313 (1985).

[3] A. Stamatovic, K. Leiter, W. Ritter, K. Stphan, and T. D. Mark, J. Chem. Phys. **83**, 2942 (1985).

[4] M. Knapp, O. Echt, D. Kresle, T. D. Mark and E. Recknagel, Chem. Phys. Lett. **126**, 225 (1985).

[5] H. Langosh, H. Harberland, Z. Phys. D **2**, 243 (1986).

[6] M. L. Alexander, M. A. Johnson, N. E. Levinger, and W. C. Lineberger, Phys. Rev. Lett. **57**, 976 (1986).

[7] T. Kondow and K. Mitsuke, J. Chem. Phys. **83**, 2612 (1985).

[8] T. Kondow, J. Phys. Chem. **91**, 1307 (1987).

[9] F. Misaizu, K. Mitsuke, T. Kondow, and K. Kuchitsu, J. Chem. Phys. **94**, 243 (1991).

[10] T. Kraft, M. W. Ruf and H. Hotop, Z. Phys. D **14**, 179 (1989).

[11] M. J. DeLuca, B. Niu, and M. A. Johnson, J. Chem. Phys. **88**, 5857 (1988).

[12] A. R. Rossi, and K. D. Jordan, J. Chem. Phys. **70**, 4422 (1979).

[13] Y. Yoshioka, and K. D. Jordan, J. Am. Chem. Soc. **102**, 2621 (1980).

[14] S. H. Fleishman, and K. D. Jordan, J. Phys. Chem. **91**, 1300 (1987).

[15] M. Tsukada, N. Shima, S. Tsuneyuki H. Kageshima, and T. Kondow, J. Chem. Phys. **87**, 3927 (1987).

[16] R. N. Compton, and P. W. Reinhardt, J. Chem. Phys. **63**, 3821 (1975).

[17] C. E. Klots, J. Chem. Phys. **71**, 4172 (1979).

[18] S. T. Arnold, J. G. Eaton, D. Patel-Misra, H. W. Sarkas, and K. H. Bowen, in *Ion and cluster ion spectroscopy and structure*, edited by Maier (Elsevier, Amsterdam 1989); and references therein.

J. Chem. Phys. **92**, 3980 (1990).

[19] T. O. Teirnan, and R. L. C. Wu, Adv. Mass Spectrom. A **7**, 136 (1974); J. F. Paulson, J. Chem. Phys. **61**, 2592 (1974); S. V. Krishna, and V. S. Venkatasubramanian, J. Chem. Phys. **79**, 6423 (1984).

[20] S. T. Arnold, J. G. Eaton, D. Patel-Misra, H. W. Sarkas, and K. H. Bowen, in *Ion and cluster ion spectroscopy and structure*, edited by Maier (Elsevier, Amsterdam 1989); and references therein.

[21] G. Markovich, S. Pollack, R. Giniger, and O. Cheshnovsky, J. Chem. Phys. **100**, 9344 (1994).

[22] J. V. Coe, J. T. Snodgrass, K. M. McHugh, C. B. Freidhoff, and K. H. Bowen.

[23] J. Fujimoto, Graduation Thesis, Keio University (1994); J. Fujimoto, T. Ikegami, and S. Iwata (unpublished result).

[24] C. E. Klots, J. Chem. Phys. **83**, 5854 (1985).

[25] T. D. Märk, and P. Sheier, J. Phys. Chem. **87**, 1456 (1978).

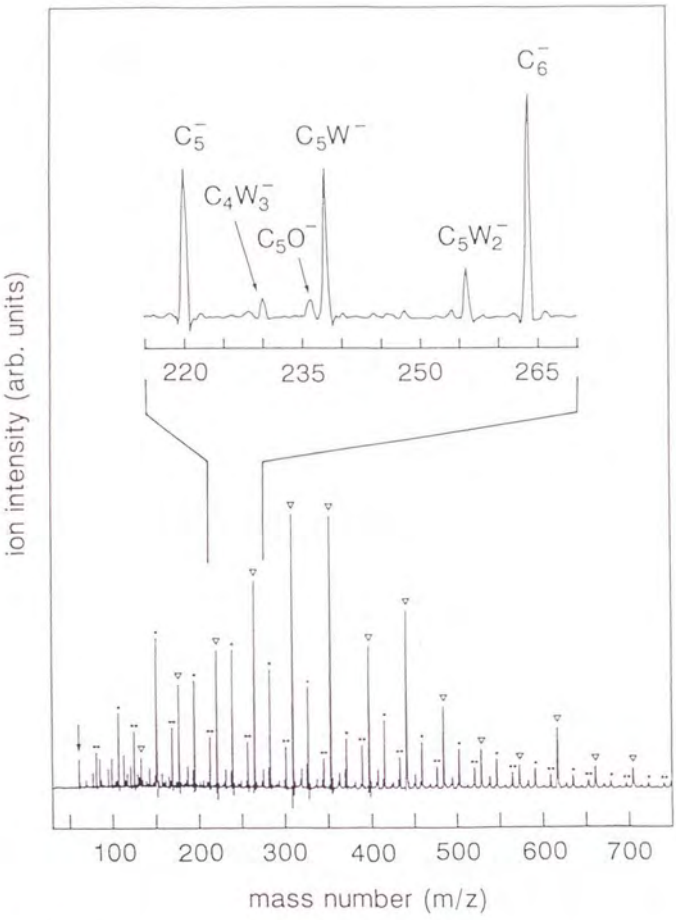

Fig. III-1 Time of flight mass spectra of anions formed by injecting electrons into supersonic expansion of CO_2 containing a small amount of H_2O; the electrons were generated by focusing excimer laser light onto a magnesium surface. The anions were dominated by $(CO_2)_n^-$ ($\triangledown$), $(CO_2)_nH_2O^-$ ($\cdot$) and $(CO_2)_n(H_2O)_2^-$ ($\cdot\cdot$). The mass range of 215–270 u is expanded in the upper trace. Here the formula $(CO_2)_nO_m(H_2O)_l^-$ is abbreviated as $C_nO_mW_l^-$.

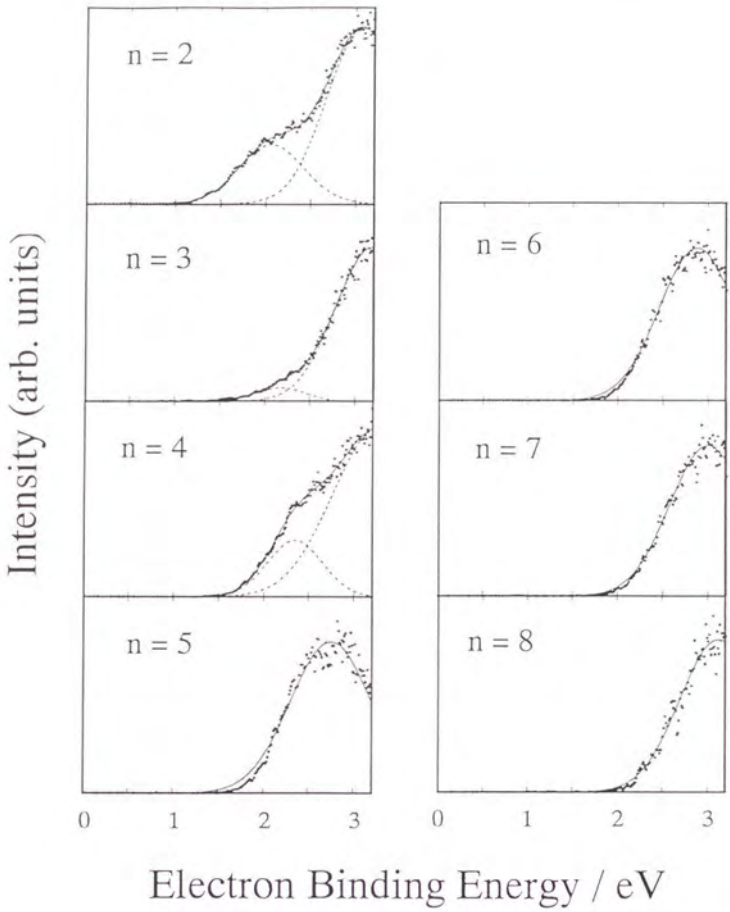

Fig. III-2 3.495 eV photoelectron spectra of $(CO_2)_nH_2O^-$ for $2 \leq n \leq 8$. Spectra are plotted as electron binding energy E_b defined $E_b = h\nu - E_{c.m.}$, where $E_{c.m.}$ is the center-of-mass electron energy (see chapter II). Dots present the experimental data. Solid curves are least square fits to a Gaussian line shape(s).

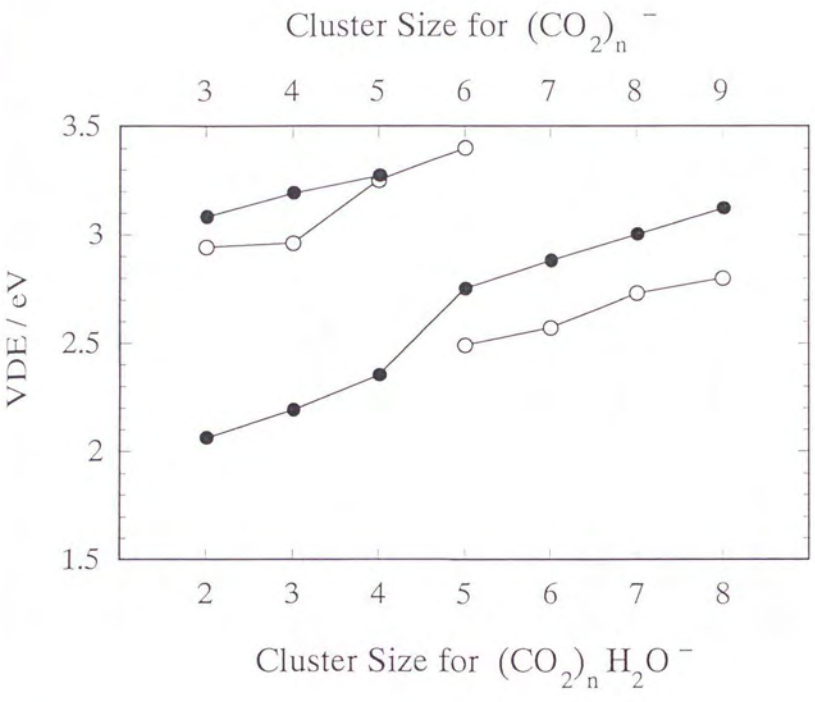

Fig. III-3 Plot of the fitted peaks of the spectra, ε_i, taken as a measure of the vertical detachment energy of $(CO_2)_nH_2O^-$ (•). The $(CO_2)_n^-$ data (○) are taken from Ref. [11].

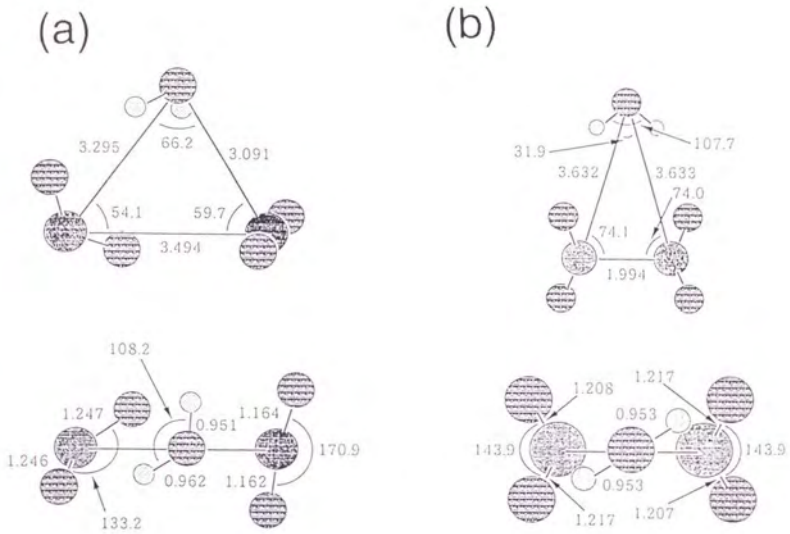

Fig. III-4 Structures for $(CO_2)_2H_2O^-$ conformations calculated by Iwata (Ref. [23]): (a) the monomer core ion, (b) the dimer core ion.

$(CO_2)_nH_2O^-$	ε_1 / eV	$FWHM_1$ / eV	ε_2 / eV	$FWHM_2$ / eV
$n = 2$	2.06	0.85	3.08	0.95
3	2.19	0.62	3.19	0.97
4	2.35	0.72	3.27	1.19
5	2.75	1.06		
6	2.88	1.00		
7	3.00	1.00		
8	3.12	1.00		

Table III-1 Cluster size dependence of the vertical detachment energies and FWHM values obtained by fitting the photoelectron spectra to the Gaussian line shape(s) (equation III.1 or III.2).

Chapter IV

Photoelectron spectroscopy of cobalt cluster anions — spin-polarized electronic structure

abstract

The photoelectron spectra of Co_n^- $(3 \leq n \leq 70)$ were measured at the photon energy of 4.025 eV by use of a XeCl excimer laser. For Co_n^- with $n = 3, 4$ and 6, the geometric and electronic structures were obtained from the spectra in comparison with the calculated spectra by the spin-polarized $DV - X\alpha$ method. The spectra observed are reproduced reasonably well by the calculation with postulating the most probable geometrical structures. It is revealed that the $3d$ band with the majority spin is separated by $1.0 \sim 2.8$ eV from that with the minority spin;the former is completely filled while the latter is partly filled and extends above Fermi level. The magnetic momenta and the average exchange energies of these cluster anions were estimated. For Co_n^- with $n \geq 7$, the observed electron affinity depends linearly on the reciprocal of the cluster radius and approach the work function of a cobalt metal, as n increases. Below $n = 6$, the electron affinity deviates from the linear dependence. This finding indicates that a size-dependent transition in the electronic structure occurs at $n \simeq 7$. The spherical conducting deop model suggests the presence of mobile electrons in Co_n^- with $n \geq 7$.

IV.1 Introduction

It is one of the fundamental issues how the properties of clusters vary with the number of the constituent atoms (cluster size) as exemplified in the evolution of a mercury cluster with the cluster size [1]- [3]. In particular, clusters of transition metal elements attract much attention because the transition metal clusters provide a unique opportunity to study the behavior of the $3d$ electrons as a function of the cluster size; the $3d$ electrons play an important role in emerging of the magnetism [4]- [8] and the catalytic activities [9]- [12] of transition metals and transition metal compounds. To this connection, photoelectron spectroscopy is one of the most promising techniques to solve such fundamental questions, with the aid of theoretical calculations. Recently, the photoelectron spectra of cluster anions constituent of Ia and Ib group metal [13]- [17], and semiconductor elements [18]- [22] have been measured. Precise *ab initio* quantum chemical calculations have also been performed for small clusters of this kind, and their geometric and electronic structures are successfully determined [23]- [25]. On the other hand, for the transition metal clusters, such precise quantum chemical calculations inherently difficult to be performed because of the presence of abundant low-lying electronic states. In addition,the photoelectron spectra of the transition metal cluster anions do not exhibit many structures [16] [17] [26], and hence precise quantum chemical calculations are not always rewarded or difficult to be performed especially for larger clusters. More qualitative calculations facilitate the analysis of the photoelectron spectra and the elucidation of the essential properties of the transition metal clusters.

Among clusters of transition metal elements, a cobalt cluster is one of the most interesting examples to be investigated, because of significant exchange interaction and electron correlation of the $3d$ band of cobalt. These specific properties are expected to be manifested in the photoelectron spectra of size-selected cluster anions of cobalt, Co_n^-. To this end, the photoelectron spectra of Co_n^- $(3 \leq n \leq 70)$ were measured, and were compared with the results of the spin-polarized $DV - X\alpha$ calculation. The $3d$ bands with the majority and the minority spins are expected to be separated in the vicinity of Fermi level because of a large

exchange interaction of cobalt itself. It is also conceivable that a size-dependent transition occurs in the electronic structure of Co_n^- because of a significant electron correlation of the transition metal element, although such a transition is not observed in the size-dependence of the ionization potential of a neutral cobalt cluster [27]. A slight difference in the electron correlation between neutral and negatively charged cobalt clusters could cause to alter the size-dependence remarkably.

IV.2 Experimental

A detailed description of the apparatus employed in this experiment is given in chapter II. Cobalt cluster anions, Co_n^-, were generated from a laser-vaporization cluster source with a small cluster growth chamber [28] [29]. A carrier gas of helium was introduced into the cluster growth chamber by a pulse valve (General Valve series 9) at a stagnation pressure of 5 atm. The second harmonics of Nd YAG laser output (Quanta Ray DCR-11) was focused on a rotating-translating sample disc and Co vapor from the disc was mixed with He carrier gas in the growth chamber. In order to prevent the He carrier gas from being contaminated, He gas having 99.9999 % purity, which was further purified by passing through three kinds of molecular sieve, was purged into the valve components before use. Cluster anions formed in the growth chamber were admitted into vacuum through a hypersonic conical nozzle, which has a 1-mm-diameter central exit hole, and a 3-mm long 90° cone facing the growth chamber, and a 10-mm long 30° cone facing the vacuum. The cluster anions were extracted collinearly by applying a pulse voltage with a width of up to 50μs and a rise time of less than 100 ns, and then were accelerated at an energy of 600 eV in two pairs of plate electrodes which are separated by 35 mm and 20 mm, respectively. They were both spatially and temporally focused [30] at a magnetic bottle type photoelectron spectrometer [31] [32] located 3 m downstream from the acceleration plates. After being mass-selected by a mass gate consisting of three grids, a cluster anion with a given size was decelerated to a kinetic energy of > 30eV by a series of grids and a potential switch. Cluster anions, Co_n^- with $n < 50$, are separable into a size-selected cluster

anion, but those with $n > 50$ are not, because of a limited sensitivity of the ion detector for larger cluster anions and the stability of the mass spectrometer. The deceleration voltage was so determined that an energy broadening of a photoelectron peak due to Doppler effect gives energy resolution, $\triangle E/E$, of less than 0.05. A size-selected cluster anion thus produced was irradiated by a XeCl excimer laser in a magnetic field of $\sim$ 1000G provided by a water-cooled solenoid of the photoelectron spectrometer. Laser fluence was in the range of $7 - 20$ mJ cm^{-2}. Photoelectrons produced by the laser irradiation were deflected by the field gradient and were guided by a weak homogeneous magnetic field of $\sim$ 10 G provided by a long solenoid covering a 2.2 m drift tube. The electrons were detected by a microchannel plate (Hamamatsu F2223-21S). Both the solenoids were mounted outside the vacuum chamber so that the solenoids can be cooled easily and the vacuum chamber is prevented from being contaminated.

Signals from the detector, which were amplified and discriminated, were stored in a transient digitizer (Iwatsu DM-2350) with a 20-ns time resolution, and were accumulated typically by 5000–20000 events. A time-of-flight of photoelectrons was converted into the kinetic energy with use of the following parameters: the flight length of the electron, the inherent delay time in the data-taking system and a contact potential of the laser interaction region [33]. These parameters were obtained by comparing the observed photoelectron spectra with the reported photoelectron spectra of NO^- [34], O_2^- [35], and Cu^- [36].

All the spectra measured were smoothed with a 0.005 eV square window. The overall energy resolution was attained to be better than $\triangle E/E = 0.1$ and the uncertainty in the kinetic energy due to stray electric field was less than 0.1 eV. The vacuum chamber for the photoelectron spectrometer was maintained at a background pressure of less than 1×10^{-8} Torr by a turbo molecular pump having a pumping speed of 150 l s^{-1}. Under this ambient pressure, the background signal associated with the ambient gas was found to be less than 10 % of the total photoelectron signals.

IV.3 Results

IV.3.1 Mass spectrum of parent cluster anions

Figure IV-1 shows a typical time-of-flight (TOF) mass spectrum of the parent cluster anions, Co_n^-. The intensities of the peaks for $n \leq 6$ are systematically smaller than those with $n \geq 7$ in the present experimental condition; the timing of actuating the pulse valve and that of triggering the laser pulse were delayed by about 800 μs and 300 μs, respectively, with respect to the rise time of the ion acceleration voltage. Evidently, the peaks with $n \leq 6$ behave differently from those with $n \geq 7$; there was a tendency that the peaks with $n \geq 7$ were more favored at a higher pressure in the cluster growth chamber, which was attained by adjusting the timing of the laser pulse, and the timing, duration and voltage of the pulse valve. When these conditions were optimized for larger clusters (up to $n = 100$), the mass spectrum in the size range above $n = 7$ was enhanced, while the mass peaks lower than $n = 6$ disappeared.

IV.3.2 Photoelectron spectra

The photoelectron spectra of Co_n^- with $3 \leq n \leq 70$ were measured at the photon energy of 4.025 eV (308 nm). The uncertainties in the relative photoelectron intensities were estimated to be less than 10 % from the reproducibility of defferent experimental runs. As mentioned in section IV-2, the uncertainties in the photoelectron energies were 0.1 eV. Figure IV-2 shows typical photoelectron spectra for $n = 3 - -7, 13, 20$ and 30. As n increases, the characteristic feature of the spectrum changes at $n = 7$; below this size the spectra have several structures, while above this size the spectra are almost structureless in the entire kinetic energy range studied. As shown in Fig. IV-2, the photoelectron spectrum of Co_3^- has a narrow and intense peak at the electron binding energy of 1.6 eV, a broad and weak peak centered at 2.6 eV, and a sharp rise above 3.2 eV. The photoelectron spectrum of Co_4^- is characterized by a narrow and intense peak at 2.0 eV and a sharp rise above 3.0 eV. In addition, there appears to be a weak structure in the 2–3 eV region. In the

spectrum of Co_6^-, the most intense peak is located at 2.4 eV, while there are two narrower peaks at 1.6 eV and 1.8 eV, and a sharp rise above 3.2 eV. In a spectrum for Co_n^- with $n \geq 7$, the intensity increases sharply at the onset and reaches a plateau, with increase in the energy. This fundamental feature does not essentially change with n, but for a gradual increase of the onset energy with the increase of n. As argued in a later section, the energy of the onset does not change significantly with n in the $n \leq 6$ range, whereas increase with n in the $n \geq 7$ range.

IV.4 Discussion

IV.4.1 Geometric and electronic structures

In order to derive information on the geometric and the electronic structures from the photoelectron spectra measured, the energies of the electronic states of the cobalt cluster anions, Co_n^-, were calculated by the spin-polarized DV – $X\alpha$ method with the self-consistent charge approximation [37]-[40]. The exchange parameter was taken to be 0.70 in all the calculations [40]. Atomic orbitals (AOs) of $1s, 2s, 2p, 3s, 3p, 3d, 4s$ and $4p$ were calculated numerically from the Hartree-Fock-Slater method and were used as the basis set. Furthermore, a well potential with the depth of 0.1 a.u. was added in the calculation of $4p$ AOs. The calculation was repeated until the nominal charge projected at each atomic orbital was converged to a certain value. All the calculations were performed on a workstation (SUN, SPARK station IPX).

The most probable structures of Co_n^- were postulated in the calculation of the electronic structure by referring the geometric structures of neutral and charged clusters, which are theoretically [41]-[46] and/or experimentally predicted [47].

The calculation was carried out for a given structure with three different bond distances between a nearest neighbor pair of cobalt atoms; the nearest neighbor distance in a cobalt metal (2.5 Å) [48], those 10 % shorter and 10 % longer (2.25 Å and 2.75 Å, respectively). It is likely that the real bond distance is in the range of 2.25–2.75 Å as described above;

for example the average bond distance of the cobalt dimer Co_2 is 2.56 Å [49] and bond elongation by addition of one electron to the dimer is 0.08 ± 0.02 Å [50].

The energy levels were calculated by filling 0.5 nominal charge in the highest occupied level of the anion, that is, this state was treated as a transition state [51]. By this method, the electron affinity is calculated properly. No essential difference was observed in the spectral feature except for an energy shift of the spectrum even when all the electronic states were treated as transition states. The discrete energy levels thus obtained were smoothed by broadening each level with a Lorentzian function having a FWHM of 0.1 eV, so that the calculated results can be compared with the experimental photoelectron spectra.

Trimer anion. The trimer anion, Co_3^-, has either a triangle or a linear structure. In a neutral nickel trimer, for example, the energy of an equilateral triangle structure is reported to be almost equal to that of an equidistance linear structure [42]- [45]. An equilateral triangle with D_{3h} symmetry and an equidistance linear structures with $D_{\infty h}$ symmetry were postulated as the candidates of the cluster anion structure in the present calculation.

The calculation showed that the spectral feature sensitively changed with the structure change as shown in Fig. IV-3. The observed spectrum is well reproduced by assuming that Co_3^- has a linear ($D_{\infty h}$) structure with a bond distance of 2.50 Å. The electron affinity of Co_3^- was calculated to be 1.50 eV, which agrees fairly well with the measured value of 1.38 eV. On the other hand, the spectral feature for the equilateral triangle structure(D_{3h}) is found to be much different from that of the photoelectron spectrum measured, so possibility of the triangular structure can be excluded with much confidence. These findings lead us to conclude that the cobalt trimer anion, Co_3^- ,has a linear structure ($D_{\infty h}$) with a bond-distance of 2.25–2.5 Å.

Tetramer anion. A nickel tetramer has been reported to have structures either with tetrahedral (T_d) [41] or rhombic (D_{2h}) [46] symmetry. In the present calculation, tetrahedral (T_d) and equilateral square (D_{4h}) structures were adopted. As shown in Fig. IV-4, a tetrahedral structure (T_d) with a bond distance of $\sim 2.25 \pm 0.2$Å reproduces the measured

photoelectron spectrum with the electron affinity of 1.65 eV. As in the case of Co_3^-, the spectral feature and the electron affinity depend sensitively on the structure adopted.

Hexamer anion. A pentagon with a cap (C_{5v}) and an octahedron (O_h) were postulated as candidates of the most probable structure [41] [46]. It is found that only slight change in the structure brings great change in the spectral feature. As shown in Fig. IV-5, the most probable structure is a pentagon with a cap (C_{5v}) having a bond distance of $\sim 2.75 \pm 0.1$Å. The calculation for larger clusters was also performed by assuming the most probable structures predicted theoretically and experimentally. The results show that geometry optimization is necessary to obtain reliable results to be compared with the experimental one.

IV.4.2 Magnetic moment and exchange energy

The energy spectrum calculated for each cluster anion mentioned in section IV-4.1 was smoothed by the Lorentzian broadening (see section IV-4.1), and the density of states (DOS) was obtained. Figure IV-6 shows the DOS curves for Co_3^-, Co_4^- and Co_6^-. As shown in Fig. IV-6, the $3d$ band having the majority spin is completely filled, while that having the minority spin is partly filled and extends above Fermi level. The difference in number between the majority and the minority spins (spin difference) were determined. The average spin-difference per Co atom for Co_3^-,Co_4^- and Co_6^- turns out to be 2.3, 1.5 and 1.8, respectively. The average exchange energies for $3d$ electrons are estimated from the energy differences between the majority and minority spin states to be 2.3 eV , 1.1 eV and 2.8 eV for Co_3^-, Co_4^- and Co_6^-, respectively. This spin polarization provides an evidence of the ferromagnetic ordering in the cobalt cluster anions.

These spin-differences are compared with the magnetic moments of a cobalt metal and neutral cobalt clusters. The total magnetic moment in the cobalt metal is 1.72 μ_B, in which 1.59 μ_B originates from the spin contribution [52] [53]. The bare magnetic moments of cobalt clusters measured by the Stern-Gerlach type deflection method are explained by the superparamagnetic model [8] in which the directions of the magnetic moments fluctuate

rapidly under thermal agitation, and hence the measured values are time-averaged ones; the 'true' magnetic moments have been derived from the analysis. In the cobalt clusters consisting of 65–215 atoms, the true magnetic moment per atom is determined to be 2.24 $\pm$ 0.14 μ_B at vibrational temperatures between 85 and 300 K [4]. Our results indicate that the magnetic moments of Co_3^-,Co_4^- and Co_6^- are in the range of $\sim 2\mu_B$, which is comparable with the value of a cobalt metal.

IV.4.3 Evolution of electronic structure

In order to examine the size evolution of the electronic structure, the electron affinities, EAs, are plotted against the reciprocal of the cluster radius, R as shown in Fig. IV-7, the radius R, was obtained from,

$$R = d\, n^{\frac{1}{3}} + r_0, \tag{IV.1}$$

where d is a half of the nearest-neighbor bond-distance and r_0 is a parameter to account for 'spilling out' of the electron charge beyond the boundary of the cluster [36]. The d value is chosen to be 1.25Å which is a half of the bond-distance in a cobalt metal [48], and r_0 is considered to be less than 0.5 Å as evaluated from the cobalt work function; here r_0 is set to be $\sim$ 0Å. It is noted that a half of the average bond length of the cobalt dimer Co_2 is 1.28 Å [49] and bond elongation by addition of one electron to the dimer is 0.08 ± 0.02 Å [50].

As shown in Fig. IV-7, the measured EA values depends linearly on the reciprocal of the cluster radius R in the $n \geq 7$ range. Below $n = 6$, the EA value deviate significantly from the linear dependence.

If a cluster can be treated as a spherical droplet of a metallic conductor, electron affinity EA of cluster is expected in terms of its radius,R, as [54]- [58],

$$EA = W - \alpha \frac{e^2}{R}, \tag{IV.2}$$

where W represents the work function of the conductor and e is the charge of an electron. The prediction of EA given by eq. (2) is also shown in Fig. IV-7 as a solid line for comparison, where α is set to be 5/8. The data points are well reproduced by the calculation,

in the range of $n \geq 7$, and the asymptotic value of the data points at a large R (or large n) agrees with the work function of the cobalt metal (5.0 eV), as expected from eq (2). The deviation of the experimental data points from the linear relationship or the prediction given by eq. (2) suggests that a size-dependent transition occurs at $n \simeq 7$ in the electronic structure of Co_n^-. The change in the essential feature of the photoelectron spectrum at $n \simeq 7$ also supports this conjecture. It seems that the valence electron is delocalized in the entire cluster system in the range of $n \geq 7$. This conclusion is not decisive because α is reported to be dependent on n in some causes [58].

IV.5 Conclusion

The photoelectron spectra of Co_n^- $(3 \leq n \leq 70)$ were measured at the photon energy of 4.025 eV. For $n = 3, 4$, and 6, the electronic structures were calculated by the spin-polarized DV – $X\alpha$ method and the energy levels are obtained by comparing the calculated spectra with the observed photoelectron spectra. The valence electrons are found to be spin-polarized; the average spin difference per atom and the average exchange energy are derived.

In the entire cluster-size range studied, the electron affinities were determined as a function of the cluster size. In the $n \geq 7$ range, the electron affinity follows the value predicted by the spherical conducting drop model, while the electron affinity deviates from the prediction in the $n < 7$ range. The deviation indicates that a metal-non-metal transition occurs at $n \simeq 7$, although such a classical picture may not provide the decisive criterion of metal-non-metal in electronic structures.

References

[1] K. Rademann, B. Kaiser, U. Even, and F. Hensel, Phys. Rev. Lett., **59**, 2319 (1987).

[2] C. Bréchignac, M. Broyer, Ph. Cahuzac, G. Delacretaz, P. Labastie, J. P. Wolf, and L. Wöste, Phys. Rev. Lett., **60**, 275 (1988).

[3] H. Harberland, H. Kornemeier, H. Langosch, M.Oschwald, and G. Tanner, J. Chem. Soc. Faraday Trans., **86**, 2473 (1990).

[4] D. C. Douglass, A. J. Cox, J. P. Bucher, and L. A. Bloomfield, Phys. Rev. B **47**, 12874 (1993).

[5] J. P. Bucher, D. C. Douglass, and L. A. Bloomfield, Phys. Rev. Lett. **66**, 3052 (1991).

[6] I. M. L. Billas, J. A. Becker, A. Châtelain, and W. A. de Heer, Phys. Rev. Lett. **71**, 4067 (1993); W. A. de Heer, P. Milani, and A. Châtelain, Phys. Rev. Lett. **65**, 488 (1990).

[7] D. M. Cox, D. J. Trevor, R. L. Whetten, E. A. Rohlfing, and A. Kaldor, Phys. Rev. B **32**, 7290 (1985).

[8] S. N. Khanna and S. Linderoth, Phys. Rev. Lett. **67**, 742 (1991).

[9] P. Fayet, A. Kaldor, and D. M. Cox, J. Chem. Phys. **92**, 254 (1990).

[10] J. L. Elkind, F. D. Weiss, J. M. Alford, R. T. Laaksonen, and R. E. Smalley, J. Chem. Phys. **88**, 5215 (1988).

[11] R. L. Whetten, M. R. Zakin, D. M. Cox, D. J. Trevor, and A. Kaldor, J. Chem. Phys. **85**, 1697 (1986).

[12] R. L. Whetten, D. M. Cox, D. J. Trevor, and A. Kaldor, Phys. Rev. Lett. **54**, 1494 (1985).

[13] S. T. Arnold, J. G. Eaton, D. Patel-Misra, H. W. Sarkas, and K. H. Bowen, in *Ion Spectroscopy and Structure*, edited by J. P. Maier (Elesevier, Amsterdam 1989)

[14] K. M. McHugh, J. G. Eaton, G. H. Lee, H. W. Sarkas, L. H. Kidder, J. T. Snodgrass, M. R. Manaa, and K. H. Bowen, J. Chem. Phys. **91**, 3792 (1989).

[15] J. Ho, K. M. Ervin and W. C. Lineberger, J. Chem. Phys. **93**, 6987 (1990).

[16] G. Ganteför, M. Gausa, K. H. Meiwes-Broer and H. O. Lutz, J. Chem. Soc. Faraday Trans. **86**, 2483 (1990).

[17] G. Ganteför, M. Gausa, K. H. Meiwes-Broer and H. O. Lutz, Faraday Discuss. Chem. Soc. **86**, 197 (1988).

[18] O. Cheshnovsky, S. H. Yang, C. L. Pettiette, M. J. Craycraft, Y. Liu, and R. E. Smalley, Chem. Phys. Lett. **138**, 119 (1987).

[19] S. H. Yang, C. L. Pettiette, J. Conceicao, O. Cheshnovsky and R. E. Smalley, Chem. Phys. Lett. **139**, 233 (1987).

[20] S. Yang, K. J. Taylor, M. J. Craycraft, J. Conceicao, C. L. Pettiette, O. Cheshnovsky and R. E. Smalley, Chem. Phys. Lett. **144**, 431 (1988).

[21] T. N. Kitsopoulos, C. J. Chick, A. Weaver and D. M. Neumark, J. Chem. Phys. **93** 6108 (1990).

[22] D. W. Arnold, S. E. Bradforth, T. N. Kitsopoulos, and D. M. Neumark, J. Chem. Phys. **95** 8753 (1991).

[23] (a)V. Bonačić-Koutecký, P. Fantucci and J. Koutecký, Chem. Rev. **91**, 1035 (1991); (b)V. Bonačić-Koutecký, P. Fantucci and J. Koutecký, J. Chem. Phys. **91**, 3794 (1989); (c)V. Bonačić-Koutecký, P. Fantucci and J. Koutecký, J. Chem. Phys. **93**, 3802 (1989); (d)V. Bonačić-Koutecký, L. Češpiva, P. Fantucci, J. Pittner and J. Koutecký, J. Chem. Phys. **100**, 490 (1994).

[24] (a)K. Raghavachari and C. M. Rohlfing, J. Chem. Phys. **94**, 3670 (1991); (b)C. M. Rohlfing and K. Raghavachari, *ibid*, **96**, 2114 (1992).

[25] J. D. Watts and R. J. Bartlett, J. Chem. Phys. **97**, 3445 (1992).

[26] K. M. Ervin, J. Ho and W. C. Lineberger, J. Chem. Phys. **89**, 4514 (1988).

[27] S. Yang, and M. B. Knickelbein, J. Chem. Phys. **93**, 1533 (1990).

[28] P. Milani and W. A. de Heer, Rev. Sci. Instrum. **61**, 1835 (1990).

[29] J. P. Bucher, D. C. Douglass, and L. A. Bloomfield, Rev. Sci. Instrum. **63**, 5667 (1992).

[30] W. C. Wiley and I. H. McLaren, Rev. Sci. Instrum. **26**, 1150 (1955).

[31] P. Kruit and F. H. Read, J. Phys. E **16**, 313 (1983).

[32] O. Cheshnovsky, S. H. Yang, C. L. Pettiette, M. J. Craycraft and R. E. Smalley, Rev. Sci. Instrum. **58**, 2131 (1987).

[33] L. A. Posey, and M. A. Johnson, J. Chem. Phys. **88**, 5383 (1988).

[34] M. W. Siegel, R. J. Celotta, J. L. Hall, J. Levine, and R. A. Bennett, Phys. Rev. A **6**, 607 (1972).

[35] R. J. Celotta, R. A. Bennett, J. L. Hall, M. W. Siegel, and J. Leine, Phys. Rev. A **6**, 631 (1972).

[36] D. G. Leopold, J. Ho and W. C. Lineberger, J. Chem. Phys. **86**, 1715 (1987).

[37] C. J. Slater, in *The Calculation of Molecular Orbitals*, (John Wiley & Sons, New York, 1979) p. 52.

[38] F. W. Averill, D. E. Ellis, J. Chem. Phys. **59**, 6412 (1973) and the related references therein.

[39] A. Rosén, D. E. Ellis, H. Adachi and F. W. Averill, J. Chem. Phys. **65**, 3629 (1976).

[40] (a) H. Adachi, M. Tsukada, C. Satoko, J. Phys. Soc. Jpn. **45**, 875 (1978); (b) C. Satoko, M. Tsukada and H. Adachi, J. Phys. Soc. Jpn. **45**, 1333 (1978); (c) H. Adachi, S. Shiokawa, M. Tsukada, C. Satoko and S. Sugano, J. Phys. Soc. Jpn. **47**,1528 (1979).

[41] M. S. Stave and A. E. DePristo, J. Chem. Phys. **97**, 3386 (1992).

[42] S. P. Walch, J. Chem. Phys. **86**, 5082 (1987).

[43] H. Basch, M. D. Newton and J. W. Moskowitz, J. Chem. Phys. **73**, 4492 (1980).

[44] S. P. Walch and W. A. Goddard III, Surf. Sci. **72**, 645 (1978).

[45] A. B. Anderson, J. Chem. Phys. **64**, 4046 (1976).

[46] M. A. Nygren, P. E. M. Siegbahn, U. Wahlgren and H. Akeby, J. Phys. Chem. **96**, 3633 (1992).

[47] E. K. Parks, L. Zhu, J. Ho and S. J. Riley, J. Chem. Phys. **100**, 7206 (1994).

[48] J. C. Slater, in *Quantum theory of molecules and solids. Vol. 2*, (McGrow-Hill Book Comp., New York, 1965).

[49] M. D. Morse, Chem. Rev. **86**, 1049 (1986).

[50] D. G. Leopold and W. C. Lineberger, J. Chem. Phys. **85**, 51 (1986).

[51] C. J. Slater, in *The Calculation of Molecular Orbitals*, (John Wiley & Sons, New York, 1979) p. 49.

[52] H. P. Myers, W. Sucksmith, Proc. R. Soc. London Ser. A **207**, 427 (1951).

[53] D. S. Rodbell, J. Phys. Soc. Jpn. **17**, Suppl. B-I, 313 (1962).

[54] D. M. Wood, Phys. Rev. Lett. **46**, 749 (1981).

[55] M. P. J. van Staveren, H. B. Brom, L. J. de Jongh and Y Ishii, Phys. Rev. B **35**, 7749 (1987).

[56] G. Makov, A. Nitzan and L. E. Brus, J. Chem. Phys. **88**, 5076 (1988).

[57] J. P. Perdew, Phys. Rev. B **37**, 6175 (1988).

[58] M. Seidel, K. -H. Meiwes-Broer, and M. Brack, J. Chem. Phys. **95**, 1295 (1991).

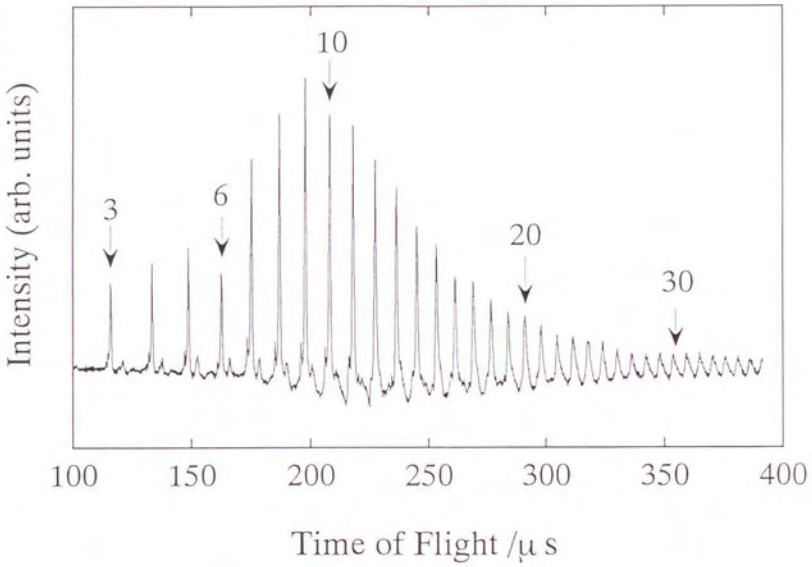

Fig. IV-1 Time of flight mass spectrum of cobalt cluster anions produced from the cluster source.

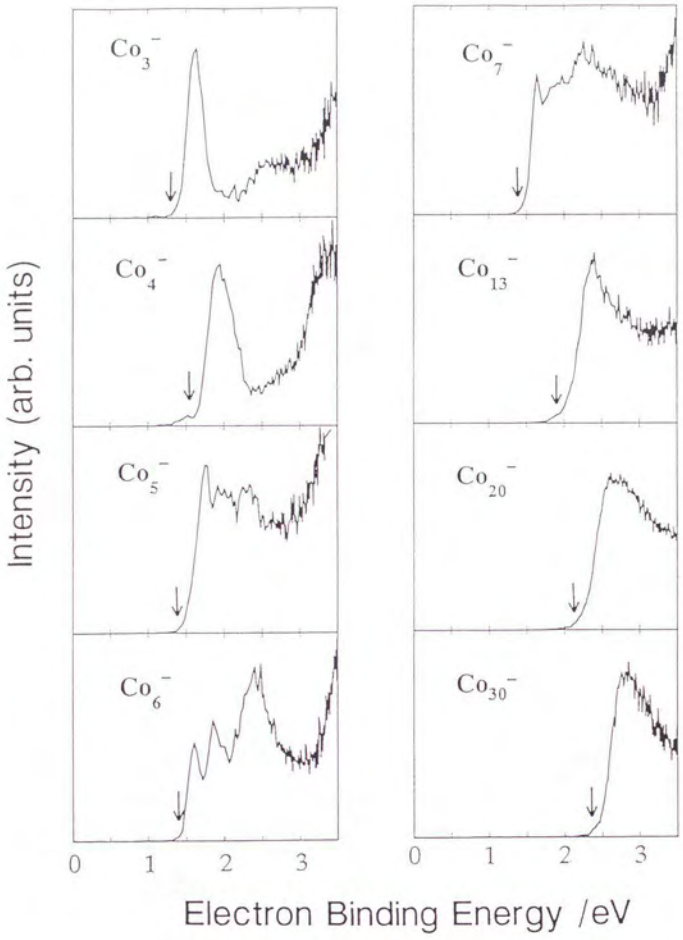

Fig. IV-2 Photoelectron spectra of cobalt cluster anions, Co_n^-, measured by use of a XeCl excimer laser (4.025 eV).

The onset energies corresponding to electron affinities,EA, are marked with arrows.

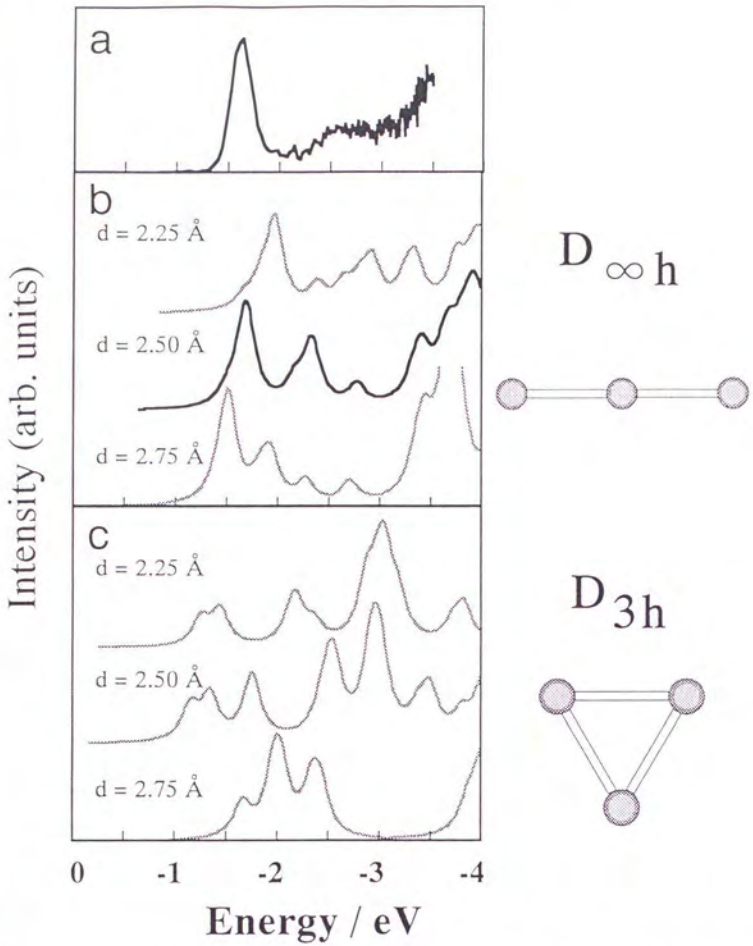

Fig. IV-3 Photoelectron spectra calculated by the spin-polarized DV $-$ $X\alpha$ method for Co_3^-, along with the measured spectrum. (a) Measured photoelectron spectrum. (b) Structure and calculated spectra for $D_{\infty h}$ symmetry. (c) Structure and calculated spectra for D_{3h} symmetry. The most probable structure is $D_{\infty h}$ having the bond-distance of 2.50 Å.

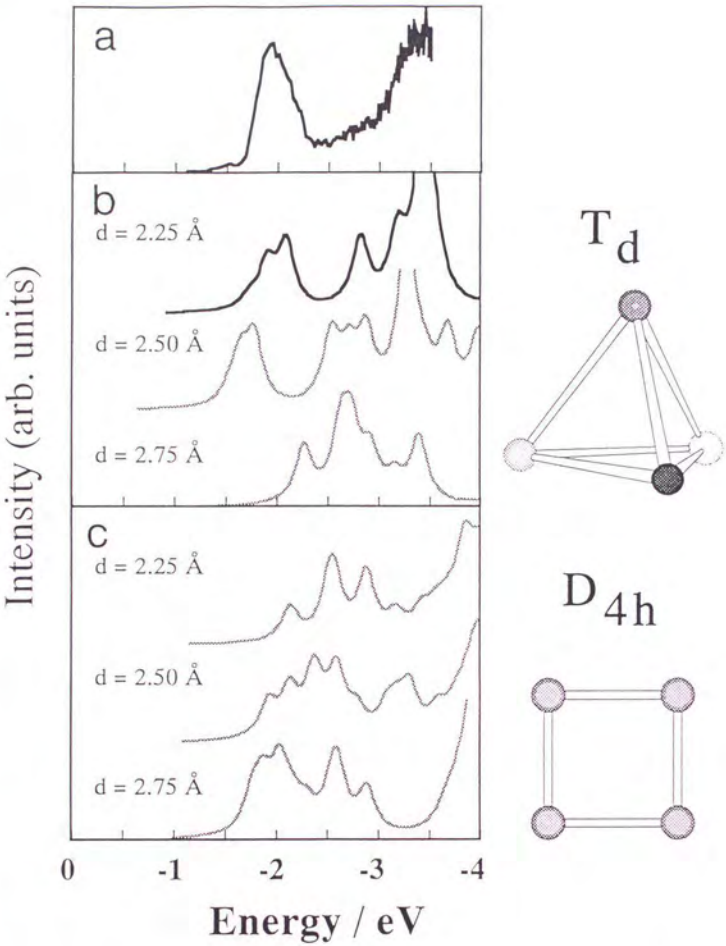

Fig. IV-4 Photoelectron spectra calculated by the spin-polarized DV – $X\alpha$ method for Co_4^-, along with the measured spectrum. (a) Measured photoelectron spectrum. (b) Structure and calculated spectra for T_d symmetry. (c) Structure and calculated spectra for D_{4h} symmetry. The most probable structure is T_d having the bond-distance of 2.25 Å.

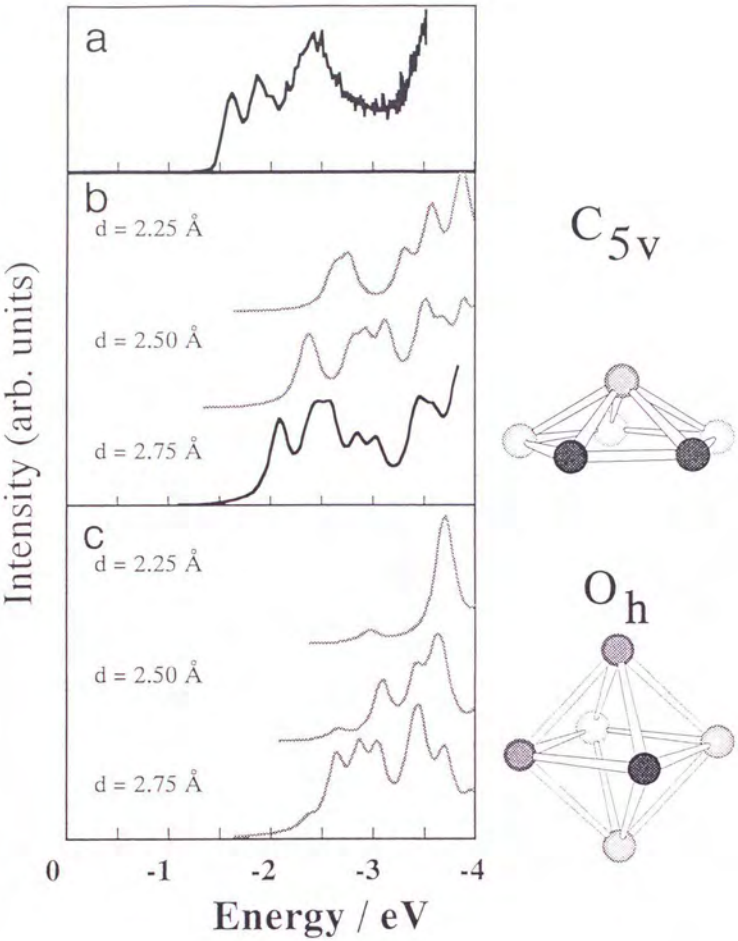

Fig. IV-5 Photoelectron spectra calculated by the spin-polarized DV – Xα method for Co_6^-, along with the measured spectrum. (a) Measured photoelectron spectrum, (b) Structure and calculated spectra for C_{5v} symmetry. (c) Structure and calculated spectra for O_h symmetry. The most probable structure is C_{5v} having the bond-distance of 2.75 Å.

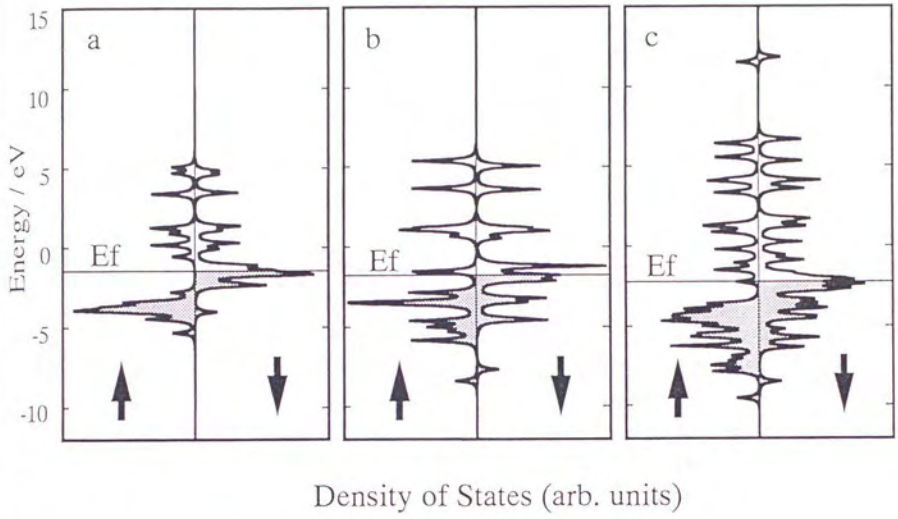

Fig. IV-6 Density of states profiles for the electronic states with the majority (left) and minority (right) spins. Fermi energies are indicated by the horizontal lines.
Co_3^- (panel a), Co_4^- (panel b), Co_6^- (panel c).

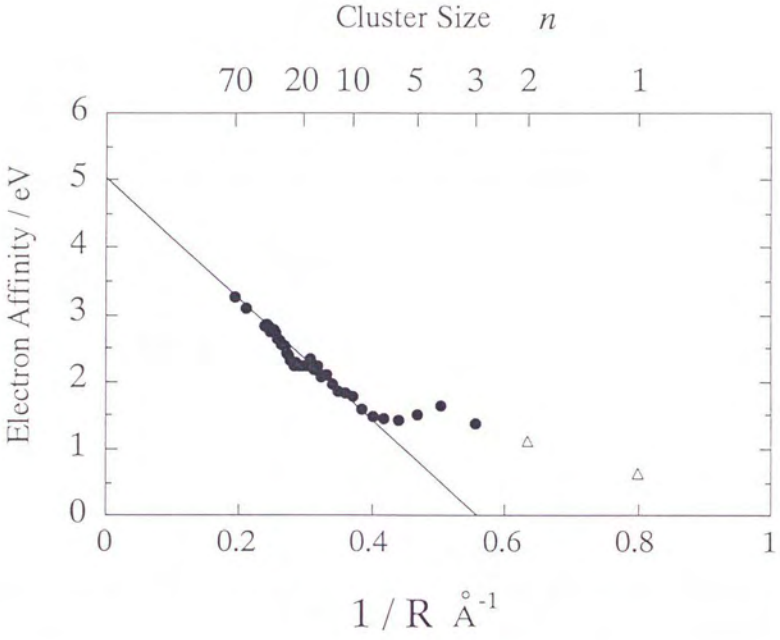

Fig. IV-7 Electron affinity vs $1/R$ plots. The open-triangle △ are taken from ref. [50]. The solid line represents the prediction by the spherical conducting drop model (see eqn. IV-2 in the text).

Chapter V

Reactivity of Co_n^- with simple molecules and electronic structure of product anions

abstract

The reactivities of Co_n^- with O_2 and CO were measured. A clear distinction between the cluster size of $n \leq 6$ and that of $n \geq 7$ was observed in the reactivities. Below $n = 6$, Co_nO^- was observed, while no Co_nCO^- was observed; but above $n = 7$, the size dependence of the intensity was almost similar between Co_nO^- and Co_nCO^-. This finding suggests that a size-dependent transition of the reactivity of Co_n^- occurs in the vicinity of $n \simeq 7$ at which the transition of the electronic structure was observed as mentioned in chapter IV. In order to elucidate these reactivity changes, the photoelectron spectra of Co_nO^- $(3 \leq n \leq 10)$, Co_nN^- and $Co_nO_2^-$ $(3 \leq n \leq 7)$ were measured by use of a XeCl excimer laser (4.025 eV).

V.1 Introduction

Understanding the processes involved in the reaction of molecules onto transition metal clusters is a research area of great interest and importance. Such studies are of interest not only from a basic scientific point of view but also because of the importance of reaction in catalysis. There have been a number of reports on the reaction experiments of transition metal clusters of copper, cobalt, nickel, niobium, palladium, iron etc. with simple molecules such as H_2, D_2,CO, N_2, and NH_3 [1]-[11]. A striking result of these experiments is the sharp size dependence of reaction rates. Since Whetten et al. [9] pointed out a correlation between the cluster ionization potential and the reaction rate, many attempts to link the reactivity to their electronic structures have been made [12] [13]. On the other hand, it was proposed that it is the geometric, rather than the electronic, properties of the clusters that are primarily responsible for the observed size selectivity [7] [8]. However, the geometric structure of the clusters in turn determines the number, energy and spatial orientation of the valence orbitals which can interact with reactant molecules. Since electronic and geometric structure are in fact synergetic, it is necessary to determine the geometric structure for each cluster together with the electronic structure involving the surface orbitals, correct ionization potential, and so on.

In this connection, the photoelectron spectroscopy is one of the most promising technique to examine the electronic and geometric structures of the cluster anions with the aid of the theoretical calculations. Recently, the photoelectron spectra of metal and semiconductor cluster anions constituent of Ia and Ib metals and semiconductor elements [14] - [23] have been measured. Comparing the photoelectron spectra with the results of the *ab initio* quantum chemical calculations, their geometric and electronic structures are successfully determined for small clusters [24] - [26].

On the other hand, little is known about the electronic and geometric structures for the transition metal clusters, because such precise quantum chemical calculations inherently difficult to be performed because of the presence of abundant low-lying electronic states. However, in the previous work (see section IV), the electronic structure of cobalt cluster

anions have been investigated by the photoelectron spectroscopy and the spin-polarized $DV - X\alpha$ calculation; a size-dependent transition of the electronic structure was found at the cluster size of $n \sim 7$. Thus this cobalt cluster anion is an excellent candidate for the study of reactivity. It is interesting to know whether the size-dependent transition in the electronic structure affects the reactivity of the cobalt cluster anions. To this end, the reactivities of Co_n^- $(3 \leq n \leq 15)$ with CO and O_2 were measured.

In most of the researches on the reactivity of metal clusters, only the correlation of the reactivity with the electronic structures of the *reactant* clusters and molecules has been considered. However, the reactivity should also be elucidated by the studies of the electronic structures of the reaction *products*, because these electronic structures closely concern the bonding between the clusters and adsorbate molecules. Recently, Rosén et al. discussed the electronic structure of the reaction products of copper neutral clusters with O_2 to explain the reactivity of the copper clusters [13]; the reactivity of the copper clusters with O_2 varies dramatically as a function of cluster size [10] [11]. They have calculated the chemisorption energy and charge transfer between the cluster and the adsorbate and successfully explained these specific size dependence in the reactivity of the copper clusters with O_2.

To examine the electronic structure of the reaction products experimentally, the photoelectron spectroscopy is the most promising technique. For this purpose, the photoelectron spectra of Co_nN^- and $Co_nO_m^-$ $(m = 1, 2)$ was measured at the photon energy of 4.025 eV.

V.2 Experimental

The apparatus employed in this experiment was described in chapter II.

Reactivity Cobalt cluster anions, Co_n^-, were generated from a laser vaporization cluster source. The Co_n^- generated collided with the reactant gas of CO or O_2 in the reactor positioned about 20 mm downstream from the nozzle of the cluster source. The reactor was consist of about 5-cm-long and 5-cm-diameter cylinder capped by two apertures of 10 mm in diameter; through these two apertures, the cluster anions enter and exit the

reactor. The reactant gases were injected into the reactor by the pulsed valve attached on the cylinder. Special care was taken to ensure that the reaction never occurred in the cluster source, because the reaction of reactant gas with high temperature plasma in the laser vaporization source may hinder a precise measurement of the reactivity. In fact, the cluster anions generated in the presence of small amount of O_2 were dominated by $Co_nO_m^-$ ($m = 1, 2$ and 3), while only weak intensity of Co_nO^- was observed in the reaction products of Co_n^- with O_2 as described below. Therefore these Co_nO^- were preferentially formed in the cluster source but were not in the reactor. The reaction products were analyzed by a reflectron time-of-flight mass spectrometer. The mass resolution was better than $\triangle m/m \simeq 200$. The relative ion intensity was determined by the area of the each peak in the mass spectrum. The accuracy was estimated to be $\sim 20\%$.

Photoelectron spectroscopy The oxide, $Co_nO_m^-$ ($m = 1, 2$), and the nitride, Co_nN^-, clusters were generated in the presence of small amount of nitrogen and oxygen gas, respectively, in the cluster source. The cluster anions thus produced were mass-selected by a time-of-flight technique and were irradiated by a XeCl excimer laser (308 nm). The kinetic energies of photoelectrons were analyzed by a magnetic bottle type photoelectron spectrometer [28] with a 2.2 m drift tube. Laser fluence was in the range of 7–20 mJ $cm^{-2}pulse^-$. Signals were accumulated typically by 5 000-20 000 events. The overall energy resolution was attained to be better than $\triangle E/E = 0.1$ and the uncertainty in the kinetic energy due to the stray electric field is less than 0.1 eV. The background signal associated with the ambient gas was found to be less than 10 % of the total photoelectron signal.

V.3 Results and Discussion

A time-of-flight spectrum of anions measured without introducing the reactant gas in the reactor is shown in Fig. V-1 (a). A series of intense peaks is assigned to Co_n^-, starting from $n = 3$. Small peaks observed among the peaks of Co_n^- arise from the cobalt oxide anions, Co_nO^- and $Co_nO_3^-$. Time-of-flight spectra measured in the presence of CO and O_2 in the reactor are shown in Figs. 1 (b) and (c), respectively. These two spectra show

the reaction product anions of Co_n^- with CO or O_2. The product anions of the reaction with CO were dominated by Co_nCO^-, starting from $n = 7$, while below $n = 6$, no product anions of Co_nCO^- were observed. Although a trace amount of Co_nO^- were observed, these anions were probably contaminants produced directly in the source as shown in Fig. V-1 (a). In the reaction with O_2, the main product anions were $Co_nO_m^-$ ($m = 2, 4$), starting from $n = 3$. Especially in higher concentration of O_2, $Co_4O_4^-$ as shown in Fig. 1(c) was the most intense, which indicates that $Co_4O_4^-$ is the most stable product anion. For $Co_nO_6^-$ with $n \geq 5$ and for $Co_nO_8^-$ with $n \geq 8$ were also observed. However, no product anions containing odd number of oxygen atoms were observed, except for a trace amount of Co_nO^-; it is not clear whether these Co_nO^- are reaction products or contaminants which is the same as shown in Fig. V-1 (a).

In order to investigate the relative reactivity of Co_n^- with CO or O_2, the ratio of the intensity of the reaction product, Co_nX^- ($X = O_2, CO$) indicated by arrows in Figs. V-1 (b) and (c), to that of the reactant (Fig. V-1(a)) ,Co_n^-, is plotted against the cluster size, n, in Fig. V-2. The coarse estimation of the relative reaction rates for O_2 or CO as a function of cluster size for Co_n^- is connected with the above ratio by the following discussion [2] [4] [6]. The reaction for Co_n^- is assumed in a single elementary step of the form

$$Co_n^- + X \xrightarrow{k_n} Co_nX \ (X = CO, O_2), \tag{V.1}$$

for which the elementary rate expression is

$$\frac{d[Co_n^-]}{dt} = -k_n\,[Co_n^-]\,[X]. \tag{V.2}$$

Assuming that X is in such excess that its concentration change is negligible, integration gives an expression for the rate constant, k_n, in terms of the measured fraction of Co_n^-, X concentration, [X], and the reaction time, t:

$$k_n = -\frac{1}{[X]t} \ln \frac{[Co_n^-]_{reaction}}{[Co_n^-]_{control}}, \tag{V.3}$$

where $[Co_n^-]_{control}$ and $[Co_n]_{reaction}$ represents the concentration of Co_n^- of before and after the reaction, respectively. If a decrease in the concentration of Co_n^- is equal to an increase

in the concentration of Co_nX^- in the course of the reaction (formula (V.1)), the rate expression (V.3) is

$$k_n = -\frac{1}{[X]t}\ln\left(1 - \frac{[Co_nX^-]}{[Co_n]_{control}}\right). \quad (V.4)$$

It is $[Co_n^-X]/[Co_n]_{control}$ that is plotted in Fig. V-2 instead of the reaction rate, k_n; the reliable reaction rate cannot be reduced from following reasons: for this studies of cluster anion reaction, we have only a rough knowledge of the average concentration of X and reaction times appropriate to the reactor. In addition, for estimating the reaction rate, such processes as collision-induced electron detachment or scattering by reactant molecules must be taken into account. Although it is possible to make reasonable estimates of these parameters and obtain the reaction rate constants for each cluster size, these qualitative values alone provide sufficient information on the insight into the reaction of the cobalt cluster anions.

The most striking result shown in Fig. 2 is the difference in the reaction pattern between CO and O_2 for $n \leq 6$ of Co_n^-. In the reaction with O_2, the reaction products of $Co_nO_2^-$ were observed from $n = 3$ and peaks at $n = 4$; in the reaction with CO, no reaction products of Co_nCO^- were observed below $n = 6$ in this measurement. On the other hand, above $n = 7$ the reactivity of Co_n^- with both O_2 and CO varies in the similar manner as a function of cluster size, except for $n = 7$ and $n = 14$. For both clusters with $n = 7$ and $n = 14$, the reactivity of Co_n^- with CO is smaller than that with O_2. These results obviously suggest that the reactivity of Co_n^- with O_2 and CO changes dramatically in the vicinity of $n \sim 7$, at which the transition of the electronic structures of Co_n^- were observed using the photoelectron spectroscopy [27].

It is interesting to compare the reactivity for the neutral cobalt clusters with the present results. The reactivity of neutral cobalt clusters with D_2, N_2 and CO were reported [6]. Among these results, the reactions of neutral cobalt clusters with CO are to be compared with the present results of cobalt cluster anion with CO. The reaction of the neutral cobalt clusters with CO was reported to be generally facile, with very little change as a function of cluster size. This reactivity pattern contrasts with that of the anion where the clear size dependence in the reactivity was observed. These results suggests that in the reaction of

the cobalt cluster anions with CO, the electron donation from CO to the cluster anion is a rate-determining step. Although no significant size dependence of neutral cobalt clusters with CO was observed, the reactivity with D_2 or N_2 varies dramatically as a function of cluster size. In addition this overall size-dependence for neutral clusters is similar to that for cation [7]. In the light of this similarity between the neutral and cation, the difference in the reactivity of the anion and neutral clusters with CO is striking.

These characteristic behavior in the reactivity should be elucidated by the understanding of the bonding between the cluster and the adsorbate. In order to examine the electronic structure of cobalt cluster-adsorbate complex anions, the photoelectron spectra of Co_nX^- (X = N, O and O_2) were measured at the photon energy of 4.025 eV. The photoelectron spectra of Co_nO^- ($3 \leq n \leq 10$) are shown in Fig. V-3, and those of Co_nN^- and $Co_nO_2^-$ ($3 \leq n \leq 7$) are in Fig. V-4. The feature of the photoelectron spectra of the nitride clusters, Co_nN^-, and the oxide clusters, Co_nO^- were similar to that of the bare cobalt clusters [27] in the high electron binding energy region (2.3 $\sim$ 3.5 eV). However, in the nitride clusters, the intensity of the peak around the Fermi level were weakened, while in the oxide clusters the intensities of the Fermi level were not only weakened but also broadened. On the other hand, in the photoelectron spectra of $Co_nO_2^-$, the envelop shifts by 0.2–0.5 eV toward higher in electron binding energy, probably due to the high electron negativity of O_2. These results indicates that the electrons around the Fermi level strongly affects the reaction process.

V.4 Conclusion

The reactivities of Co_n^- with both CO and O_2 were measured. The results suggest that the size-dependent transition of the reactivity of Co_n^- in the vicinity of $n \sim 7$. This transition will correlate with that of the electronic structures of Co_n^- observed by the photoelectron spectroscopy. In addition, below $n = 6$, the reactivities of Co_n^- show much difference between CO and O_2.

The mechanism of the reactivity change depending on the cluster size and on the material

of the adsorbate should be elucidated by the study of the photoelectron spectra of the reaction products. To this end, the photoelectron spectra of $Co_nO_2^-$ $(3 \leq n \leq 10)$, Co_nO^- and Co_nN^- $(3 \leq n \leq 7)$ were measured at the photon energy of 4.025 eV. To discuss the electronic structure involving the charge transfer and the bonding between the cluster and the adsorbate, the theoretical analysis is now undertaken.

References

[1] D. M. Cox, D. J. Trevor, R. L. Whetten, E. A. Rohlfing, and A. Kaldor, Phys. Rev. B **32**, 7290 (1985); D. J. Trevor, R. L. Whetten, D. M. Cox, and A. Kaldor, J. Am. Chem. Soc. **107**, 518 (1985); R. L. Whetten, D. M. Cox, D. J. Trevor, and A. Kaldor, Surf. Sci. **156**, 8 (1985); M. R. Zakin, R. O. Brickman, D. M. Cox, K. C. Reichmann, D. J. Trevor, and A. Kaldor, J. Chem. Phys. **85**, 1198 (1986); P. Fayet, A. Kaldor, and D. M. Cox, *ibid.* **92**, 254 (1990).

[2] D. M. Cox, K. C. Reichmann, D. J. Trevor, and A. Kaldor, J. Chem. Phys. **88**, 111 (1988).

[3] S. C. Richtsmeier, E. K. Parks, K. Liu, L. G. Pobo, and S. J. Riley, J. Chem. Phys., **82**, 3659 (1985); K. Liu, E. K. Parks, S. C. Richtsmeier, L. G. Pobo, and S. J. Riley, *ibid.* **83**, 2882 (1985).

[4] E. K. Parks, K. Liu, S. C. Richtsmeier, L. G. Pobo, and S. J. Riley, J. Chem. Phys. **82**, 5431 (1985).

[5] M. E. Geusic, M. D. Morse, and R. E. Smalley, J. Chem. Phys. **82**, 590 (1985); J. L. Elkind, F. D. Weiss, J. M. Alford, R. T. Laaksonen, and R. E. Smalley, *ibid.* **88**, 5215 (1988).

[6] M. D. Morse, M. E. Geuic, J. R. Heath, and R. E. Smalley, J. Chem. Phys. **83**, 2293 (1985).

[7] P. J. Brucat, C. L. Pettiette, S. Yand, L.-S. Zheng, M. J. Craycraft, and R. E. Smalley, J. Chem. Phys. **85**, 4747 (1986).

[8] J. M. Alford, F. D. Weiss, R. T. Laaksonen, and R. E. Smalley, J. Phys. Chem. **90**, 4480 (1986).

[9] (a) R. L. Whetten, D. M. Cox, D. J. Trevor, and A. Kaldor, Phys. Rev. Lett. **54**, 1494 (1985); (b) R. L. Whetten, M. R. Zakin, D. M. Cox, D. J. Trevor, and A. Kaldor, J. Chem. Phys. **85**, 1697 (1986).

[10] B. J. Winter, E. K. Parks, and S. J. Riley, J. Chem. Phys. **94**, 8618 (1991).

[11] M. Andersson, J. L. Persson, and A. Rosén, Nanostr. Mater., **3**, 337 (1993).

[12] I. Panas, P. Siegbahn, and U. Wahlgren, Mechanism for H_2 dissociation on transition metal clusters and surface, in *The Challenge of d and f electrons* (American Chemical Society, 1989), p. 125.

[13] H. Grönbeck, M. Andersson and A. Rosén, Surf. Sci. (in press).

[14] S. T. Arnold, J. G. Eaton, D. Patel-Misra, H. W. Sarkas, and K. H. Bowen, in *Ion Spectroscopy and Structure,* edited by J. P. Maier (Elesevier, Amsterdam 1989).

[15] K. M. McHugh, J. G. Eaton, G. H. Lee, H. W. Sarkas, L. H. Kidder, J. T. Snodgrass, M. R. Manaa, and K. H. Bowen, J. Chem. Phys. **91**, 3792 (1989).

[16] J. Ho, K. M. Ervin and W. C. Lineberger, J. Chem. Phys. **93**, 6987 (1990).

[17] G. Ganteför, M. Gausa, K. H. Meiwes-Broer and H. O. Lutz, J. Chem. Soc. Faraday Trans. **86**, 2483 (1990).

[18] G. Ganteför, M. Gausa, K. H. Meiwes-Broer and H. O. Lutz, Faraday Discuss. Chem. Soc. **86**, 197 (1988).

[19] O. Cheshnovsky, S. H. Yang, C. L. Pettiette, M. J. Craycraft, Y. Liu, and R. E. Smalley, Chem. Phys. Lett. **138**, 119 (1987).

[20] S. H. Yang, C. L. Pettiette, J. Conceicao, O. Cheshnovsky and R. E. Smalley, Chem. Phys. Lett. **139**, 233 (1987).

[21] S. Yang, K. J. Taylor, M. J. Craycraft, J. Conceicao, C. L. Pettiette, O. Cheshnovsky and R. E. Smalley, Chem. Phys. Lett. **144**, 431 (1988).

[22] T. N. Kitsopoulos, C. J. Chick, A. Weaver and D. M. Neumark, J. Chem. Phys. **93** 6108 (1990).

[23] D. W. Arnold, S. E. Bradforth, T. N. Kitsopoulos, and D. M. Neumark, J. Chem. Phys. **95** 8753 (1991).

[24] (a)V. Bonačić-Koutecký, P. Fantucci and J. Koutecký, Chem. Rev. **91**, 1035 (1991); (b) J. Chem. Phys. **91**, 3794 (1989); (c) **93**, 3802 (1989); (d)V. Bonačić-Koutecký, L. Češpiva, P. Fantucci, J. Pittner and J. Koutecký, *ibid.* **100**, 490 (1994).

[25] (a) K. Raghavachari and C. M. Rohlfing, J. Chem. Phys. **94**, 3670 (1991); (b) C. M. Rohlfing and K. Raghavachari, *ibid*, **96**, 2114 (1992).

[26] J. D. Watts and R. J. Bartlett, J. Chem. Phys. **97**, 3445 (1992).

[27] H. Yoshida, A. Terasaki, K. Kobayashi, M. Tsukada, and T. Kondow, J. Chem. Phys. (in press).

[28] P. Kruit and F. H. Read, J. Phys. E **16**, 313 (1983).

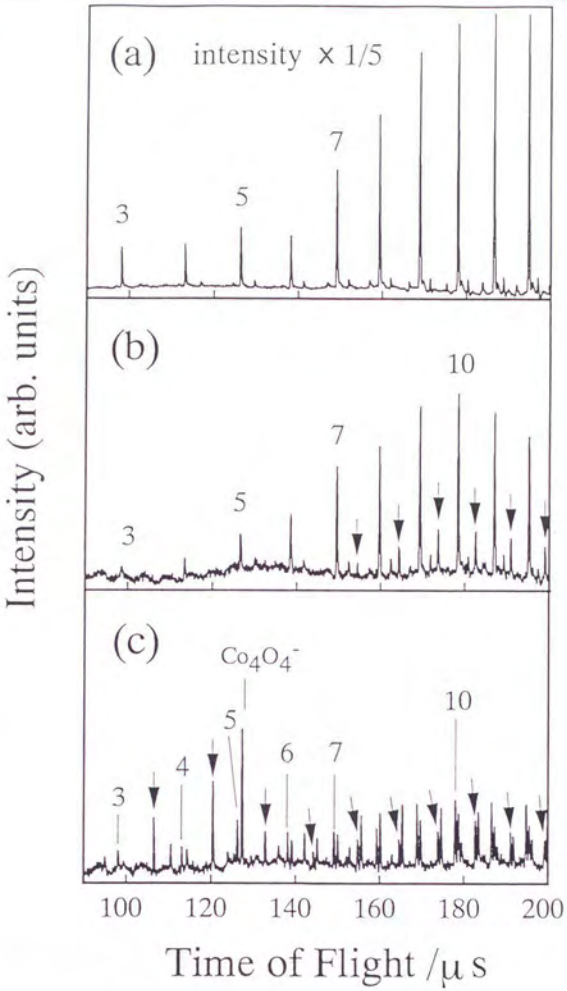

Fig. V-1 Time-of-flight spectra of cobalt cluster anions and reaction product anions. The control spectrum (panel a) was measured without injecting the reactant gas in the reactor. The lower two spectra were taken injecting CO (panel b) and O_2 (panel c) in the reactor. The numbers beside the peaks refer the size of the bare cobalt cluster anions, Co_n^-. The arrows indicates Co_nCO^- and $Co_nO_2^-$ in the panels (a) and (b), respectively.

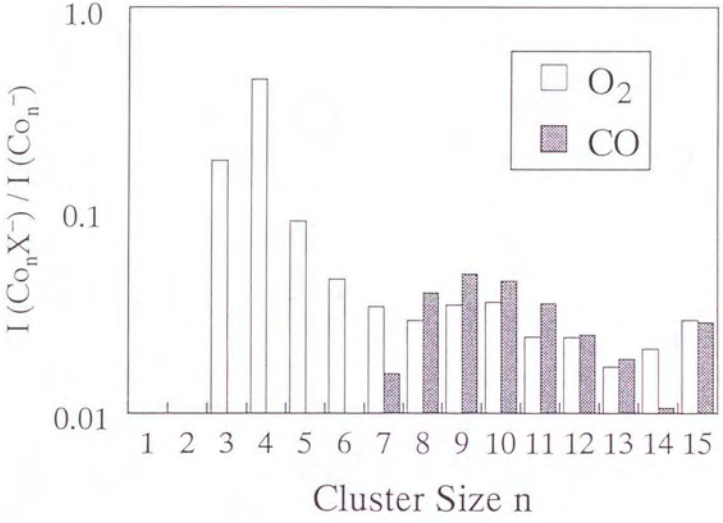

Fig. V-2 Reaction ratio (intensity of product, Co_n^-X (X = O_2, CO), divided by intensity of reactant of cobalt cluster anion, Co_n^-) as a function of cluster size n.

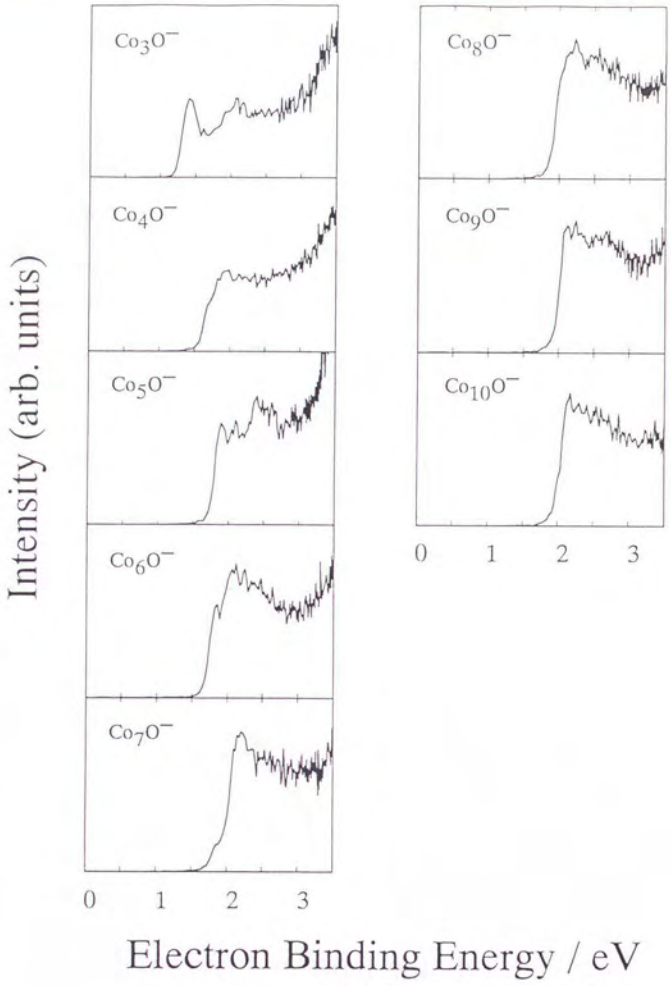

Fig. V-3 Photoelectron spectra of cobalt oxide cluster anions, Co_nO^-, measured by use of a XeCl excimer laser (4.025 eV).

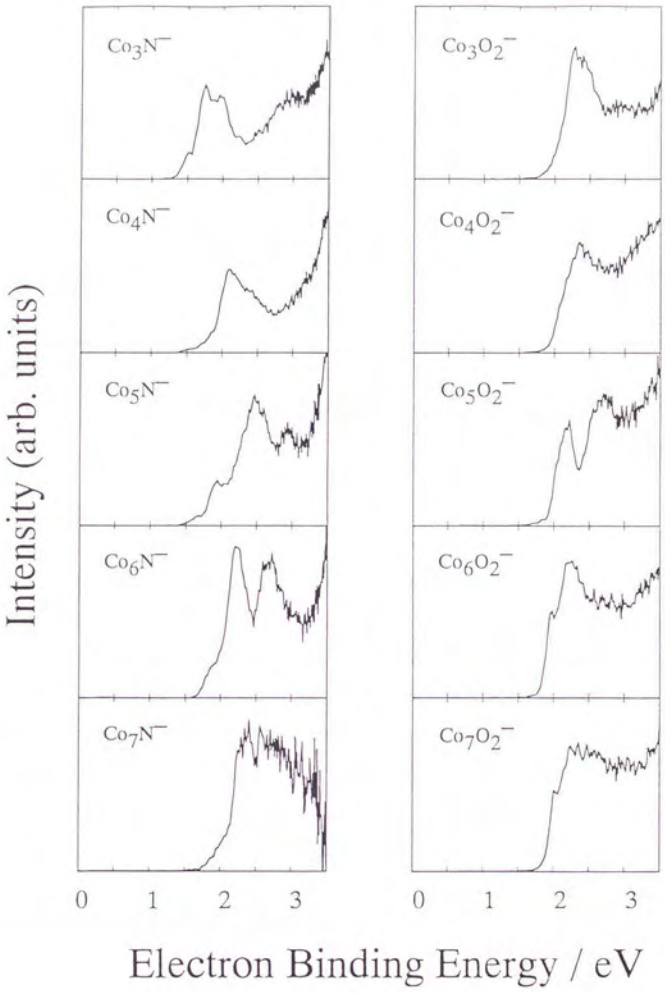

Fig. V-4 Photoelectron spectra of cobalt mono-nitride cluster anions, Co_nN^-, and cobalt dioxide cluster anions, $Co_nO_2^-$, measured by use of a XeCl excimer laser (4.025 eV).

Chapter VI

Photoelectron spectroscopy of V_n^-

abstract

Photoelectron spectra of vanadium cluster anions, V_n^- ($3 \leq n \leq 100$), were measured by 3.495-eV light. Electron affinities were determined from the onset of the photoelectron spectra. The values were compared with that predicted by the spherical conducting drop model; it is found that the electron affinities above $n \simeq 9$ are well represented by the model, while the electron affinities deviate from the prediction by the model below $n \simeq 8$. This finding suggests that the size-dependent transition occurs in the electronic structure of V_n^-. In the spectral feature, a clear distinction was observed between $n = 16$ and $n = 17$. Below $n = 16$, the spectral feature varies dramatically as a function of cluster size, while above $n = 17$ the overall feature does not change. This size-dependence in the spectral feature below $n = 16$ suggests that the $4s$ and $4p$ electrons were observed in the photoelectron spectra.

VI.1 Introduction

The development of the electronic band structure in a small particle with increase number of constituent atoms is of fundamental interest and importance in cluster research. Transition metal clusters in particular have received extensive attention because of the interests that have d electron orbitals available for bonding; these d electrons play an important role in emerging of the catalytic activities and magnetism.

Among the transition metals, coinage metal (copper, silver, and gold) clusters are widely investigated because they are relatively simple. Each of the ground state atoms has a closed d shell and a single s valence electron; the properties of the s electrons in the coinage metal clusters are well described by the electronic shell model [1] in which the electrons are totally delocalized within the boundary of the clusters. On the other hand, the properties of the d electrons are not described by the simple shell model because the electrons are localized around the core of the atoms [2]. Smalley and coworkers demonstrated the evolution of d in the copper and gold cluster anions using the photoelectron spectroscopy [3]. Further more, the evidence of the sp-d hybridization was reported in the coinage metal clusters [3] [4].

In contrast, the electronic structure of clusters consisting of the transition metal having the partially filled d shell is not clear. The detailed information on the electronic structures such as the bonding of d and s electron orbitals and $sp-d$ hybridization were limited to the dimers or trimers [5]. Involvement of electronic configurations with partially filled d shells can produce a large number of low-lying electronic states, making theoretical treatment inherently difficult and spectral feature complicated.

In the previous work, we measured the photoelectron spectra of cobalt cluster anions, Co_n^- [6]. It was found that a size-dependent transition in the electronic structure occurs in the vicinity of $n = 7$. In addition, the spin states for Co_3^-, Co_4^-, and Co_6^- were examined by comparing the experimental photoelectron spectra with the spin-polarized DV-$X\alpha$ calculations. It was found that the electron energy levels with the majority spins and the minority spins split by 1.0–2.8 eV with the spin difference of about 2 electron per cobalt

atom. These results provide the evidence of ferromagnetic ordering in Co_n^-.

In recent years, the magnetism of the vanadium clusters, V_n, are extensively discussed theoretically, because both a low-spin and a high-spin states might be exist depending on the interatomic parameters [7]-[9]. The Stern-Gerlach-type magnetic deflection experiments on clusters of V_n^- with $8 \leq n \leq 99$ showed no deflection within experimental error [10]. On the basis of the superparamagnetism [11], the upper limits of the magnetic moments were determined to be 0.59 μ_B for V_9. This result was good agreement with the calculated magnetic moment of the low-spin states of V_9 [7]. However, the high-spin states might be observed in smaller clusters or in different charge states, i. e. anions or cations.

In the present work, we measured photoelectron spectra of vanadium cluster anions, V_n^-, with the cluster size ranging between $n = 3$ and $n = 100$. The photoelectron spectra may provide the excellent information on the magnetism of V_n^-. It is also interesting to see whether the same size-dependent transition occurs in the electronic structure of V_n^- as that observed in Co_n^-.

Another focus of this work was the experimental investigation of the properties of the s and p electrons in larger clusters consisting of the transition metals having a partially filled d shell; it is expected the energy levels of the s and p electrons vary dramatically as a function of cluster size, while those of d electrons change gradually as seen in the coinage metal clusters. The previous experiments little information on the s electrons, probably because the s band were hidden behind the thick d band [6] [12]. Regarding the number of s electrons relatively to that of d electrons, the cluster anions consisting of vanadium whose atomic configuration is represented as $3d^34s^2$ are excellent candidate to examine the d bands. The clear influence of $4s$ and $4p$ electrons on the electronic structure is probably observed in the photoelectron spectra.

VI.2 Experimental

A detailed description of the apparatus used in this experiment is given in chapter II. Vanadium cluster anions, V_n^-, were generated from a laser vaporization source. Metal

vapor was produced by focusing the second harmonics of Nd YAG laser (Quanta Ray DCR-11) onto a vanadium sample disc. The metal vapor generated was mixed and cooled by carrier gas of helium introduced by a pulsed valve (General Valve series 9) to form both negatively and positively charged metal clusters along with neutral. The cluster anions thus produced were extracted by a pulsed voltage of 150–1000 V which was chosen to be roughly proportional to the cluster size of interest, and were temporally and spatially focused at 3 m downstream. Then, the anions of interest were selected by a mass-gate and were decelerated to 10–20 % of the initial kinetic energy in order to suppress the broadening of the photoelectron energies due to the Doppler effect. These anions were thus irradiated by either the third harmonics (355 nm) or the second harmonics (532 nm) of a Nd YAG laser (Spectra Physics GCR-250-10) at a repetition rate of 10 Hz. The kinetic energy of the photoelectron was analyzed by a magnetic bottle type photoelectron spectrometer. The energy resolution of this photoelectron spectrometer was depend on the electron energy and varied from about 50 meV at one electron volt to about 150 meV at three electron volts. Photoelectron spectra was calibrated using Cu^- as a standard [13]. The uncertainty of the absolute value of the electron energy was estimated to be less than 0.1 eV

Signals from an electron detector were recorded by a 1-GHz time-to-digital converter (LeCroy TDC4208) and each spectrum represented an accumulation of between 20 000 to 50 000 shots. Laser fluence was in the range of 20–40 mJ cm^{-2} $pulse^{-1}$ and no power dependent processes were observed.

VI.3 Results

VI.3.1 Mass spectra

A typical time-of-flight mass spectrum of V_n^- are shown in Fig. VI-1. A series of intense peaks are V_n^- starting from $n = 3$. A series of satellite peaks which are 12 u. larger than each corresponding vanadium cluster peak are assignable to V_nC^-. The cluster anions of V^- or V_2^- were never observed under this source condition; the timing of actuating

the pulsed valve was delayed by 700-1000 μs with respect to firing the vaporization laser. However, under the completely different condition where the duration of 500 μs between actuating the pulsed valve and firing the vaporization laser, intense V^- and V_2^- were produced as shown in Fig. VI-2 while no larger clusters than $n = 3$ were observed.

VI.3.2 Photoelectron spectra

The photoelectron spectra of V_n^- $(3 \leq n \leq 100)$ are shown in Fig. VI-3. In V_3^-, the photoelectron spectrum consists of a series of sharp peaks from 1.0 eV to 2.4 eV and an unresolved broad peak above 2.4 eV. In V_4^-, the spectrum reveals a series of sharp peaks from 1.3 eV to 2.5 eV, while an unresolved envelope is observed above 2.5 eV. Both in V_3^- and V_4^- , each photoelectron spectrum measured by 355-nm light is essentially the same as that measured by 532-nm light except that the energy resolution is improved in stead of the limitation of the energy region. The photoelectron spectra of V_5^- and V_6^- are qualitatively similar to each other; both spectra are consist of two unresolved broad peaks centered around 1.5 eV and 2.0 eV, respectively, and sharp rise above 2.8 eV. Although each peak observed in these spectra seems to contain fine structures, these structures are not reproduced reasonably. Thus we conclude that these fine structures are noise. In $n = 5$ and $n = 6$, the photoelectron spectra were also measured by 532-nm light; the spectrum is essentially the same as that measured by 355-nm light except for improvement of the energy resolution.

For larger clusters from V_7^- up to V_{100}^-, the photoelectron spectra were measured by only 355-nm light. The spectra of V_7^- and V_8^- reveal partially resolved broad envelopes ranging from about 1.2 eV to 2.8 eV and a sharp rise above 2.8 eV. In V_9^-, the spectra consists of a sharp peak centered at 1.8 eV in a broad peak centered around 2.3 eV. From V_{10}^- to V_{16}^-, the photoelectron spectra seems to be characterized by two different components which overlaps each other in the electron energy region. The first components have asymmetric bell-shapes with no reproducible fine structures. This components gradually evolves in shape along with the gradual shifts of the maxima centered from about 1.8 eV for V_{10}^- to

about 2.0 eV for V_{16}^- as the increase of the cluster size, n; this evolution of the spectral shape continues from V_8^- toward at least V_{100}^- which was the largest cluster investigated in this work. In addition, in larger clusters, the shapes resemble that of the bulk photoelectron spectrum. On the other hand, the second components vary dramatically both in shapes and in energies as a function of the cluster size. For example, a broad peak at 2.1 eV observed in the photoelectron spectrum of V_{11}^- is also observed at 2.3 eV in the photoelectron spectrum of V_{12}^-, but the intensity of the peak is lowered. This peak is again observed at 2.4 eV with higher intensity in the photoelectron spectrum of V_{13}^- and continue to be observed up to V_{16}^-. In V_{16}^-, another small peak centered at 1.75 eV was observed.

Above $n = 17$, the spectrum reveals only asymmetric bell-shape which is quite similar to that of bulk photoelectron spectrum. This fundamental feature does not change with the cluster size except for a gradual shift of the maxima.

VI.4 Discussion

The finite of the clusters will cause the electron affinity, EA, to be lower than the work function, W (4.3 eV for vanadium). The electrostatic "conducting spherical drop model" was invoked to account for the size dependence of these differences [14]. This model assumes that the metallic clusters are perfectly conducting spheres, that the charging energy of the sphere and the interaction between the detached electron and the image charge on the cluster is responsible for the following relation between EA and W, where

$$EA = W - \alpha \frac{e^2}{R}, \tag{VI.1}$$

where e is the electron charge, R is the effective radius of the cluster. α is a coefficient which is put between 1/2 and 5/8 [15] - [18].

In order to compare the EA of V_n^- with the predicted values by eq. (VI.1), the EAs were derived from the onset of the photoelectron spectra. The EAs are plotted against the reciprocal of cluster radius, $1/R$, in Fig. VI-4. The cluster radius, R, was determined by the formula,

$$R = d\, n^{1/3} + r_0, \tag{VI.2}$$

where d assumes the radius of the constituent atom, and r_0 is a parameter to account for "spilling out" of the electronic charge of the cluster. The d value is chosen to be 1.31 Å which is a half of the bond-distance in a vanadium metal. The spilling out parameter, r_0, of 0.1 Å was obtained by comparing the measured EA with that predicted by eq. VI.1; for $\alpha = 5/8$, r_0 of 0.1Å fit the experimental data well. In Fig. VI-4, the predicted EAs given by eq. VI.1 with $\alpha = 5/8$ and $\alpha = 1/2$ are presented by a solid and a dashed lines, respectively, for comparison.

As shown Fig. VI-4, the data were well reproduced by eq. VI.1 above $n \simeq 9$, while below $n \simeq 8$ the data were not reasonably reproduced; the EAs measured were higher than that predicted by the model in $n \leq 8$. Moreover, the discontinuity between $n = 8$ and $n = 9$ were observed in the intensity of the cluster anions in the mass spectrum as mentioned in section VI-3. These findings suggest that a size-dependent transition occurs around $n = 9$ in the electronic structure of V_n^-.

The same transition was also observed in the electronic structure of Co_n^- with $n \simeq 7$ [6]. In Co_n^- with $n \leq 6$, EAs were also higher than that predicted by the model. Moreover, the discontinuity in the intensity of the cluster anions in the mass spectrum were also observed at this cluster size. These coincidence strongly suggests the mechanism of the transition observed in V_n^- is the same as that in Co_n^-.

In the spectral feature, another size dependent change was observed at the cluster size of $n = 17$ as mentioned in section VI-3. Above $n = 17$, the photoelectron spectra are characterized by the single broad features which do not vary significantly as a function of cluster size except for the shift of the maxima. This overall feature is similar to that of d band observed in the bulk photoelectron spectra. In addition, the position of this envelop gradually moves toward that of d band of the bulk. Therefore, the spectra will arise from the d electrons of V_n^-. In contrast, below $n = 16$, the spectra seems to be comprised of two components; one varies dramatically and irregularly as a function of cluster size, while the other vary gradually. The dramatic size-dependence of the spectral feature of the first component suggests that these feature arise from s electrons, i.e. the s-derived band or the band caused by $s - d$ hybridization.

These assignments are rationalized by that of Cu_n^- and Au_n^- reported by Smalley and coworkers [3]. The photoelectron spectra of Cu_n^- are characterized by a shallow broad structure with the sharper broad feature rising 2 eV deeper than the onset of the spectra; comparing with the bulk photoelectron spectra, they assigned these two features to s and d bands, respectively. The spectral feature of s band varies dramatically, while that of d band varies gradually as a function of cluster size. In Au_n^- with $n \leq 20$, the spectral features which did not show clear distinctions of s and d bands are interpreted as the *sp-d* hybridization [3]; the feature of these hybridized band also varies dramatically as a function of cluster size. Therefore the possibility of the *sp-d* hybridization does not conflict with the above explanation of the size-dependence of the spectral feature.

These size dependence of spectral features together with the essential change in spectral feature at the cluster size of $n = 17$ can be explained by the simple model proposed by Fujima and Yamaguchi [2]; using the model they predicted the size dependence of the magnetism of the nickel, cobalt and iron clusters. In this model, d electrons are localized around the core of the atoms to form a narrow band, while s electrons are entirely delocalize within the boundary of the cluster to form the electronic shell structure in the same manner as in alkali and coinage metal clusters [1]. Since the s and d bands are close in energy, the number of the s and d electrons are determined so as to minimize the total electron energy. Therefore with the increase of the cluster size, the number of d electron change abruptly corresponding to the shell closing of the s electrons where the number of s electrons are 8, 18, 20, and so on. Obviously the number of s electrons is not directly correspond to that of cluster size, n. If this model can be applied to the electronic structure of V_n^-, not only the spectral feature for $n \leq 16$ of V_n^- but also the size dependent transition in spectral feature at $n = 17$ can be explained.

If the transition observed at $n = 17$ are really caused by the shell closing of the $4s$ electrons, the same transition should occur at larger cluster size such as $n = 18, 19, 20$, in the neutral or cations. Indeed, the ionization potentials of neutral vanadium cluster measured show a sharp discontinuity between $n = 18$ and $n = 19$ [19]. On the other hand, such a discontinuity was observed in the electron affinity between $n = 16$ and $n = 17$ as

pointed by an arrow in Fig. VI-4; obviously this discontinuity would correspond to the transition in the spectral feature as discussed above. This fact would support the above prediction.

VI.5 Summary

The photoelectron spectra of V_n^- $(3 \leq n \leq 100)$ were measured at the photon energy of 3.495 eV. The electron affinities determined by the onset of the photoelectron spectra were compared with the values predicted by the spherical conducting drop model. As a result, above $n \simeq 9$ the electron affinities measured are well represented by the model, while below $n \simeq 8$ the electron affinities deviate from the prediction. This finding together with the discontinuity observed in the mass spectrum suggests that a size-dependent transition occurs around $n = 9$ in the electronic structure of V_n^-. This transition parallels to that of cobalt cluster anions where the cluster size of the transition was in the vicinity of $n = 7$. Although this transition seems to be a metal-non-metal transition, it is not decisive because the simple electrostatic model is not a definite criterion of metal and non-metal.

On the other hand, the feature of the photoelectron spectra show a sharp difference between $n \leq 16$ and $n \geq 17$. Below $n = 16$, the spectrum shows rich structure which varies sensitively and dramatically as a function of the cluster size, while above $n = 17$ the spectrum shows single broad feature which does not vary significantly; the latter is similar to that of the balk d band. These rich structures likely arise from the $4s$ and $4p$ electrons.

Regarding the magnetism, preliminary DV-$X\alpha$ calculations of the tetramer anion show that the electron energy levels with the different spin states split with the spin difference of 1.1 electrons per vanadium atom. This result provides the evidence of the ferromagnetic spin coupling in V_n^-. Further analysis are now undertaken.

References

[1] W. A. de Heer, Rev. Mod. Phys. **65**, 611 (1993).

[2] N. Fujima, and T. Yamaguchi, J. Non-Crystal. Solid, **117/118**, 2885 (1990).

[3] K. J. Taylor, C. L. Pettiette-Hall, O. Cheshnovsky, and R. E. Smalley, J. Chem. Phys. **96**, 3319 (1992).

[4] C.-Y. Cha, G. Ganteför, and W. Eberhardt, J. Chem. Phys. **99**, 6308 (1993).

[5] (a) D. G. Leopold, and W. C. Lineberger, J. Chem. Phys. **85**, 51 (1986); (b) K. M. Ervin, J. Ho, and W. C. Lineberger, *ibid.* **89**, 4514 (1988); (c) J. Ho, M. L. Polak, K. M. Ervin, and W. C. Lineberger, *ibid.* **99**, 8542 (1993).

[6] H. Yoshida, A. Terasaki, K. Kobayashi, M. Tsukada, and T. Kondow, J. Chem. Phys. (in press).

[7] K. Lee and J. Callaway, Phys. Rev. B **48**, 15 358 (1993).

[8] F. Liu, S. N. Khanna, and P. Jena, Phys. Rev. B **43**, 8179 (1991)

[9] (a) J. Dorantes-Dávila and H. Dreyssé, Phys. Rev. B **47**, 3857 (1993); (b) P. Alvarado, J. Dorantes-Dávila and H. Rreyssé, *ibid.* **50**, 1039 (1994).

[10] D. C. Douglass, J. P. Bucher, and L. A. Bloomfield, Phys. Rev. B **45**, 6341 (1992).

[11] S. N. Khanna and S. Linderoth, Phys. Rev. Lett. **67**, 742 (1991).

[12] (a) G. Ganteför, M. Gausa, K.-H. Meiwes-Broer, and H. O. Lutz, Faraday Discuss. Chem. Soc, **86**, 197 (1988);(b) G. Ganteför, M. Gausa, K.-H. Meiwes-Broer, and H. O. Lutz, J. Chem. Soc. Faraday Trans. **86**, 2483 (1990).

[13] D. G. Leopold, J. Ho and W. C. Lineberger, J. Chem. Phys. **86**, 1715 (1987).

[14] D. M. Wood, Phys. Rev. Lett. **46**, 749 (1981).

[15] M. P. J. van Staveren, H. B. Brom, L. J. de Jongh and Y Ishii, Phys. Rev. B **35**, 7749 (1987).

[16] G. Makov, A. Nitzan and L. E. Brus, J. Chem. Phys. **88**, 5076 (1988).

[17] J. P. Perdew, Phys. Rev. B **37**, 6175 (1988).

[18] M. Seidel, K. -H. Meiwes-Broer, and M. Brack, J. Chem. Phys. **95**, 1295 (1991).

[19] M. D. Morse, Chem. Rev. **86**, 1097 (1986)

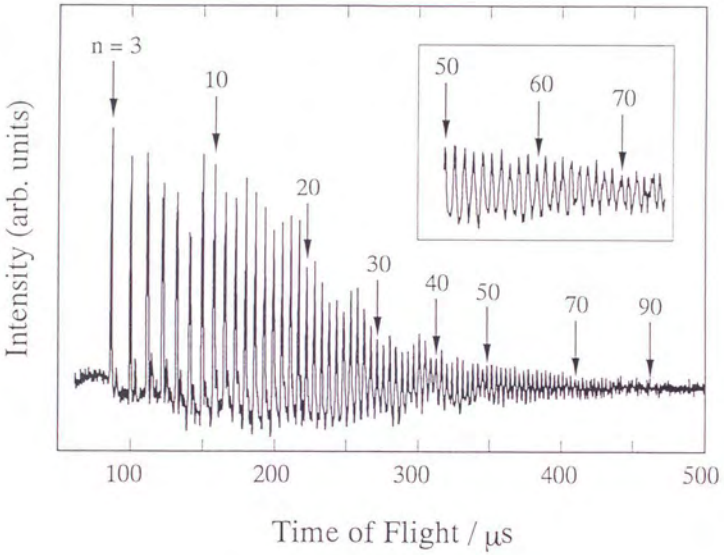

Fig. VI-1 Time of flight mass spectrum of vanadium cluster anions with $n \geq 3$ produced from the cluster source. Under this source condition, neither monomer nor dimer was observed.

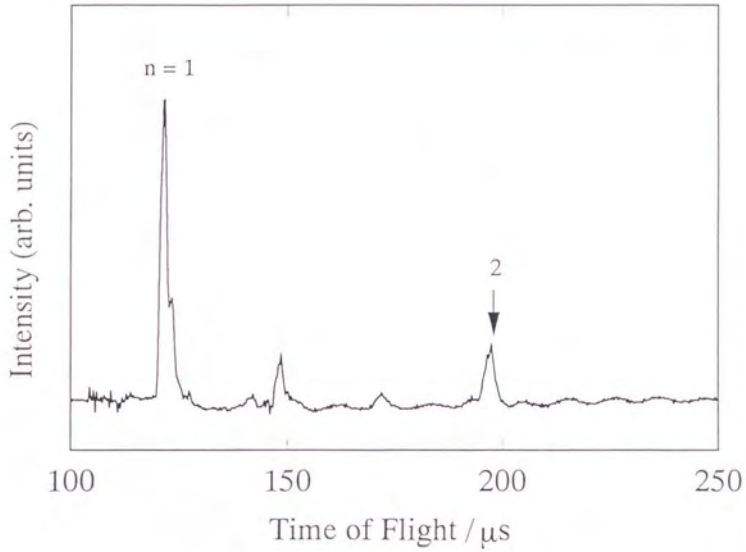

Fig. VI-2 Time of flight mass spectrum of vanadium cluster anions. The source condition was optimized to produce the monomer and dimer anions. Here no larger cluster anions than the trimer were observed.

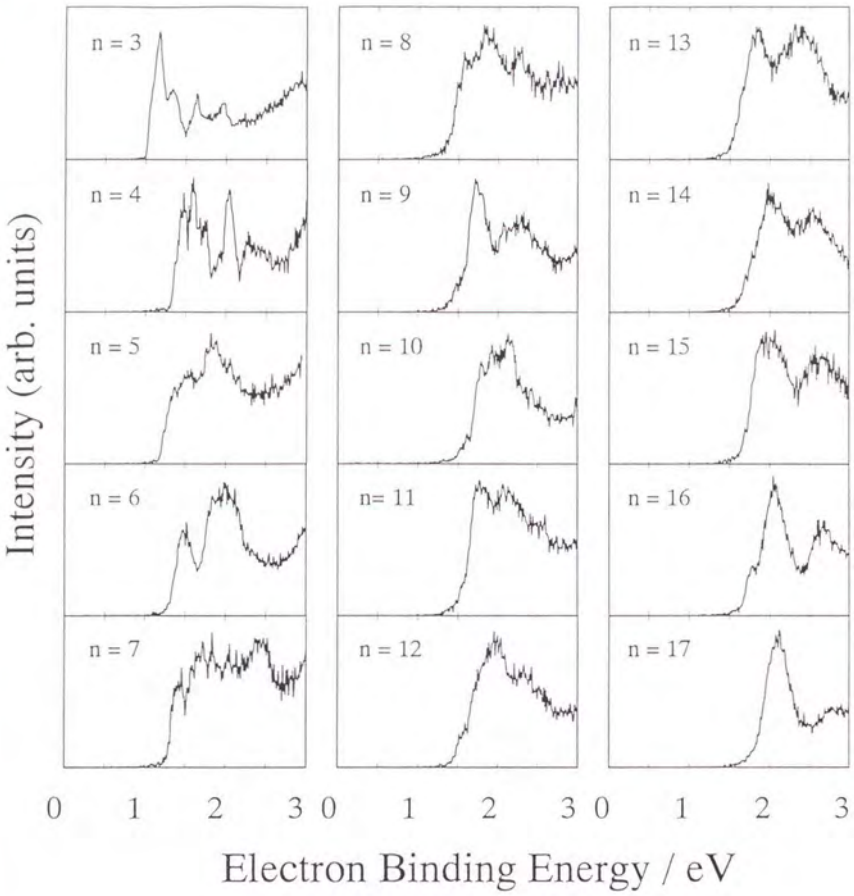

Fig. VI-3 Photoelectron spectra of vanadium cluster anions, V_n^-, measured by use of the third harmonics of a Nd YAG laser (3.495 eV).

(continued on the next page.)

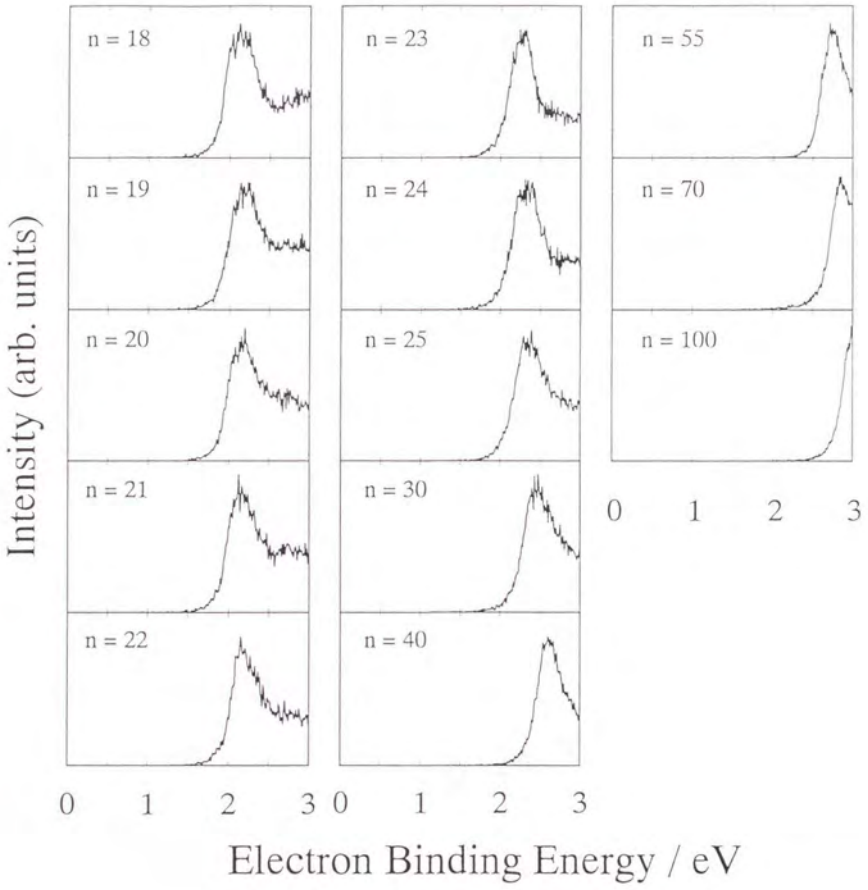

Fig. VI-3 (continued from the previous page.)

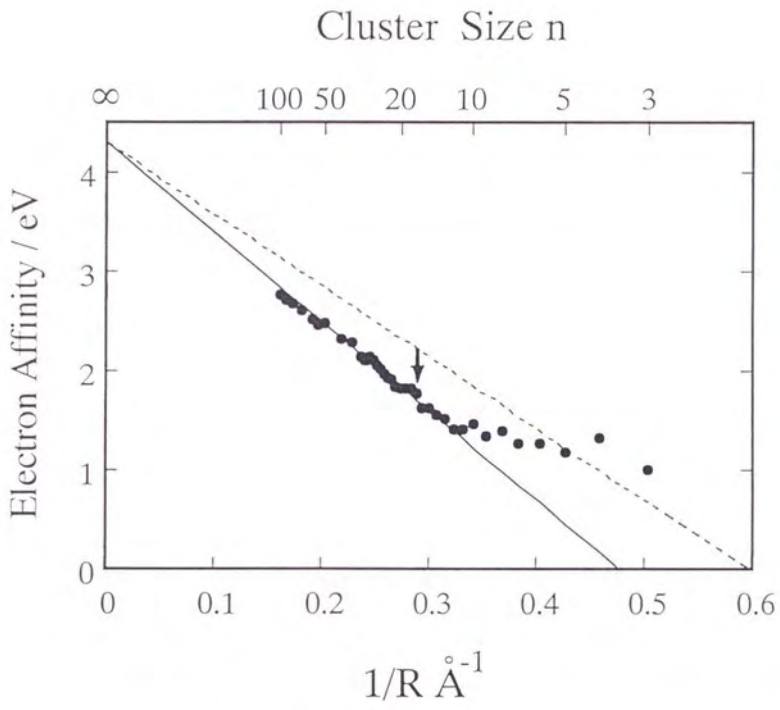

Fig. VI-4 Electron affinity vs $1/R$ plots. The solid and doted lines represent the prediction by the spherical conducting drop model with $\alpha = 5/8$ and $\alpha = 1/2$, respectively (see eqn. VI.1 in the text). The electron affinities show a clear discontinuity between $n = 16$ and $n = 17$ (pointed by the arrow).

Chapter VII

Concluding Remarks

The present work was focused on the study of the electronic structures of van der Waals and transition metal clusters using photoelectron spectroscopy and the spin-polarized DV–$X\alpha$ calculation. In order to perform the study, the photoelectron spectrometers and the cluster sources used were designed and constructed (chapter II).

At first, we investigated isomerization of $(CO_2)_nH_2O^-$ as a function of the cluster size and found that two isomeric forms exist simultaneously in $(CO_2)_nH_2O^-$ (chapter III); the stability of the two isomers sensitively depended on the cluster size. The *ab-initio* calculation now undertaken will provide a further explanation about the function of the water molecule and the mechanism of the isomerization.

We further studied the electronic structures of cobalt (chapter IV) and vanadium (chapter VI) cluster anions. In addition to the measurement of the photoelectron spectra, the electronic structures of the cobalt cluster anions, Co_n^-, with $n = 3, 4$ and 6 were calculated by the spin-polarized DV–$X\alpha$ method. It was found that the electron energy levels with the majority and the minority spins were split by 1.0–2.8 eV with the spin difference of about 2 electrons per cobalt atom. This result indicates ferromagnetic spin coupling in the cobalt cluster anions. In the vanadium clusters, preliminary calculations of the tetramer anion show that the electron energy levels with the different spin states split with the spin difference of 1.1 electrons per vanadium atom. As far as we know, this is the first experimental evidence for the ferromagnetic spin coupling in the vanadium clusters.

We also found size-dependent transitions in the electronic structures of both the cobalt and the vanadium cluster anions. Comparing the measured electron affinities with those predicted by the "spherical conducting drop model", the transition observed seems to be a metal-non-metal one. However, this classical model cannot provide a definitive criterion of metal and non-metal, because quantum effects such as the electron correlation which are neglected in this model are expected to play an important role in the transition metal clusters.

The electronic and magnetic properties of the transition metal clusters shown here are strongly correlated with the nature of their d electrons. It is well known that the correlation effects in d-electron systems are significant, because these d electrons tend to be

localized around the cores of the atoms and have high states densities. Therefore, the nearly-free-electron theory which is successfully applied to typical metal clusters cannot be valid anymore.

In addition, the reactivity of the cobalt cluster anions with simple molecules were investigated (chapter V). It was found that the size-dependent transition of the reactivity occurs at the transition size ($n \simeq 7$) for the electronic structures. For elucidating the reaction mechanism, the photoelectron spectra of the reaction product anions were also measured. The photoelectron spectra presented here provide important information on the bonding of the clusters and the adsorbates.

As shown in this thesis, the photoelectron spectroscopy of the cluster anions provides quantitative information on the electronic structures such as electron affinities and low-lying electronic states. Moreover, the theoretical calculations on the photoelectron spectroscopy provide insight into not only the electronic structures but also the geometrical structures, the magnetism and so on. Further studies of cluster anions by the technique of photoelectron spectroscopy will doubtlessly lead to a more thorough understanding of the chemistry and physics of clusters and cluster anions.

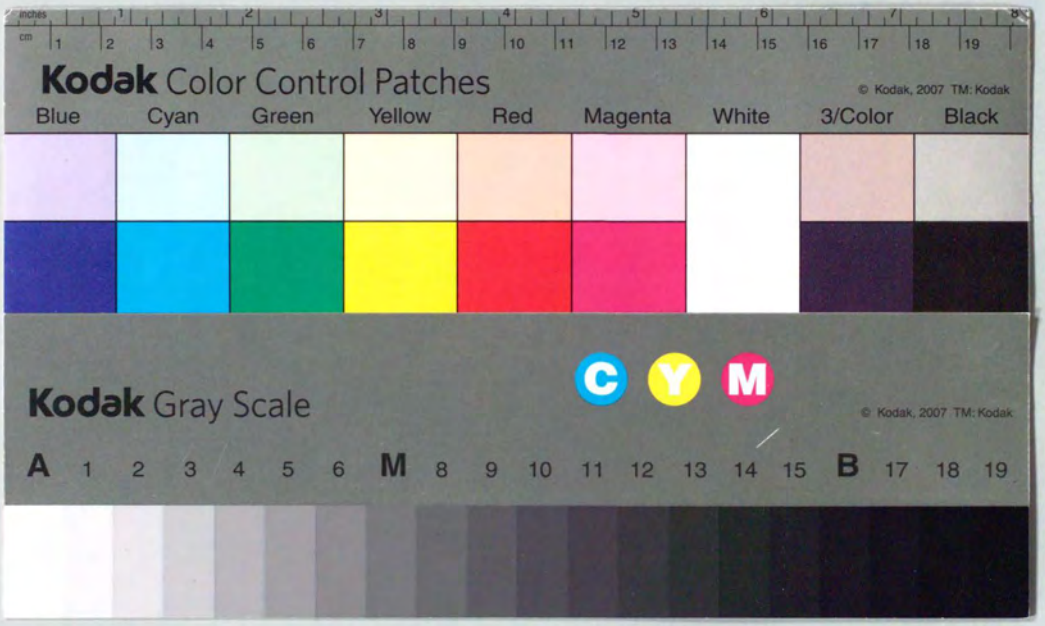
inches
cm
Kodak Color Control Patches
© Kodak, 2007 TM: Kodak
Blue
Cyan
Green
Yellow
Red
Magenta
White
3/Color
Black
C
Y
M
Kodak Gray Scale
© Kodak, 2007 TM: Kodak
A 1 2 3 4 5 6 M 8 9 10 11 12 13 14 15 B 17 18 19